Branching Growth in Stony Corals
a modelling approach

Vertakkende groei bij steenkoralen
een modelbenadering

Branching Growth in Stony Corals
a modelling approach

ACADEMISCH PROEFSCHRIFT

ter verkrijging van de graad van doctor
aan de Universiteit van Amsterdam
op gezag van de Rector Magnificus
prof. mr. P. F. van der Heijden
ten overstaan van een door het college voor promoties
ingestelde commissie, in het openbaar te verdedigen
in de Aula der Universiteit
op woensdag 7 mei 2003 te 14:00 uur

door

Roeland Mattheus Hermanus Merks

geboren te Groningen

Promotiecommissie:

Promotor:	prof. dr. P. M. A. Sloot
Co-promotores:	dr. ir. A. G. Hoekstra dr. J. A. Kaandorp
Overige leden:	prof. dr. R. P. M. Bak prof. dr. A. V. Bogdanov dr. A. Deutsch prof. dr. ir. F. C. A. Groen prof. dr. P. Hogeweg prof. dr. H. V. Westerhoff
Faculteit:	Natuurwetenschappen, Wiskunde en Informatica

— maar nieuwe elementen worden na het begin niet meer toegevoegd, de schrijver had ze allemaal al klaargezet in de opening en hoefde ze alleen nog maar te gebruiken, net zoals een goede kok eerst alle benodigde ingrediënten klaarzet voor hij begint te koken, en net zoals een schaakspeler speelt met de stukken die al vanaf het begin op het bord staan, zonder bij te zetten.

Thomas Rosenboom, *Aanvallend spel*

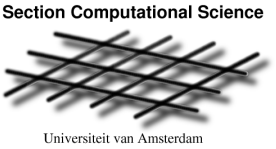

This work was carried out in the Section Computational Science

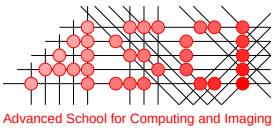

This work was carried out in the ASCI graduate school
ASCI dissertation series number 86

Cover design
Han van Eijk
Eijkpunt Grafische Vormgeving, Utrecht

Cover photography
Louis van der Laan (real corals, *Madracis mirabilis*)
Ronald van Weeren (coral models)

Printing
Ponsen & Looijen, Wageningen

ISBN 90-5776103-3

www.roelandmerks.nl
post@roelandmerks.nl

Contents

CHAPTER

ONE

General Introduction

Understanding morphogenesis, the generation of shape, is one of the most fascinating and fundamental problems in biology. A single fertilised egg cell, or a small fragment of the parental organism, seemingly contains enough information about how the organism's shape will unfold during its life-time. This information, sometimes called the *developmental program*, is encoded in the genome, which is stored as DNA in every cell of the organism. It seems to be often overlooked, however, that this is only part of the story. Imagine we would be able to obtain the genetic sequences of a life-form living in some parallel universe, governed by physical laws unknown by us. Would we in principle be able to decode this information and reconstruct the morphologies of the life forms encoded by it? The answer would of course be 'no'. We would have no knowledge about the material from which the organism would be constructed, and moreover, we would have no idea of how this material were to interact with the information stored in the genetic code. We would be in the same position as the archaeologist uncovering a pile of punch cards a thousands years from now; he may be able to transcribe a long list of ones and nods, but without knowledge of the PDP/11 computer that these were once fed to, this would not help him very much. Hence to start understanding morphogenesis, we both need a thorough understanding of the *software* – the DNA – and of the *hardware*, the tissue, cells, and skeleton. This fact was realised long before the first DNA was sequenced. In his seminal book *On Growth and Form*, Thompson (1917) studied biological morphologies by using concepts from physics, such as surface tension and close packings, to explain biological morphology. We call such comparisons *physical metaphors* in this thesis, and we will make extensive use of them to shed light on the physical mechanisms of morphogenesis.

In most organisms the genome seems to strictly guide the organism's development. Such species would not be the best model organisms for studying the physical mechanisms of morphogenesis, as this would require detailed understanding of the complex interactions between the genome and the organism's proteins, cells and tissues. Recently, the view is coming up that early during the evolution of multicellular organisms, development was less strictly regulated than in present day organisms (Newman

& Muller, 2000, see also Buss, 1987). This view argues that "the present relationship between genes and phenotype is a derived condition, a product of evolution rather than its precondition" (Newman & Muller, 2000), and emphasises the role of epigenetic mechanisms, such as the inductive interactions between cells and tissue. The original function of the genes would have been to deliver structural building blocks. Ideally, we would study such an early, hypothetical product of multicellular evolution, in which morphogenesis would be less strictly genetically controlled.

Instead of searching for the ideal, loosely genetically regulated multicellular organism, we take a different approach and study colonial multicellular organisms that collectively shape their colony, such as gorgonians and stony corals. Although the morphology of the separate modules of these organisms is often very stable[1], suggesting strict genetic developmental regulation, the morphologies of colonies formed by the repetition of the modules is highly variable, and is easily influenced by environmental factors such as light availability, water flow and sedimentation (see Section 1.3 for discussion). This may suggest that the morphogenesis of the coral colony is not under strong genetic control, suggesting that it may be possible to understand it to a large extent from epigenetic mechanisms alone. This would enable us to explain coral morphogenesis starting from the level of the individual polyp. We could take into account the physical mechanisms of morphogenesis, ignoring possible higher-level regulation through inter-modular signalling. It is often thought, however, that coral morphogenesis is under strict genetic control (Rinkevich, 2001; Rinkevich, 2002). Using computational modelling approaches, we aim to unravel for which aspects of the morphogenesis of stony corals the interactions between the deposition of coral skeleton, the resource uptake by the polyps and the environment can provide sufficient explanation, and for which aspects genetic regulation must be responsible.

In the remainder of this introductory chapter, we will first introduce the role of computational methods in the study of biological morphogenesis. Then we will introduce models used for understanding branching morphogenesis in physics and biology and give a biological introduction to the morphogenesis of branching corals. Thereafter we will introduce previous computational approaches to the study of morphogenesis and give an overview of this thesis.

1.1 Computational Approaches for Morphogenesis

The role of modelling and simulation in biology differs somewhat from its role in physics. It is often possible to construct models of physical systems which closely reproduce reality. Thus, quantitative comparisons can be made in order to validate the models, and, importantly, the model can be used to make predictions about the system's future behaviour. For example, using Newton's laws of motion, it is possible to predict the orbit of a planet around a star, or even to statistically (the systems are chaotic) predict the evolution of star clusters (see for example Makino, 1996; Hut & Makino, 1999; Portegies Zwart *et al.*, 2001). For many biological problems such an

[1] Note, however, that the polyps of many stony corals show some environmental variation, see Section 1.3.

approach would be impossible, due to their enormous complexity. But modelling has a second important role, which is to analyse or to reconstruct the minimal set of processes that is *sufficient* to reproduce the observed phenomenon. Studying such a simplified model system makes it easier to understand which mechanisms are responsible for the observations in the real system, just as it often gives more insight to study gears by building a LEGO model than by taking apart a clockwork. In such a simplified model system it becomes more difficult to make quantitative predictions about the real system. When the main objective is to understand mechanisms, however, this is a minor disadvantage. How well it may reproduce the observations, a simulation system that contains too many details of the original system may become as complicated and as opaque as the real system. This would not be a problem, or might even be desirable when the real-world system cannot easily be studied, because it is too large or when the processes under study take too long to be studied in a life-time, which for example is the case for astrophysical simulations. For studies of biological morphogenesis this is mostly not the case. A simplified system may provide insight in the processes that produce the observations in the real system. We take the latter approach in this thesis.

The computational approaches taken in biological morphogenesis can be roughly distinguished into two classes. The first class, which we call "phenomenological models" here, starts with an analysis of the biological shape, and aims to find a computational model which reproduces it. Using such a "top-down" analysis one may reconstruct interactions between lower-level entities that have possibly produced the observed morphology. The second approach is a "bottom-up" approach; it starts with the observation of the interactions between low-level entities, say the cells, and aims to reconstruct the higher level structure, the morphology, which is produced by these interactions. We call such an approach a "mechanistic approach", since it focuses on the mechanisms producing the morphology. A typical modelling study would mostly combine these two approaches. Both high-level and low-level observations are mostly carried out, and when interactions between low-level entities have been reconstructed, it will be tested whether these interactions reproduce the observed morphology in a mechanistic modelling study. In this section we will discuss several examples of models of morphogenesis, in the light of this rough classification.

Turing, in his most influential paper "The Chemical Basis of Morphogenesis" (Turing, 1952), must have been the first to apply numerical methods to the study of biological morphogenesis. Turing developed a simple partial differential equation model, simulating a system with two chemicals, which he called morphogens in the sense of "a form producer"(Turing, 1952). These hypothetical morphogens were produced at a fixed rate from some external source. One of the chemicals, later called the *activator* by Gierer & Meinhardt (1972) (see also Meinhardt & Gierer, 2000), was produced by an autocatalytic reaction. It was converted into the second morphogen, called the *inhibitor* by Gierer & Meinhardt (1972), which catalyzed the destruction of the activator, and had a short life time itself. When the inhibitor diffused much quicker than the activator, spatial patterns would arise from a homogeneous, disturbed initial condition. Thus Turing provided a possible mechanism of symmetry breaking by which patterns could arise from an initially homogeneous distribution of morphogens. In a developing organism such a pattern could function as a "pre-pattern" used as a template to structure

periodic patterns in the organism.

Although the conditions needed for Turing's system may seem quite unrealistic, indeed Turing patterns have been realised in experimental systems (see Lee *et al.*, 1994; Castets *et al.*, 1990). They also have been hypothesised to play a role in stripe patterns found on the marine fish *Pomacanthus*, where new stripes are inserted as the fish grows larger (Kondo & Asai, 1995). Using models similar to the Turing system and to the Gierer-Meinhardt system, Meinhardt simulated the patterns occuring on tropical seashells such as *Conus textilae* (Meinhardt, 1995).

The last decennium several computational approaches have been developed to study morphogenesis in cellular aggregates and tissues. Aiming to reconstruct tissue dynamics from the collective behaviour of the individual cells, these models are very helpful in describing, analysing and understanding developmental mechanisms in phenomena ranging from the life-cycle of the cellular slime mould *Dictyostelium discoideum* and the growth of plant tissue, to tumour growth and the evolution of morphogenesis in multicellular organisms. Although some of these approaches keep the position of the cells relative to each other fixed (such as in plant tissues, see for example Lantin, 1999; Holloway & Lantin, 2002), mostly they focus on animal tissues which consist of mobile cells. In such models aggregates of hundreds to thousands of cells are simulated, where the adhesive forces between the cells and the cells and extracellular matrix, and often also chemo-attractive movements are taken into account. Palsson (2001) carries out Newtonian force calculations between individual ellipsoidal cells, using which he recovers the viscoelastic behaviour of cell-aggregates and he simulates differential adhesion-driven engulfment of one cell type by the other. Another approach is to model cell or animal aggregation using lattice gas cellular automata (see for example Bussemaker *et al.*, 1997; Parrish & Edelstein-Keshet, 1999; Börner *et al.*, 2002). In such models cells are represented by individual particles that live on a discrete grid, hopping from one lattice node to the next depending on their discrete velocity. This approach for modelling morphogenesis is applied, amongst others, in studies of ripple formation in myxomycetes (Börner *et al.*, 2002), germinal centre dynamics (Meyer-Hermann *et al.*, 2001) and avascular tumour formation (Dormann & Deutsch, 2002).

The *Glazier & Graner* (G&G)-method (Glazier & Graner, 1993) is currently becoming a commonly used and promising method for modelling cell and tissue dynamics. Its elegance lies in the fact that it mesoscopically models the cell surface dynamics while the identity of the individual cell is retained. The G&G method, also called *the extended large Q-Potts model*, is a lattice-based Monte-Carlo method originally developed to study the structure of soap froths (Holm *et al.*, 1991; now used to study foam rheology, see e.g. Jiang *et al.*, 1999) and was later extended to simulate differential adhesion driven cell rearrangement (Glazier & Graner, 1993). It focuses on morphogenesis due to cell rearrangement in cell-aggregates, driven by differential cell-cell adhesion through cellular adhesion molecules (CAMs), and quantitatively reproduces cell sorting experiments. In the G&G-method, biological cells are represented on the lattice by a patch of sites in the same state, where the state identifies a cell. Cell-cell contacts are represented as bonds between sites of unlike state, where the bond strength is determined by the types of "cellular adhesion molecules" (CAM) of the cells to which both sites belong. During a Monte-Carlo step, the cells attempt to make new bonds

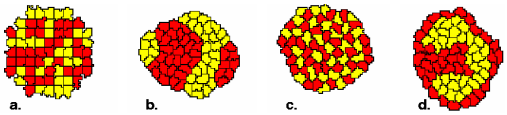

Fig. 1.1: Simple set-up of the Glazier & Graner model (Glazier & Graner, 1993). a) Initial condition. Using different bond-strength settings between dark cells, light cells and the surrounding medium (b) cell sorting, (c) mosaic, and (d) engulfment patterns are obtained.

to neighbouring cells, trying to copy the state of a site into a neighbouring site where a Hamiltonian favours stronger bonds over weaker bonds. An example is given in Fig. 1.1. Several additions and improvements have been made to the G&G algorithm, including cell growth, cell division, apoptosis and cell differentiation (Hogeweg, 2000), chemotaxis (Savill & Hogeweg, 1997), the simulation of extracellular materials (Marée & Hogeweg, 2002) and cell polarity (Zajac *et al.*, 2000; Hogeweg, *pers. comm.*). The G&G algorithm is becoming a widely used computational tool in the study of biological morphogenesis, and has been used to simulate the full development of the cellular slime mould *Dictyostelium discoideum* (Savill & Hogeweg, 1997; Marée & Hogeweg, 2001; Marée & Hogeweg, 2002)[2], convergent extension in early vertebrate embryos (Zajac *et al.*, 2000), tumour invasion (Turner & Sherratt, 2002) and skeletal formation in the vertebrate limb (Newman and Glazier, in preparation).

An approach often taken to classify simulated biological morphology is the *theoretical morphology* approach (Raup, 1962; Raup & Michelson, 1965; McGhee, Jr., 1999). In this approach one aims to construct parameterised descriptions of morphology. The parameters span up a theoretical space, called *morphospace* in which existing, but also *non-existing* morphology is ordered. The theoretical morphospace is then used to order present and extinct morphologies, in order to find which regions in morphospace have, and which have not been occupied by biological evolution. The next step is to explain why some parts of morphospace have remained empty, for example due to chance, functional constraints or physical impossibility, while others may be densely filled (see McGhee, Jr., 1999). A major drawback of this approach may be the fact that one most often uses *descriptions* of morphology, rather than models of morphogenesis. The "empty" regions in the morphospace may have very well remained empty because these morphologies cannot be produced by morphogenesis. The parameters of a morphospace can also be set by the parameters of a morphogenetic process, in which case a *developmental morphospace* is constructed (see for example Ellers, 1993; Eble, 1999).

[2]Now also in three dimensions, presented by Dr. A. F. M. Marée, University of British Colombia at the European Conference on Mathematical Modelling and Computing in Biology and Medicine, Milano, 2002.

1.2 Modelling Branching Growth

In this thesis we aim to shed light on the morphogenesis of branching corals. Branching structures are common in biology, and are studied in many contexts, such as in branching organisms like fungi, seaweeds, sponges, plants, and corals, and in branching organ systems and cells, such as lung development, the formation of blood vessels (angiogenesis) and branching of axons and dendrites in neurons. In the present section we describe some of the work and methods used in the study of biological branching systems.

Much work on plant development has been done using models based on rewriting grammars (Lindenmayer, 1968). These models, called L-systems after its developer, are formalised descriptions of (mostly branching) development that make use of a rewriting grammar (Chomsky). An L-system consists of an initial condition, called the *axiom*, a set of symbols, called the *alphabet* and a set of rewriting or *production* rules. In this grammar some symbols can signify the initiation or ending of a branch, for which mostly [and] are used. An example of an L-system is,

$$
\begin{aligned}
&V = \{F, X, +, -\} \\
&w = X \\
&P = \{F \to FF, X \to F[+X][-X]FX, [\to [,] \to], + \to +, - \to -\},
\end{aligned}
$$

where V is the alphabet, w is the axiom and P is the set of production rules. The first two rewritings of the system produce,

$$
\begin{aligned}
X &\to F[+X][-X]FX \\
&\to FF[+F[+X][-X]FX][-F[+X][-X]FX]FFF[+X][-X]FX.
\end{aligned}
$$

This example is context-independent, the rewriting rules depend exclusively on the symbol itself, and not on the neighbouring symbols. Most L-systems are context-dependent. It was first realised by Hogeweg & Hesper (1974) that the string-descriptions from some L-systems produce surprisingly life-like branching morphologies when they are *interpreted* in a post-processing step to produce morphologies like the ones in Fig. 1.2. Such approaches were later adapted by the computer graphics community to generate images of plant-like structures. An excellent review is given by Prusinkiewicz & Lindenmayer (1990).

Another biological branching process that is often studied using computational approaches is angiogenesis, the formation of blood vessels, and angiogenesis, the formation of new blood vessels towards an organ or a tumour. Most of these studies focus on the development of a branching pattern, while they include branch splitting as a model assumption. Anderson & Chaplain (1998) and McDougall *et al.* (2002) developed a discrete model of tumour induced angiogenesis, in which vessels are represented as interconnected patterns of cells in a cellular automata model. The growth of these vessels and the formation of side branches is governed by an external field of diffusing morphogens. In a simular model, Tong & Yuan (2001) study bFGF-induced angiogenesis

Fig. 1.2: Branching morphologies generated by graphical post-processing of a string produced by an context sensitive L-system (Hogeweg & Hesper, 1974). Images taken from Prusinkiewicz & Lindenmayer (1990).

in the cornea, where the vessels are represented as line pieces. The length increase of these vessels and the growth direction is determined by the gradient of "bFGF". The formation of side branches is determined by a rule linking the probability of branch formation to the concentration of the morphogen. The model by Gödde & Kurz (2001) focuses on remodelling of vascular systems due to hemodynamics and oxygen transport. In this model an initial system of afferent and efferent vessels was randomly generated, after which a pressure difference was applied over the system. Pressure drops and shear stresses in the vascular elements were calculated using an analytical model of Newtonian viscous fluid flow in linear tubes. Vessels were then added or removed based on pressure drops or shear stresses. A model similar to the angiogenesis model by Tong & Yuan (2001) was applied in a simulation of the morphogenesis of the branching sponge *Raspailia inaequalis* (Abraham, 2001). In this simulation, the growth pattern is controlled by an external field of a diffusing chemical. This diffusing chemical is absorbed by the branches, which generates a local gradient whose direction controls the branch's growth direction. Most of the models described above focused exclusively on the morphologies developing from branching processes, where branch splitting was taken as an assumption of the model. By contrast, most model studies of branching processes occuring in abiotic systems, focus on the phenomenon of branch splitting itself. Here branching is not put in as an assumption to the model, but it emerges from lower level dynamics in the system itself.

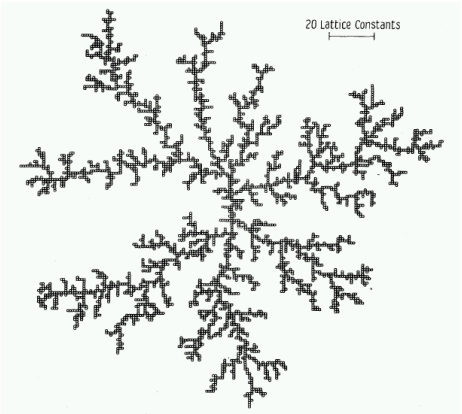

Fig. 1.3: A two-dimensional cluster generated by an lattice based diffusion limited aggregation (DLA) model. Picture taken from Witten Jr. & Sander (1981).

Branching occurs in many physical systems, such as crystallisation (think of snow crystals), aggregation, electrical discharge (see for example Pasko *et al.*, 2002) and viscous fingering. Models of such processes can be roughly divided in diffusion limited aggregation models (DLA), as introduced by Witten Jr. & Sander (1981), and Laplacian growth models (see for example Bensimon *et al.*, 1986; Arrayás *et al.*, 2002). In a DLA model (Witten Jr. & Sander, 1981), a field is initialised with a solid particle. A second particle is released at some distance from the initial seed and carries out a random walk. As soon as the free particle hits the solid seed, it solidifies, sticking irreversibly to the initial seed. A new particle is released and the procedure is repeated until a cluster has formed (see Fig. 1.3). Such pattern formation is often seen as an inherently irreversible and dissipative process (Nicolis & Prigogine, 1989; Nicolis & Prigogine, 1977). Indeed diffusion-limited aggregation is a dissipative and irreversible process, but such irreversibility is only apparent at the macroscopic level and is merely due to the low probability of the time-reversed process. The underlying microscopic physical laws of aggregation processes are reversible although this is mostly neglected in DLA models. D'Souza & Margolus (1999) have developed a thermodynamically reversible generalisation of diffusion-limited aggregation which produces clusters similar to those formed in DLA models. Many variations of the DLA model have been studied, such as off-lattice diffusion limited aggregation in which the aggregates undergo an off-lattice random walk (Schwarzer *et al.*, 1991), cluster-cluster aggregation models where both the particles and the developing clusters undergo random walks (Meakin, 1983b; Kolb *et al.*, 1983) and ballistic aggregation (Meakin *et al.*, 1986) where the particles move according to a biased random walk. For recent reviews on DLA and related models see Meakin (1999) and Halsey (2000).

The essential difference between DLA and Laplacian growth is that growth in DLA occurs particle by particle, whereas Laplacian growth is layer by layer (Barra *et al.*, 2001). Typical growth processes modelled by Laplacian growth models are viscous

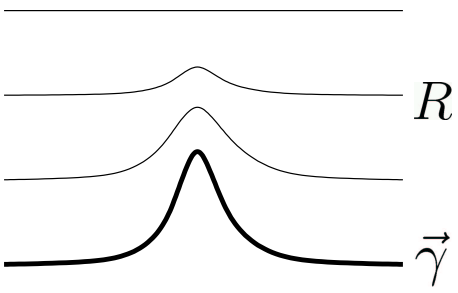

Fig. 1.4: The Mullins-Sekerka instability. A small bump in the interface $\vec{\gamma}$ results locally in a larger gradient in the field R. Thick line, interface $\vec{\gamma}$; thin lines, isolines of field R.

fingering (see e.g. Bensimon *et al.*, 1986; Arnéodo *et al.*, 1989; Lajeunesse & Couder, 2000 and references therein), discharge patterns (see e.g. Pasko *et al.*, 2002; Arrayás *et al.*, 2002 and references therein) and, with anisotropy, dendritic solidification (see e.g. Plapp & Karma, 2000b; Plapp & Karma, 2000a; Al-Rawahi & Tryggvason, 2002). In Laplacian growth models, the displacement of an interface $\vec{\gamma}$ is governed by a field of some quantity R which satisfies Laplace's equation,

$$\nabla^2 R = 0. \tag{1.1}$$

The quantity R can represent various quantities, for example a pressure field, as in viscous fingering models, an electric field, as in electric discharge models, or a growth resource. In the latter case the Laplace equation would represent an equilibrated diffusion process. Mostly $R = 0$ at the interface, i.e. $R(\vec{\gamma}) = 0$. The displacement of the interface is given by,

$$\partial_t \vec{\gamma}(t) = \vec{\nabla} R(\vec{\gamma}), \tag{1.2}$$

indicating that the local displacement of the interface $\partial_t \vec{\gamma}(t)$ is proportional to the gradient of the field, $\vec{\nabla} R(\vec{\gamma})$. Central to understanding the mechanism of branching in DLA and Laplacian growth is the so-called Mullins-Sekerka instability (Mullins & Sekerka, 1963; Mullins & Sekerka, 1964). As soon as a tiny bump of the interface $\vec{\gamma}$ appears, the gradient of the surround field R at the bump will be slightly larger than elsewhere (see Fig. 1.4). Hence, it grows a little bit faster, enlarging the bump which sets off the instability. An essential parameter in determining the shape of these bumps is the so-called *ultraviolet cutoff* (see e.g. Ball & Somfai, 2002). This cutoff refers to the minimum wavelength of the developing pattern and is driven by stabilising forces at the surface, such as the surface tension. Without this ultraviolet cutoff the Mullins-Sekerka instability leads to cusp singularities in the interface (Shraiman & Bensimon, 1984); these are non-differentiable points of the interface.

Diffusion-limited aggregation and Laplacian growth have been traditionally considered to belong to the same universality class and were thus expected to give rise to

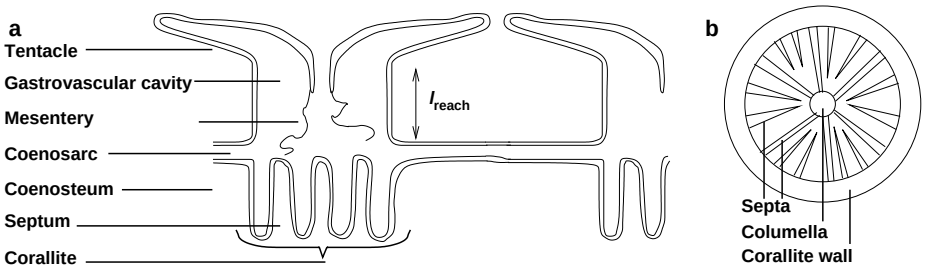

Fig. 1.5: Diagrams of a) a coral polyp (longitudinal section) in the skeletal cup and b) the skeletal cup or calix (transversal section). Modified after Dorit *et al.* (1991)

patterns with the same fractal dimensions (see e.g. Paterson, 1984; Nittmann & Stanley, 1986; Sander, 1986; Arnéodo *et al.*, 1989; Ball, 1998; Halsey, 2000). However, recently Barra *et al.* (2001) calculated the lower bound of the fractal dimension of Laplacian growth patterns using conformal mapping techniques, and proposed that it should always be higher than 1.85 for two-dimensional Laplacian growth. Since this lower bound is considerably higher than the fractal dimension of two-dimensional DLA clusters, which is 1.71, it was deduced that patterns grown with these two mechanisms cannot have the same fractal dimensions. Hence they concluded that DLA and Laplacian growth should be considered members of different universality classes. These models have been recently brought together in a theoretical framework of diffusion controlled growth (Ball & Somfai, 2002), in which indeed Laplacian growth and DLA take different positions.

1.3 The morphogenesis of branching corals

In this thesis, we use the physical metaphors of diffusion-limited aggregation and Laplacian growth to study the morphogenesis of branching corals. To see how these metaphors can be applied to understand branching in coral growth, we briefly introduce the biology of coral growth and the biological questions addressed in this thesis. Then we will introduce previous models of coral growth, and discuss how these models relate to the biological and physical models of branching growth we have introduced in Section 1.2.

Most stony corals are colonial organisms consisting of tightly interconnected polyps that collectively build an external skeleton of aragonite, a crystal form of calcium carbonate. The coral polyps reside in skeletal structures called the calices or skeletal cups (Fig. 1.5a.). These consist of a central cylinder, the columella, from which radial septa project onto a surrounding cylindrical or polygonal wall (Fig. 1.5b.). In some coral species, called *cerioid* corals, neighbouring polyps share the calix wall, whereas in *plocoid* species each polyp has its own wall and is separated from neighbouring polyps by a skeletal region called the coenosteum. The polyps feed on organic suspended material and zooplankton, which is digested in the gastrovascular cavity.

The gastrovascular cavity is in open connection to neighbouring polyps through tissue bridges called the coenosarc. There is evidence that the coenosarc is used to transport nutrients between the polyps (Rinkevich & Loya, 1983; Oren *et al.*, 1997). In addition to heterotrophic feeding, many coral species make use of photosynthesis, which is made possible by endosymbiotic algae, called *zooxanthellae*.

The coral skeleton grows as the polyps vertically extend their calix walls and septa, that are thickened secondarily. During such *skeletal growth*, the polyps periodically retreat from the skeleton, closing off the space they leave behind with a horizontal skeletal structure, called the dissepiment (Barnes, 1973; Barnes & Lough, 1992; Vermeij *et al.*, 2001). In order to keep the expanding coral surface covered with coral polyps, new polyps are formed, a process called *tissue growth*.

Because polyps need space on the skeleton in order to divide, and the skeleton is generated by the polyps, the growth of tissue and skeleton is tightly linked. Tissue growth and skeletal growth are however not necessarily limited by the same factors (Barnes & Lough, 1992; Darke & Barnes, 1993). The skeletal growth rate depends on the availability of light (Marubini *et al.*, 2001), on the saturation state of dissolved calcium carbonate (Kleypas *et al.*, 1999; Langdon *et al.*, 2000; Marubini *et al.*, 2001) and on the concentration of a number of dissolved inorganic nutrients, such as phosphate, nitrate or inorganic carbon (Lesser *et al.*, 1994). In some species, the skeletal growth rate has been reported to depend also partly (Miller, 1995; Wellington, 1982) or completely (Marshall, 1996) on the availability of organic nutrients, such as zooplankton and suspended material. The availability of such organic nutrients has been hypothesised to determine the rate of tissue production (Barnes, 1973; Graus & Macintyre, 1982; Darke & Barnes, 1993). Recent measurements of feeding on fine particulate matter in stony corals are argued to provide evidence for this hypothesis (Anthony, 1999).

The coral growth process generates a wide range of corallum morphologies, for example branching, spherical or plate-like morphologies. In this thesis we focus on branching morphologies such as those of *Madracis mirabilis* shown in Fig. 1.6. The morphogenesis of corals is driven by the interplay between genetic and environmental factors. It is thought that genetic factors regulate the branching patterns of corals, since in many corals the branches are added according to strict architectural rules (Dauget, 1991). In *Stylophora pistillata* such rules can generate nearly spherical colonies, that regenerate when damaged (Loya, 1976, reviewed in Rinkevich, 2001; Rinkevich, 2002). Such genetic regulation is sometimes thought to be mediated by hypothetical extracellular signalling molecules called “isomones”, excreted by the polyps in the surrounding water (Rinkevich & Loya, 1985). Molecular evidence for such genetic regulation is sparse, however. Coral polyp cells host many nuclear receptors for small lipophylic signalling molecules such as retinoic acid (Grasso *et al.*, 2001), but it is unknown whether such signalling molecules are used to convey signals between polyps.

Within the limits set by genetics, some coral species form a wide range of morphologies through the effect of the environmental conditions under which they grow, such as the availability of light and the amount of water flow. An example of such *morphologic plasticity* may be given by colonies of *Montastrea annularis* that are hemispherical at shallow growth sites, whereas columnar, foliaceous and sheet-like

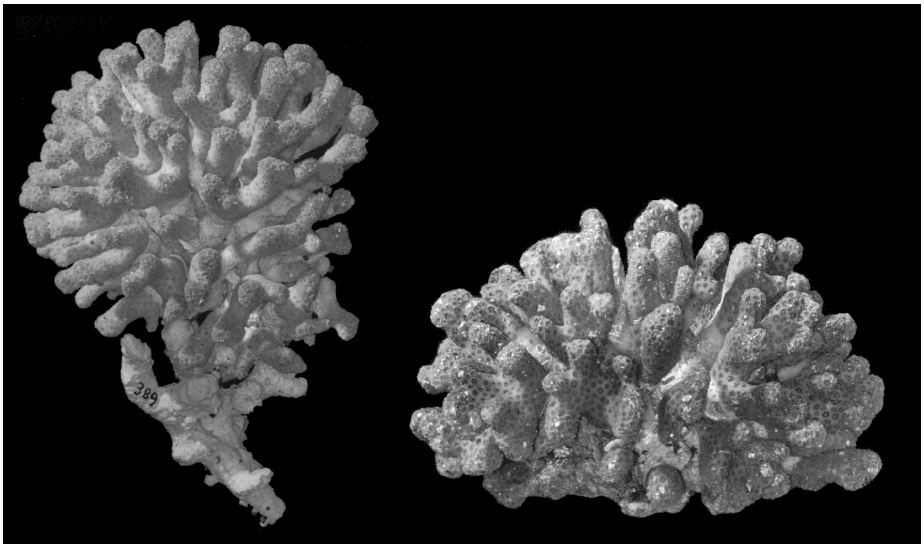

Fig. 1.6: Branching morphologies of *Madracis mirabilis*. Pictures from Kaandorp (2001). The corals are in the collection of the Zoological Museum Amsterdam. Photography by Louis van der Laan (Zoological Museum Amsterdam). Corals were kindly provided by Mark Vermeij (Cooperative Institute for Marine and Atmospheric Research) and Rolf Bak (Netherlands Institute of Sea Research and UvA), and are used in a collaborative project "Modelling and analysing growth and form of *Madracis*" (J.A. Kaandorp, P.M.A. Sloot, M.J.A. Vermeij, R.P.M. Bak and L.E.H. Lampmann).

morphologies are found at deeper growth sites. Although originally described as three species, *Montastrea annularis* was later treated as a single species containing three morphotypes. The morphological differences were attributed to morphological variation, such as the availability of light (see Barnes, 1973; Graus & Macintyre, 1976; Graus & Macintyre, 1982 and references therein). More recently significant enzymatic differences and behavioural differences were found between the morphotypes (Van Veghel & Bak, 1993) and the original three species were resurrected (Weil & Knowlton, 1994), which was further supported by fluorescence analysis (Manica & Carter, 2000). This suggests that the morphologic differences may be genetically influenced. Extreme morphological variation of a single species is nevertheless not ruled out, due to the occurrence of intermediate morphologies and because of the fact that none of the allelic differences could be considered diagnostic for the morphotypes (Manica & Carter, 2000). Another possible example of environmental variation is found in *Porites sillimaniani* which forms branching colonies at brightly illuminated growth sites and flat, plate-like colonies at dim growth sites (Muko *et al.*, 2000). *Madracis mirabilis* forms wider branches at deep growth sites than at more shallow site, which may be either attributed to the lower water flow or to the lower irradiation found in deep reef habitats (Sebens *et al.*, 1997). Recent measurements have indicated that such mor-

phological variation in the *Madracis* genus may be directly related to the light regime (Vermeij & Bak, 2002). Evidence that coral morphologies are affected by water flow is given by the analysis of Kaandorp (1999) who finds that the branches of *Pocillopora damicornis* growing in fast water currents are more tightly spaced than those of colonies growing in slow flows.

Also the structure of calices and the coenosteal skeleton has been found to be subject to environmental variation (Foster, 1979; Foster, 1980; Zilberberg & Edmunds, 1999). For example, the calices of *Montastrea annularis* are increasingly widely spaced with depth, which is most likely attributed to the poor irradiance at deeper growth sites (Graus & Macintyre, 1982). In contrast, in *Madracis mirabilis* the calices of specimens growing under dim growth conditions are more closely spaced (Bruno & Edmunds, 1997). The ability for such environmental variation certainly also has a genetic component. This was already recognised by Foster (1979, 1980), who showed that in *Montastrea annularis* micromorphological traits such as the calix size and the porosity of coenosteum were found to vary with light intensity and food supply, whereas in *Siderastra siderea* another set of traits, such as the spacing of the dissepiments, varies with the sedimentation rate. Phenotypic plasticity is also genetically variant within species. Bruno & Edmunds (1997) found in experiments with *Madracis mirabilis* that the response to environmental effects is similar in magnitude among clones, but differs significantly between genotypes.

Hypotheses explaining morphologic plasticity in stony corals can be divided roughly in two categories, adaptive and mechanistic hypotheses. Adaptive hypotheses interpret morphologic plasticity as an adaptation to the varying environmental conditions in which a newly spawned specimen can find itself. These studies thus attempt to demonstrate the fitness advantages of morphologic plasticity. Using a mathematical model, Muko *et al.* (2000) explain the plasticity in *Porites sillimaniani* as an optimisation problem in which a maximum number of viable polyps must be supported. At growth sites with high irradiation, a branched morphology maximises the surface area, thus supporting a large number of polyps. At sites of lower irradiation, the polyps must be oriented perpendicular to the light direction in order to receive enough light, and a flat morphology becomes the optimal morphology. Several authors have experimentally studied the functional advantage of branch spacing in varying water flow conditions. Sebens *et al.* (1997) have shown that colonies of *Madracis mirabilis* with wide branch spacing, typically found in deep, low flow habitats, capture most particles at low water flow speeds. At higher flow velocities the polyps in these colonies flatten, which inhibits particle capture. Conversely, tightly spaced morphologies (typically found in more shallow, high flow speed habitats) capture most particles at high flow habitats, as the flow is slowed down between the densely packed branches. Also for *M. mirabilis* Bruno & Edmunds (1998) have shown that the respiration rate, indicative for the metabolic rate of the coral polyps, increases in specimens of *Madracis mirabilis* both with branch spacing and with flow speed. In such adaptive hypotheses morphologic plasticity is often thought to be controlled by plasticity genes (Pigliucci, 1996; Callahan *et al.*, 1997; see also Rinkevich, 2002).

Mechanistic hypotheses attempt to explain morphological plasticity as a physical or biological modification of the growth dynamics by the environment. In these studies

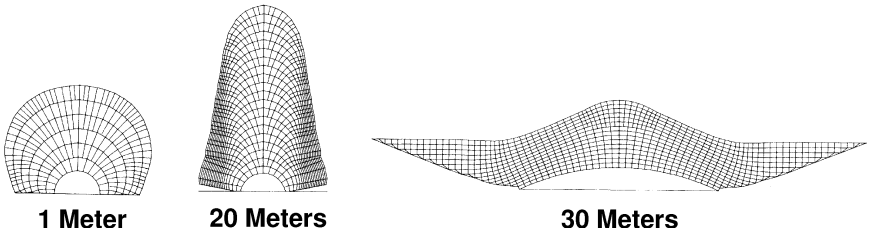

Fig. 1.7: Light dependent morphological plasticity of *Montastrea annularis*, as reproduced in the mechanistic model by Graus and Macintyre (1976, 1982). Figure modified from Graus & Macintyre (1976)

morphologic plasticity is not necessarily interpreted as an adaptation. One of the first of these mechanistic hypotheses was coined by Goreau (1963) in order to explain the flattening of colonies of *Montastrea annularis* with depth. If tissue growth is normal, but the skeletal growth rate is low due to low irradiation, "tissue growth is faster than skeletal accretion with the result that the colony must spread out, becoming much thinner and flatter" (Goreau, 1963). This explanation was further developed by Barnes (1973) to include the formation of columnar-lobate morphologies in *Montastrea annularis* in which tissue growth may not be able to keep up with skeletal accretion, resulting in separated columns only covered by tissue at the tops. Unfortunately, experimental testing of such mechanistic hypotheses is far from trivial. It is difficult to distinguish a direct, not necessarily adaptive, physical or biological modification of the morphogenetic process by the environment, from an adaptive, genetically guided modification of morphogenesis initiated by an environmental signal. Computational models of the hypothesised mechanism can be helpful in indicating whether a mechanistic hypothesis may be *sufficient* to explain a case of morphological plasticity. In the next section we introduce such computational approaches and discuss to what extent they can be used to understand coral morphogenesis and morphologic plasticity.

1.4 Computational Studies of Coral Morphogenesis

The hypothesis of Goreau (1963) was investigated by Graus and Macintyre (1976, 1982) who studied a two-dimensional computer model of light dependent accretive coral growth. They modelled skeletal accretion using a two-dimensional surface normal deposition model, where curves consisting of skeletal elements are built upon previous layers. Thus skeletal accretion occurs in a direction normal to the coral surface. The thickness of these layers, hence the growth rate, depends on the amount of light received by the simulated coral surface. A model rule guaranteed a minimum rate of tissue growth, according to the suggestion by Goreau (1963) that the rate of tissue growth is independently regulated by the supply of food. At shallow growth sites, where enough light is available, the accretive growth process produced a hemispherical morphology. The resulting coral surface expansion allowed for sufficient tissue growth

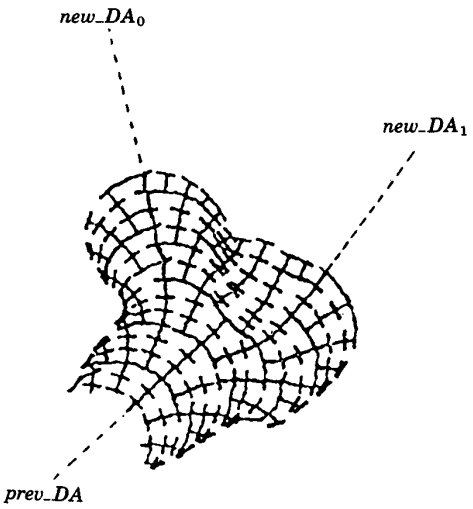

Fig. 1.8: Generation of new growth axes (new_DA_0 and new_DA_1) in the two-dimensional coral growth model by Kaandorp (1994b). Picture taken from Kaandorp (1994b).

to satisfy the minimum rate. However, at deeper growth sites skeletal growth became so slow that insufficient space is generated on the skeleton to keep up with the minimum tissue growth rate. As a result, the tissue extended laterally, resulting in more flattened colonies. Their mechanistic model reproduced the environmental range from hemispherical, to columnar towards plate-like morphologies of *Montastrea annularis* (see Fig. 1.7).

The morphogenesis and morphologic plasticity of *branching* accretive growth in sessile organisms, such as corals and sponges, was first assessed in model studies by Kaandorp *et al.* In Kaandorp (1991) and Kaandorp (1994b) a two-dimensional model of branching accretive growth was introduced, which was based on the model by Graus and Macintyre (1976, 1982). In these models, the thickness of the deposited layer was determined by a set of functions, the *growth functions*, which returned local measurements of the current growth form and of a simulated environment of the organism. Each of the branches contained an explicit *growth axis*, whose direction governed the growth of the branch. Through one of the growth functions, the angle between the coral surface and the growth axis determined the thickness of the branch, thus generating a rod shaped branch. Branch splits were initiated by generating new growth axes at local extrema, as shown in Fig. 1.8. Environmental influences were introduced using growth functions which captured the effect of the environment on the growth form. An example of such a growth function is the so-called *curvature rule*; this function makes growth highest at sections of the organism with a high curvature, whereas growth is made lower or even suppressed at flat or hollow sections. It was motivated by arguing

that the transport system of the sessile organism (sponges in particular) had a better access to the nutrients at sections of high curvature (Kaandorp, 1994b). Also it was necessary to introduce an *avoidance rule*[3] preventing the branches to intersect, and a function which added some noise to the growth rate (Kaandorp, 1991). The combination of these rules generated branching structures resembling the sponge *Haliclona oculata*. A variant of this model also included the availability of nutrients transported by diffusion (see Kaandorp, 1994b). These models were later extended to three dimensions (Kaandorp, 1995), using a method which forms the basis of the accretive growth models presented in Chapters 4 and 5.

Arguably, these models of branching accretive growth could be placed somewhere half-way between the traditional biological models of branching growth, where branching is put in as an assumption of the model, such as L-systems (Lindenmayer, 1968) and the models of abiotic growth processes as DLA and Laplacian growth (see Section 1.2). Although in these models specific rules were introduced to enforce the splitting of branches, branch splitting was not initiated by an externally enforced signal or rule, like in L-systems and in most models of angiogenesis. Contrarily, a branch split was initiated by a local extremum on the surface, mostly generated by means of the curvature rule. The coral growth models were placed further from traditional biological models by removing the assumption of a growth axis in each branch (Kaandorp & Sloot, 2001). In this model, the local growth rate was made dependent on the external field of a nutrient, which was transported by means of flow and diffusion. This study assessed the water flow driven plasticity of branch spacing and colony compactness. Increasingly compact growth forms were reported for an increasing influence of water flow (a similar result was reported in a model related to DLA with added advection, see Kaandorp *et al.*, 1996). However, the curvature rule was still necessary to generate branching structures.

1.5 Overview of this Thesis

In this thesis we aim to understand coral morphogenesis from the behaviour of low-level elements in the system, the skeleton, the tissue layer or the individual polyps and the transport of growth resources by the surrounding water; doing so, we aim to argue that branching coral growth possibly emerges from the interaction between resource uptake, skeleton deposition and tissue production. Importantly, we refrain from introducing "high-level" rules or functions which may initiate branches or force branch splitting, as the ones that were reviewed in the previous section. Even though such functions may be supported by biological facts or measurements, their introduction would lead us away from understanding the *mechanism* of coral morphogenesis; moreover, it would make it impossible to understand how environmental or genetic effects may affect such processes. The growth mechanisms which we hypothesise based on the results of these model studies, are based on the physical mechanisms of DLA and Laplacian growth which we introduced in Section 1.2.

[3] Since the avoidance rule directly affects the growth rate, we prefer to call it a growth function in this thesis.

In Chapter 2 we introduce the method used for modelling the advective-diffusive transport of growth resources in the environment. We validate the method against analytic benchmarks, and analytically calculate its limits. We apply this method in Chapter 3, in which we reassess the aggregation model of coral growth in a moving fluid (Kaandorp *et al.*, 1996). In contrast to that work, we did not find an effect of laminar flows on the compactness of DLA clusters within the limits of applicability of the advection-diffusion solver. We discuss the differences between our work and the work by Kaandorp *et al.* (1996) and show under which conditions their results can be reproduced. We postpone the consequences of these results for coral morphogenesis to Chapter 4, where we study coral growth as a Laplacian growth process, and show that branching growth can indeed be generated based on low-level interactions between skeleton, tissue and resource transport. Calculating the time-scales at which these processes take place, we discuss whether it is correct to consider coral growth a Laplacian growth process. We also study the effect of laminar flows on this growth model, and find that within the limits of the methods presently available, flow induced compactification does not occur in the accretive growth model, contrasting Kaandorp & Sloot (2001). The cause of these contrasting results is discussed. In Chapter 5 we add more biological detail, by introducing the concept of the individual polyp in our models. We show how this generates a mechanism for branching growth in stony corals, which is more robust against environmental disturbances than the Laplacian growth model. With these models, we show how the polyps' micromorphological traits can affect, through their effects on morphogenesis, the coral colony's macromorphology. Such micromorphological traits can be affected by genetic factors and by the environment. In order to fully understand the mapping from micromorphology to macromorphology, one may want to carry out a theoretical morphological analysis (Raup, 1962; Raup & Michelson, 1965; McGhee, Jr., 1999), and analyse which morphologies are found in real corals, and which ones are not. The mechanistic models which we introduce in this thesis, however, are computationally very expensive. This makes it difficult to carry out such extensive analyses, for which large amounts of morphologies would need to be simulated. In Chapter 6 we discuss the computational aspects of our models and introduce a prototypical problem solving environment (PSE) for coral morphogenesis. The aim of this PSE is twofold. Firstly, the PSE hides implementation details of the models, and assists a computationally untrained marine biologist to actively cooperate in carrying out simulation research. Secondly, the aim is to facilitate morphospace analyses, by providing assistance in scheduling the computations of large sets of simulations on large computing architectures. We briefly discuss recent developments in distributed computing which enables such an approach in the future. Finally, in Chapter 7 we summarise and conclude the work presented in this thesis, and we describe possible lines of future research.

CHAPTER

TWO

The moment propagation method for advection-diffusion in the lattice Boltzmann method[1].

We numerically validate the moment propagation method for advection-diffusion in a lattice Boltzmann simulation against the analytic Taylor-Aris prediction for dispersion in a three-dimensional Poiseuille flow. Good agreement between simulation and theory is found, with relative errors smaller than 2%. The Péclet-number limits on the moment propagation method are studied, and maximum parameter values are obtained. The maximum lattice Péclet-number vanishes towards zero in the low Reynolds number limit. We show that a modification of the moment propagation method allows advection-diffusion simulations with higher Péclet numbers, in particular in the low Reynolds number limit where the maximum Péclet-number is $\sqrt{2}$ for the D_3Q_{19}-lattice.

2.1 Introduction

In the previous chapter we discussed that we aim to understand coral morphogenesis from the interaction between the deposition of coral skeleton by the polyps and their uptake of growth resources. Corals are sessile structures; thus, the polyps' uptake of nutrients and other soluble growth resources depends on what the water flow takes to them. Consequently, the shape of coral's is often affected by water flow. Thus, modelling the transport water soluble resources is an essential step in constructing a model of coral morphogenesis. In this chapter, we introduce the lattice Boltzmann method (LBM), a computational method for simulating fluid dynamics, which we use

[1]This chapter is based on: R.M.H. Merks, A.G. Hoekstra and P.M.A. Sloot (2002). The moment propagation method for advection-diffusion in the lattice Boltzmann method: validation and Péclet-number limits. *Journal of Computational Physics* **183**, 563–576

in conjunction with the moment propagation method to simulate the solute. LBMs are widely used in fluid dynamics applications as an alternative to numerical solutions of the Navier-Stokes equations (Chen & Doolen, 1998; Succi, 2001). They are well suited for parallel simulation (Kandhai *et al.*, 1998) and they are especially useful in problems with obstacles of complex geometry (see for example Clague *et al.*, 2000; Kaandorp *et al.*, 1996; Kandhai *et al.*, 1998; Koponen *et al.*, 1998).

The transport of growth resources through the flowing water is an advection-diffusion problem. Efficient solvers for the advection-diffusion equation are important in many applications, for example in the study of contaminant spreading in ground water (Bedient *et al.*, 1993), the transport of heat and water vapour from seed potato packagings (Van der Sman, 1999) and tracer dispersion in rough fractures (Drazer & Koplik, 2001). Apart from numerical solutions of the macroscopic advection-diffusion equation (see for example Succi *et al.*, 1999; Van der Sman & Ernst, 2002; Koopman, 2002), several methods have been developed to solve advection-diffusion using tracer particle distributions. In stochastic methods, discrete particles carry out a random walk that is biased by the velocity field (Maier *et al.*, 1998). Mesoscopic advection-diffusion methods use particle densities, rather than discrete particles. Examples of such mesoscopic methods are the method of Flekkøy and coworkers (Flekkøy, 1993), or the method of Dawson *et al.* (Dawson *et al.*, 1993; Kumar *et al.*, 1999). These methods solve a multiple species miscible flow using the LBM. A similar method is Van der Sman's method (Van der Sman & Ernst, 2000). Van der Sman solves a lattice Boltzmann equation for advection-diffusion, in which the collision operator is biased by an externally imposed velocity field. The method of Calí *et al.* uses the fourth velocity component in a four-dimensional flow projected onto a lower-dimensional lattice as a tracer (Calí *et al.*, 1992).

Another mesoscopic method is the moment propagation method (Lowe & Frenkel, 1995) that we aim to validate in this chapter. In this method a single scalar per site for each tracer species is propagated. The direction of propagation is biased by the velocity field. The moment propagation method was originally developed to efficiently calculate the velocity autocorrelation function (VACF) in lattice gas cellular automata (Frenkel, 1989; Frenkel & Ernst, 1989; Van der Hoef & Frenkel, 1990), and was later used to calculate the VACF in the lattice Boltzmann method (Lowe & Frenkel, 1995; Lowe & Frenkel, 1996). The moment propagation method has been used to solve the advection-diffusion equation in a simulation of the transport of nutrients to a growing coral colony (Kaandorp *et al.*, 1996), and was further developed to solve electroviscous transport problems (Warren, 1997).

The moment propagation method has a few advantages relative to other tracer dispersion methods. In many applications one needs a preaveraged, smooth distribution of tracer. For these applications a stochastic method (Maier *et al.*, 1998) may not be most efficient. Since the moment propagation method uses only a single scalar per site for each tracer species, the computational and memory requirements are much lower than for the other methods. Also, the addition of extra tracer species is relatively easy. Hence, the moment propagation method seems to be a good choice for solute dispersion applications.

We are unaware of any attempts to numerically validate the moment propagation

method against analytic benchmarks. Here we undertake such validation by comparing the moment propagation method against the analytic Taylor-Aris result of solute dispersion in three-dimensional tubes (Aris, 1956).

In addition, we study the Péclet-number limits of the moment propagation method. We find a maximum value of the Péclet number, beyond which non-realistic negative solute concentrations occur. We present a modification of the moment propagation method, which allows higher Péclet-numbers than the standard moment propagation method.

2.2 Simulation methods

2.2.1 Lattice Boltzmann BGK method

To obtain the flow field in which the solutes were dispersed, we applied a special form of the lattice Boltzmann method, the Lattice Boltzmann BGK (Bhatnager, Gross, Krook)-method (denoted hereafter as LBGK) (Qian *et al.*, 1992). The lattice Boltzmann equation is solved on a discrete lattice x. On each lattice point there is a set of particle densities f_i of discrete velocity $\vec{c}_i/\Delta t$. For each time step Δt, the density f_i is propagated along the lattice according to its lattice velocity $\vec{c}_i/\Delta t$. The discrete lattice velocities $\vec{c}_i/\Delta t$ are such that in one time step the particle densities stream from one lattice site to a neighbouring lattice site. Next, the particle densities are redistributed according to the collision operator Ω_i. The general form of the lattice Boltzmann equation is

$$f_i(\vec{x} + \vec{c}_i, t + \Delta t) = f_i(\vec{x}, t) + \Omega_i, \tag{2.1}$$

in which Ω is the collision operator and $\vec{c}_i/\Delta t$ is the velocity of the particle density f_i.

The density ρ and the fluid velocity $\vec{u}$ are obtained from the first and second order moments of the particle distributions

$$\rho(\vec{x}, t) = \sum_i f_i(\vec{x}, t), \tag{2.2}$$

and

$$\vec{u}(\vec{x}, t) = \frac{\sum_i f_i(\vec{x}, t)\vec{c}_i}{\rho(\vec{x}, t)}. \tag{2.3}$$

We used the D_3Q_{19} model on a cubic lattice. This model is isotropic and satisfies the Navier-Stokes equations (Chen & Doolen, 1998).

The collision operator Ω_i can take different forms. In the LBGK method (Qian *et al.*, 1992), the particle distribution f is relaxed towards the equilibrium distribution f^{eq}, through:

$$\Omega_i = \frac{1}{\tau}(f_i^{\mathrm{eq}}(\vec{x}, t) - f_i(\vec{x}, t)). \tag{2.4}$$

The equilibrium distribution $f^{\mathrm{eq}}(\vec{x},t)$ is a function of the local density $\rho(\vec{x},t)$ and the local velocity $\vec{u}(\vec{x},t)$,

$$f_i^{eq}(\rho,\vec{u}) = t_p\rho\left(1+\frac{\vec{c_i}.\vec{u}}{c_s^2}+\frac{(\vec{c_i}.\vec{u})^2}{2c_s^4}-\frac{\vec{u}.\vec{u}}{2c_s^2}\right), \tag{2.5}$$

in which c_s is the speed of sound, the index $p=\vec{c_i}.\vec{c_i}$ is the square length of the lattice vectors and t_p is the corresponding equilibrium density for $\vec{u}=0$ and $\rho=1$ (Qian *et al.*, 1992). For the D_3Q_{19}-lattice that we use throughout this thesis, $t_0=\frac{1}{3}$, $t_1=\frac{1}{18}$ and $t_2=\frac{1}{36}$.

The relaxation parameter τ determines the kinematic viscosity ν of the simulated fluid. For the D_3Q_{19}-lattice $\nu=(2\tau-1)/6$ (Chen & Doolen, 1998). In this thesis, $\tau=1.0$ ($\nu=\frac{1}{6}$). This value for τ is well above the safe lower limit of τ (Qian *et al.*, 1992). At solid boundaries, a half-way bounce back boundary condition was applied (Kandhai *et al.*, 1999).

To speed up the computation of a stable flow field, we routinely use the *iterative momentum relaxation* technique (Kandhai *et al.*, 1999). In this technique, a body force is iteratively balanced with the frictional forces of the obstacle. The iterative momentum relaxation is started as soon as the fluid velocity exceeds a pre-set minimal velocity.

2.2.2 The moment propagation method

After the iteration of Eq. 2.1 until a stable flow field $f(\vec{x})$ is obtained, the dispersion of tracers using the moment propagation method (Lowe & Frenkel, 1995) is started. In this method, a scalar quantity $R(\vec{x},t)$ is released in the lattice. A fraction Δ/ρ of $R(\vec{x},t)$ stays on the lattice node and the remaining fraction is distributed over the neighbouring nodes according to the probability $f(\vec{x}-\vec{c}_i,t)$ that a carrier fluid particle moves with velocity $\vec{c}_i$ after collision, giving

$$R(\vec{x},t+1)=\sum_i \frac{(f_i(\vec{x}-\vec{c}_i)-\Delta/b)R(\vec{x}-\vec{c}_i,t)}{\rho(\vec{x}-\vec{c}_i)}+\Delta\frac{R(\vec{x},t)}{\rho(\vec{x})}, \tag{2.6}$$

where b is the number of velocities in the lattice (in our case $b=19$). The parameter Δ is used to set the molecular diffusion coefficient D_m. The dependence of D_m on Δ for a D_3Q_{19} lattice is found as follows. Assuming that the moment propagation method solves the advection-diffusion equation, we can find the diffusion constant by considering the dispersion of tracer after one time step. A δ-pulse of tracer is released in a flow field in equilibrium at $t=0$. At $t=1$, the first and second order moments $\vec{m}_1$ and m_2 are

$$\vec{m}_1=\sum_i \frac{f_i^{\mathrm{eq}}(\vec{u},\rho)-\frac{\Delta}{19}}{\rho}\vec{c}_i=\vec{u} \tag{2.7}$$

and

$$m_2 = \sum_i \frac{f_i^{\mathrm{eq}}(\vec{u},\rho) - \frac{\Delta}{19}}{\rho} \vec{c}_i.\vec{c}_i = 1 + \vec{u}.\vec{u} - \frac{30}{19}\frac{\Delta}{\rho}. \tag{2.8}$$

Using $D_m = \frac{1}{6}\frac{d(m_2 - \vec{m}_1.\vec{m}_1)}{dt} = \frac{1}{6}\left[m_2 - \vec{m}_1.\vec{m}_1\right]_{t=1}$, we find that

$$D_m = \frac{1}{6} - \frac{5}{19}\frac{\Delta}{\rho}. \tag{2.9}$$

We measured D_m in a D_3Q_{19} model for a wide range of values of Δ. These measurements agreed with Eq. 2.9 with a residual sum of squares of 4.10^{-17} (data not shown).

The diffusion coefficient can also be derived from the moment propagation method without the prior assumption that it solves the advection-diffusion equation. Following the method used by Warren (1997) where a uniform flow field is assumed, it is straightforward to show (see Appendix) that the moment propagation method (Eq. 2.6) approximates to second order the advection-diffusion equation

$$\frac{\partial R}{\partial t} + \vec{u}.\mathrm{grad}R = D_m \nabla^2 R. \tag{2.10}$$

This analysis results in the following expression for the diffusion coefficient D_m,

$$D_m = \frac{1}{2}\left(c_s^2 - \frac{1}{bd}\sum_i \vec{c}_i.\vec{c}_i\frac{\Delta}{\rho}\right), \tag{2.11}$$

with b the number of velocities in the lattice and d the dimensionality of the lattice. Note that for the D_3Q_{19} lattice, for which $c_s = 1/\sqrt{3}$ (Qian *et al.*, 1992), this equation agrees to the result obtained in Eq. 2.9. At solid boundaries, a half-way bounce back boundary condition was used; tracer that is propagated into a solid point bounces back immediately and stays where it was.

2.3 Results

2.3.1 Taylor-Aris dispersion in 3D Poiseuille flow

The moment propagation (MP) method was validated against the analytic Taylor-Aris prediction of tracer dispersion in a fluid flowing through a straight cylindrical tube (Aris, 1956). In this theory, the dispersion coefficient K describes the dispersion of tracer about a point moving with the mean flow velocity $\bar{u}$; $K = \frac{1}{2}\frac{\partial(\sigma_{xx}^2 - (\sigma_x)^2)}{\partial t}$, where σ_x and σ_{xx}^2 are the first and second order moments of the spatial tracer distribution along the flow direction. Aris has shown that the dispersion coefficient K is the sum of the molecular diffusion coefficient D_m and of a contribution by advection,

$$K = D_m + \kappa\alpha^2\bar{u}^2/D_m, \tag{2.12}$$

D_m	$\bar{u}$	tube length
< 0.1	$\bar{u} < 0.02$	800
< 0.1	$0.02 \leq \bar{u} < 0.04$	1600
< 0.1	$0.04 \leq \bar{u} < 0.07$	3200
< 0.1	$\bar{u} \geq 0.07$	6400
0.166	$\bar{u} < 0.01$	800
0.166	$0.01 \leq \bar{u} < 0.03$	1600
0.166	$0.03 \leq \bar{u} < 0.05$	3200
0.166	$\bar{u} \geq 0.05$	6400

Table 2.1: Settings of the tube length.

where in the case of a three-dimensional Poiseuille flow, $\kappa = \frac{1}{48}$ and α is the tube radius.

The simulations were carried out in a simulation box with a cross section of 54×54 lattice units, in which a tube of radius 25 was constructed. We initiated the simulation with a δ-pulse of solute in the middle of the tube. The first and second order moments parallel to the flow direction σ_x and σ_{xx}^2 were measured, from which the spatial variance $V = \sigma_{xx}^2 - (\sigma_x)^2$ was computed. After an initial transient, approximately the time needed for the solute to reach the wall of the tube by diffusion, the tracer variance V increased linearly with a slope of $2K$. This linear dependence no longer holds when a fraction of tracer reaches the end of the tube and re-enters the tube over the periodic boundary. This time of re-entry is dictated by advection and diffusion along the flow direction.

The size of the simulation box was set by considering estimations of the length of the initial transient and of the tracer re-entry time. In this way it was ensured that the two time scales did not overlap, enabling the observation of the linear domain, which was needed for measuring the dispersion coefficient. The length of the initial transient was estimated as follows. The initial pulse of solute diffuses perpendicular to the flow direction as a Gaussian. Using $t_D = \frac{r^2}{2D_m}$, for the range of diffusion constants considered, the time t_D at which 68% of the tracer has reached the walls of the tube is in the range $1750 < t_D < 3500$. The tracer re-entry time depends on the length of the tube. The time needed for 1% of solute in a fluid moving at a uniform velocity $u_{\max}$ to travel a distance Δx by means of diffusion and advection was estimated by solving the equation $ut + 3\sqrt{2D_m t} = \Delta x$. Hence the settings of the simulation box length were based on the mean velocity and on the diffusion coefficient (see Table 2.1), thus compromising between tracer re-entry times and computational resources.

A stable (paraboloid) flow field was computed for a range of mean flow velocities between 0.0 and 0.103 in lattice units per time step. For a 3D Poiseuille flow, the maximum velocity $u_{\max} = 2\bar{u}$, giving a maximum flow velocity of 0.206, These flow velocities correspond to Reynolds-numbers ($Re = \frac{\bar{u}L}{\nu}$, where $L = 25$ l.u. is the tube radius) between 0.0 and 15.5, which are all in the laminar regime. The maximum velocity of 0.206 is well beyond the normal applicability region of lattice-BGK (Succi,

2001). In this way it was ensured that the full region of commonly used lattice velocities was covered by the validation experiments. We measured the lattice Péclet-number $\mathrm{Pé}_{\mathrm{lat}} = \frac{u_{\max} L}{D_m}$, in which $L = 1$ l.u. The lattice Péclet-number is locally defined with respect to the lattice nodes of the advection diffusion simulation, and is independent of the size of the obstacle. The maximum lattice Péclet-numbers occurring in the simulations were between 0.0 ($u_{\max} = 0.$, $D_m = \frac{1}{6}$) and 1.892 ($u_{\max} = 2\bar{u}_{\max} = 0.182$, $D_m = 0.096$).

In Fig. 2.1 we have plotted the time dependent dispersion coefficient $D(t) = \frac{1}{2}\frac{dV(t)}{dt}$. At $t = 0$, the dispersion coefficient was equal to the molecular diffusion coefficient $D(0) = D_m$. As the initial delta pulse spread in the y and z-directions by diffusion, the dispersion coefficient increased until it reached the Taylor-Aris prediction (the dotted lines). It is easy to see that the dispersion coefficient should increase as the delta pulse spreads over the paraboloid flow field; the initial field of solute expands ever more quickly as the tracer diffuses into layers of lower velocity and lags behind the tracer moving in flow layers of higher velocity. The duration of the initial transient t_D was somewhat shorter than our estimation earlier in this section. This shows that it was a conservative assumption that 68% of the tracer should have reached the tube wall for the initial transient to end.

We measured the dispersion coefficient D in a time window well after our estimate of the initial transient and well before the estimation of the onset of tracer reentry. The dispersion coefficients were plotted together with the prediction according to the Taylor-Aris theory in Fig. 2.2. All simulated values were within a 2% range from the analytical Taylor-Aris result. Hence, our simulation results are in good agreement with the Taylor-Aris theory.

2.3.2 Limits to the Péclet-number

In the moment propagation method (Eq. 2.6) the diffusion coefficient is set using the parameter Δ, which is the probability that a tracer particle stays at the same lattice site. This poses a limit onto the maximum Péclet-number that can be simulated using the MP-method. The reason is that negative tracer concentrations may appear, if the value $f_i(\vec{x}_i - c_i) - \frac{\Delta}{b}$ in Eq. 2.6 becomes negative. In this section we investigate the maximum Péclet-number that can be used in an MP-simulation, ensuring that $\forall_{\vec{x},i} : \frac{\Delta}{b} \leq f_i(\vec{x})$.

The maximum lattice Péclet-number follows from the maximum Δ for which each streamed tracer quantity $f_i(\vec{x} - c_i) - \Delta/b \geq 0$ (see Eq. 2.6). Assuming to first approximation that $f_i \approx f_i^{\mathrm{eq}}$, we can write ($f_{\min} = \min(f_i)$),

$$\Delta_{\max}(\rho, \vec{u}) = b f_{\min}^{eq}(\vec{u}_{\max}, \rho), \tag{2.13}$$

in which $b = 19$ for the D_3Q_{19} model, and f^{eq} is the equilibrium distribution (Eq. 2.5). The maximum lattice Péclet-number is calculated using the diffusion coefficient (Eq. 2.9), giving

$$\mathrm{Pé}_{\max} = \frac{|\vec{u}_{\max}|}{D_{\min}} = \frac{|\vec{u}_{\max}|}{\frac{1}{6} - 5 f_{\min}^{eq}(\vec{u}_{\max}, \rho)}, \tag{2.14}$$

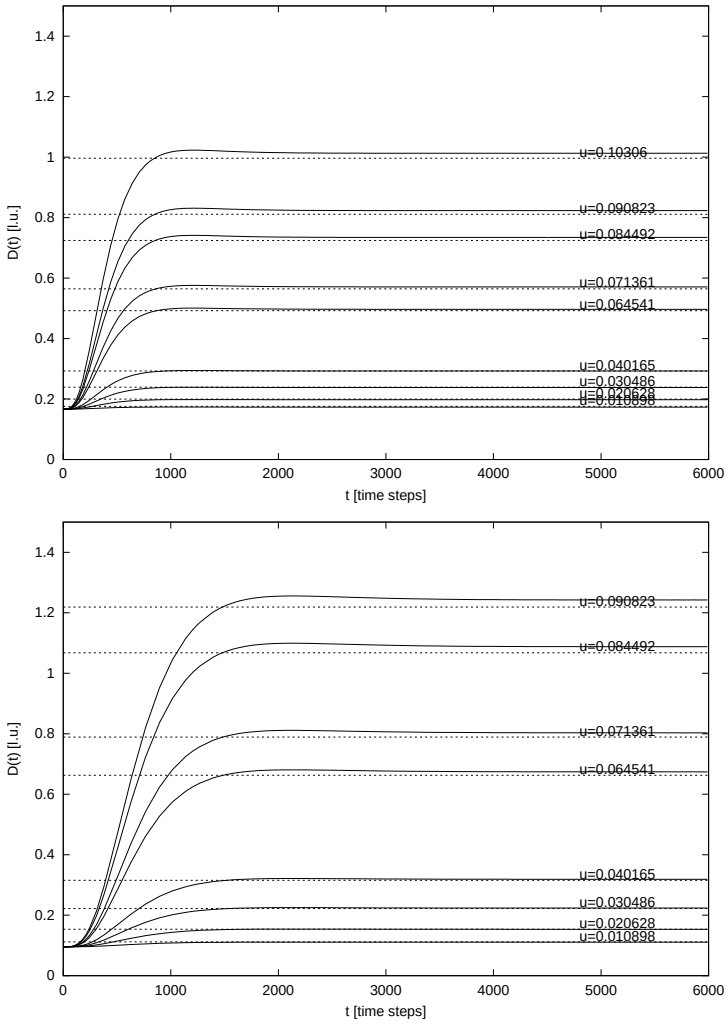

Fig. 2.1: Validation of the moment propagation scheme. The time dependent dispersion coefficients $D(t) = \frac{1}{2}\frac{dV(t)}{dt}$, in which $V = \sigma_{xx}^2 - (\sigma_x)^2$, were measured in a 3D Poiseuille flow in a tube of radius 25. $\Delta = 0$ ($D_m = \frac{1}{6}$) and $\Delta = .27$ ($D_m = 0.096$) for the upper and lower panels respectively. The tube lengths were set according to Table 2.1. The mean flow velocity $u = \frac{1}{2}u_{\max}$ is given for each line in lattice units. The Taylor-Aris predictions of the dispersion coefficients are shown as dashed lines.

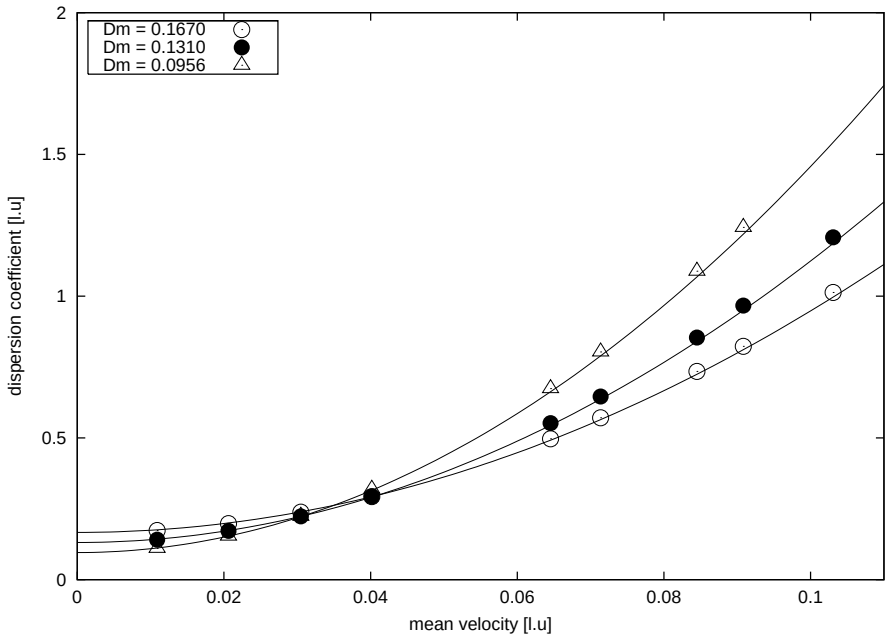

Fig. 2.2: Dispersion coefficients computed with the moment propagation method for a three-dimensional Poiseuille flow in a cylindrical tube of radius 25. The Taylor-Aris prediction is shown as a solid line. The length of the tube was varied between 800 and 6400 l.u., depending on the flow velocity and the diffusion coefficient. See text for further details. All experimental values were within a 2% interval from the prediction.

in which $|\vec{u}_{\max}|$ is the maximum velocity occurring in the simulation.

In Fig. 2.3 we have plotted the maximum lattice Péclet-number for which the MP-method still gives valid results. The maximum allowed lattice Péclet-number is plotted for three flow directions. Of these three flow directions, the direction (1,1,0) gives the lowest allowed Péclet-number. For this flow direction the smallest possible value of f_i will occur opposite to the dominating flow direction. In the D_3Q_{19} model, the velocities $|\vec{c}_i| = \sqrt{2}$ will generally have the lowest density f_i. For these velocities $t_p = \frac{1}{36}$ (see Eq. 2.5).

2.3.3 A modification of the moment propagation method

In the standard MP-scheme, the molecular diffusion coefficient D_m is lowered by subtracting an equal amount of tracer $\frac{\Delta}{b}$ from the tracer moving to the neighbouring sites. As we argued in section 2.3.2, this may lead to negative tracer values especially for the relatively small values of f_i for the velocities $|\vec{c}_i| = \sqrt{2}$.

This problem can be diminished by using the following modification of the moment propagation method. In this modified scheme, the amount of resting tracer particles is

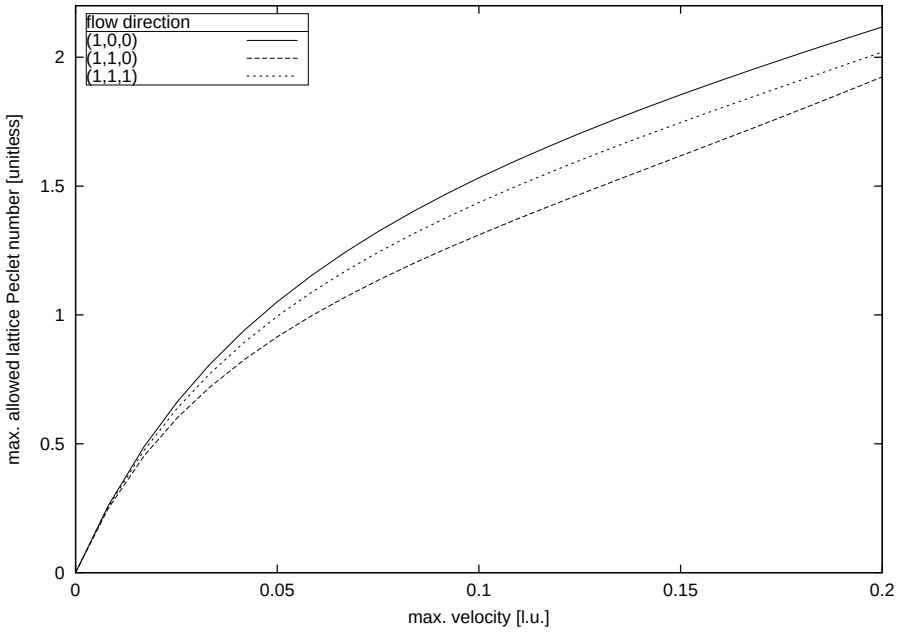

Fig. 2.3: The maximum lattice Péclet-numbers that can be simulated using the moment propagation method and the LBGK-method on a D_3Q_{19} lattice is plotted against the norm of the maximum velocity occurring in the simulation. Velocities directed along the two lattice vectors (1,0,0) and (1,1,0), and along the non-lattice vector (1,1,1) are shown. The use of lattice Péclet-numbers higher than the maximum allowed Péclet-number may result in negative tracer concentrations.

weighted according to the equilibrium distribution for a resting fluid $f_i^{\mathrm{eq}}(u=0,\rho)$,

$$R(\vec{x},t+1) = \sum_i \left[\frac{(f_i - \Delta^* f_i^{\mathrm{eq}}(\vec{u}=0,\rho))R}{\rho} \right]_{\vec{x}-\vec{c}_i,t} + \Delta^* R(\vec{x},t), \tag{2.15}$$

where the whole quantity inside $[\ldots]$ is evaluated at $(\vec{x}-\vec{c}_i,t)$. Hence we adjust the amount of extra rest particles to the streaming direction. The dimensionless parameter Δ^* is the fraction of tracer remaining at the same lattice site after propagation. Note from Eq. 2.5 that $f_i^{\mathrm{eq}}(\vec{u}=0,\rho) = t_p\rho$, so we can rewrite Eq. 2.15 to

$$R(\vec{x},t+1) = \sum_i \left[\left(\frac{f_i}{\rho} - t_p\Delta^* \right) R \right]_{\vec{x}-\vec{c}_i,t} + \Delta^* R(\vec{x},t), \tag{2.16}$$

which is equivalent to the moment propagation method introduced by Warren (1997).

The molecular diffusion coefficient D_m is set using parameter Δ^*, like in the standard MP-scheme. Releasing a δ-pulse, after one time step the first and second order

moments $\vec{m}_1$ and m_2 are

$$\vec{m}_1 = \sum_i \frac{f_i^{\mathrm{eq}}(\vec{u},\rho) - \Delta^* f_i^{\mathrm{eq}}(\vec{u}=0,\rho)}{\rho}\vec{c}_i = \vec{u} \tag{2.17}$$

and

$$m_2 = \sum_i \frac{f_i^{\mathrm{eq}}(\vec{u},\rho) - \Delta^* f_i^{\mathrm{eq}}(\vec{u}=0,\rho)}{\rho}\vec{c}_i.\vec{c}_i = 1 + \vec{u}.\vec{u} - \Delta^*. \tag{2.18}$$

Thus, the diffusion coefficient $D_m = \frac{1}{6}\frac{d(m_2 - \vec{m}_1.\vec{m}_1)}{dt} = \frac{1}{6}\left[m_2 - \vec{m}_1.\vec{m}_1\right]_{t=1}$ depends on Δ^* as

$$D_m = \frac{1}{6} - \frac{1}{6}\Delta^*. \tag{2.19}$$

Our measurements agreed to this expression with a residual sum of squares of 1.10^{-16} (data not shown). Warren (1997) has shown analytically for a uniform flow field that this scheme approximates to second order the advection-diffusion equation (Eq. 2.10) with $D_m = \frac{1}{2}{c_s}^2(1-\Delta^*)$. Note that this expression for the diffusion coefficient agrees to Eq. 2.19.

Using the reformulation of the MP-scheme, we can reach higher Péclet-numbers without obtaining negative tracer concentrations. As in section 2.3.2, the Péclet-number limits of the modified moment propagation scheme (MMP-scheme) are calculated from the maximum allowed Δ^*, $\Delta^*_{\max}(\vec{u})$, which can be obtained from Eq. 2.15,

$$\Delta^*_{\max}(\vec{u}) = \min\left(\frac{f_i^{\mathrm{eq}}(\vec{u},\rho)}{f_i^{\mathrm{eq}}(\vec{u}=0,\rho)}\right). \tag{2.20}$$

The maximum allowed lattice Péclet-number follows from Eqs. (2.19) and (2.20):

$$\mathrm{P\acute{e}}_{\max}(\vec{u}_{\max}) = \frac{|\vec{u}_{\max}|}{D_{\min}} = \frac{|\vec{u}_{\max}|}{\frac{1}{6} - \frac{1}{6}\Delta^*_{\max}(\vec{u}_{\max})}. \tag{2.21}$$

In Fig. 2.4 the maximum allowed lattice Péclet-number in the MMP-scheme is plotted against the maximum velocity occurring in the simulation.

For typical velocities of 0.05 l.u. to 0.1 l.u. the maximum Péclet-number in the MMP-scheme is 1.7 to 1.3 times higher than in the MP-scheme. For lattice velocities in the limit to 0, the maximum lattice Péclet-number is still at least $\sqrt{2}$ for the MMP-scheme, whereas in the MP-scheme the maximum lattice Péclet-number approaches 0. From Eq. 2.20 it follows that for the MMP-scheme $\lim_{u\to 0}\Delta^*_{\max} = 1$, so $(D_m)_{\min} = 0$. This means that in the low lattice velocity limit, the normal operational limit of the LBGK method, one can still set the diffusion coefficient small enough to reach Péclet-numbers up to $\sqrt{2}$. In the MP-scheme however, $\lim_{u\to 0}\Delta_{\max} = 19 f_{\min}^{\mathrm{eq}}(\vec{u}=0,\rho) = \frac{19\rho}{36}$, giving $(D_m)_{\min} = \frac{1}{36}$. So, in the low lattice velocity limit, in the MP-method one cannot set D_m small enough to reach high Péclet-numbers.

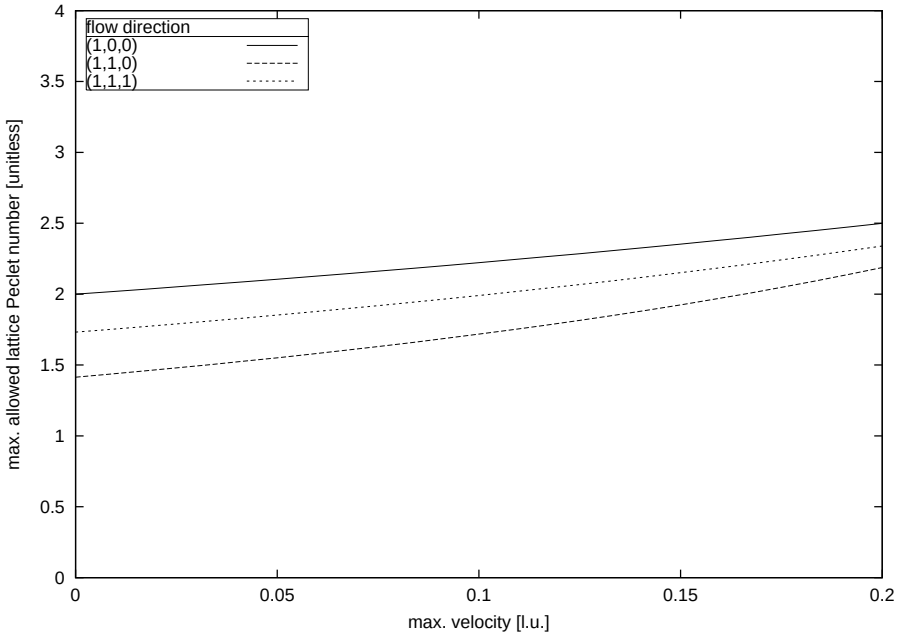

Fig. 2.4: The maximum lattice Péclet-numbers that can be simulated using the modified moment propagation method and the LBGK-method on a D_3Q_{19} lattice. Velocities directed along the two lattice vectors (1,0,0) and (1,1,0), and along the non-lattice vector (1,1,1) are shown. The use of lattice Péclet-numbers higher than the maximum allowed Péclet-number may result in negative tracer concentrations.

2.3.4 Validation of the modified moment propagation method

We did also validate the MMP scheme against the Taylor-Aris prediction of dispersion in a three-dimensional Poiseuille flow. We set $\Delta^* = 0.50$, for which $D_m = 0.083$. This value of Δ^* is very close to the maximum allowed Δ^* for $u_{\max} = 0.2$ ($\Delta^*_{\max} = 0.52$). The tube lengths were set according to Table 2.1.

In Fig. 2.5 the time dependent dispersion coefficient $D(t)$ is plotted. After the initial transient, the dispersion coefficients approached the Taylor-Aris prediction. In Fig. 2.6 we have plotted the measured Taylor-Aris dispersion coefficients for $D_m = 0.083$, for $D_m = 0.1250$ and for $D_m = \frac{1}{6}$, together with the Taylor-Aris prediction. Note that for $D_m = \frac{1}{6}$, there is no difference between the MP and the MMP-schemes. All our measurements were less than 2% above the Taylor-Aris prediction.

2.4 Discussion

In summary, our simulations of dispersion in a three-dimensional Poiseuille flow, using the moment propagation method in the LBGK-method, reproduced the analytical

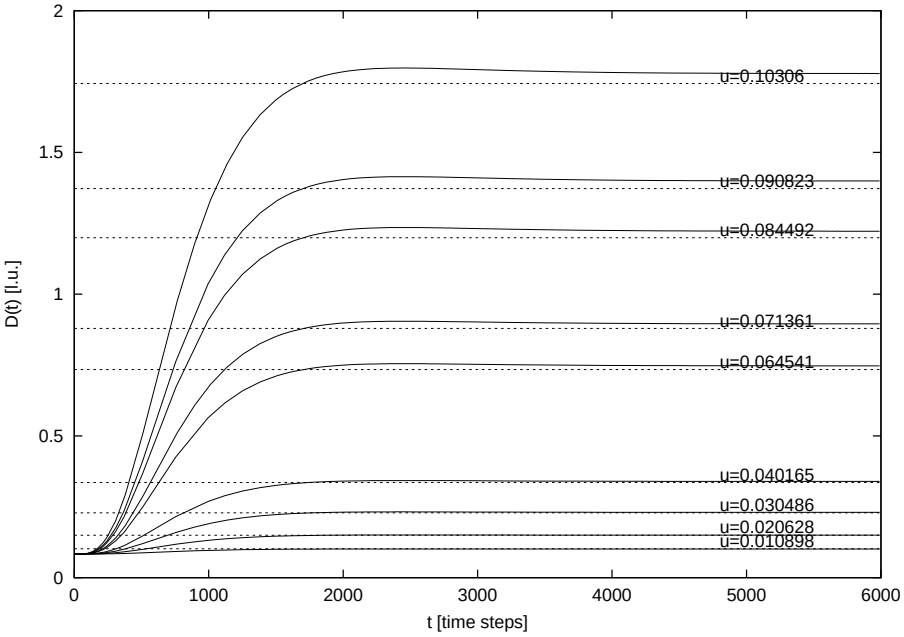

Fig. 2.5: Validation of the modified moment propagation method. The time dependent dispersion coefficient $D(t) = \frac{1}{2}\frac{dV(t)}{dt}$, in which $V = \sigma_{xx}^2 - (\sigma_x)^2$, was measured in a 3D Poiseuille flow in a tube of radius 25. $\Delta^* = 0.50$, for which $D_m = 0.083$. The tube length was set according to Table 2.1. The flow velocity in lattice units is given for each line. The Taylor-Aris predictions of the dispersion coefficients are shown as dashed lines.

Taylor-Aris result (Aris, 1956).

For the three-dimensional tube flows, the measured dispersion coefficients were never further than 2% from the Taylor-Aris prediction. The same experiments were carried out for a 2D Poiseuille flow in tubes of width 50 and of 100 l.u. (Merks *et al.*, 2001). In these experiments, all dispersion coefficients were closer than 1% to the Taylor-Aris prediction. The fact that we still found accurate agreements to the Taylor-Aris prediction in narrow, coarsely discretised circular tubes, suggests that the moment propagation method is a suitable method for advection-diffusion problems in complex geometries, such as the transport of nutrients and other chemicals towards a growing coral colony (Kaandorp *et al.*, 1996).

The dispersion coefficients as obtained in our three-dimensional simulations were systematically slightly larger than the Taylor-Aris prediction. In two-dimensional simulations the dispersion coefficients approached the Taylor-Aris prediction from below (Merks *et al.*, 2001). This observation agrees to the findings by Calí *et al.* (1992). Using their method in a two-dimensional Poiseuille flow, they also found dispersion coefficients that were systematically slightly smaller than the Taylor-Aris prediction.

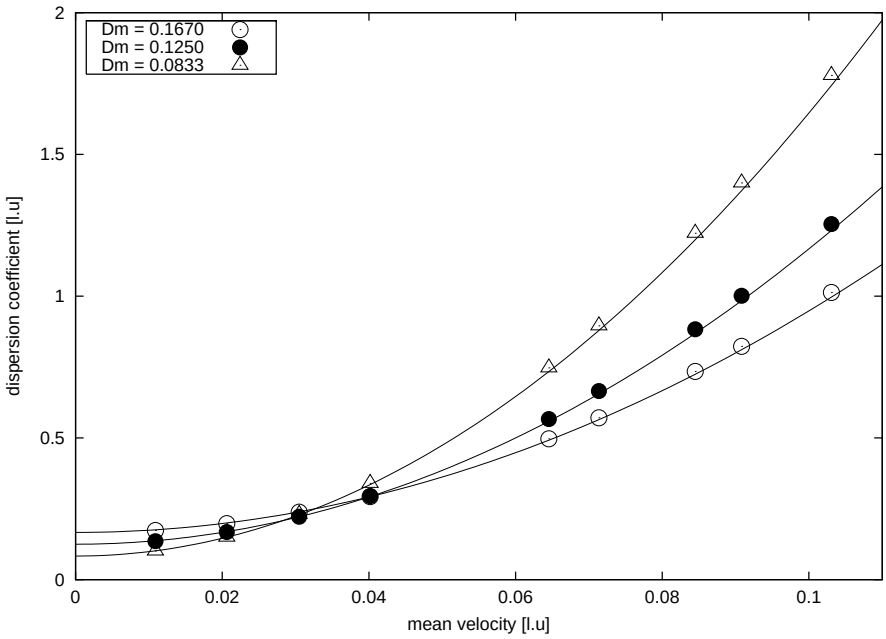

Fig. 2.6: Dispersion coefficients computed with the modified moment propagation method for a three-dimensional Poiseuille flow in a cylindrical tube of radius 25. The Taylor-Aris prediction is shown as a solid line. Mean flow speeds are given in lattice units. The length of the tube was varied between 800 and 6400 l.u., depending on the flow velocity and the diffusion coefficient. See text for further details. All experimental values were within a 2% interval from the prediction.

These authors attributed their systematic error "to the fact that the assumption on which [the Taylor-Aris prediction] is based", namely that the radial diffusion has come to an equilibrium and that the axial concentration gradient becomes uniform over the tube's cross-section in the long time limit, "is less and less valid as the Péclet-number increases" (Calí *et al.*, 1992). The asymptotic behaviour of the dispersion coefficient $D(t)$ (see Figs. 2.1 and 2.5) suggests however that the radial diffusion also equilibrises at high flow velocities. The systematic error may thus be attributed to the radial non-uniformity of the axial tracer concentration gradient.

Note that our simulations also agreed to the Taylor-Aris prediction for values of Δ and Δ^* for which negative concentrations occur (data not shown). Also, measurements of the diffusion coefficient D_m agreed to the predictions in Eqs. (2.9) and (2.19) far beyond the maximum values of Δ and Δ^*. However, such parameter values give unphysical results because some tracer concentrations will be negative. It is therefore important to check whether negative concentrations occur in a simulation using the moment propagation method.

Using the modification of the moment propagation method shown in this paper,

higher Péclet-numbers can be reached than in the standard moment propagation method. As we have shown in section 2.3.3, this holds in particular for the low lattice velocity limit, where the LBM produces more accurate flow fields (Chen & Doolen, 1998). To reach the maximum Péclet and Reynolds-numbers that are correctly simulated with the moment propagation method, the lattice velocity should be kept at moderate values (< 0.1 l.u.), the diffusion coefficient should be set to the minimum value still allowed by Eq. 2.20 and the kinematic viscosity must be set to a minimal value. In steady state flows the Péclet-number limits are independent of the kinematic viscosity. However, in unsteady flows the assumption that $f_i \approx f_i^{\mathrm{eq}}$ may not always be valid and the Pèclet-number limits may consequently be lower.

The moment propagation method has some advantages in comparison to other mesoscopic methods. The memory requirements are low; for each tracer species we need a single scalar per lattice node. By comparison, for most of the other mesoscopic methods (the methods by Flekkøy (1993), Dawson *et al.* (1993) and Van der Sman & Ernst (2000)), we would need nineteen extra scalars per lattice node for each tracer species in the D_3Q_{19} model. On the machine we use (a Linux Beowulf cluster, on which a `double` is eight bytes long), for a typical lattice of 256^3 we need 2 Gb memory for the flow field and only an extra 128 Mb of memory per tracer species for the moment propagation method. For the other mesoscopic methods we would have needed an extra amount of 2 Gb per tracer species. Calí's method (Calí *et al.*, 1992) does not need extra memory for the tracer, because it uses a quantity in the flow field itself as a tracer. However, in Calí's method it is not possible to tune the molecular diffusion coefficient D_m like in the moment propagation method. Also, no extra tracer species can be added, which is a straightforward operation in the moment propagation method. The numerical scheme by Succi *et al.* (1999) also requires only a single extra scalar per lattice node, and using this method higher lattice Péclet-numbers can be reached. However, the scheme is computationally more intensive and relies on the velocity fields, while the moment propagation method straight-forwardly uses the particle distributions from the lattice Boltzmann method. This makes the moment propagation method better suited for low-Péclet-number, large scale advection-diffusion problems.

In summary, in the range of Péclet and Reynolds-numbers studied, our simulations of the moment propagation method accurately reproduced the Taylor-Aris prediction of the dispersion coefficient. We found limits to the Péclet-numbers, beyond which the moment propagation method produces unphysical results. If these limits to the Péclet-number are taken into account, the moment propagation method is a valuable and valid computational tool for the simulation of advection-diffusion processes.

Appendix

To recover the macroscopic equations of the original moment propagation method, we follow the method by Warren (1997). He analyses the modified moment propagation method in a uniform flow by approximating $R(\vec{r} - \vec{c}_i, t)$ with a Taylor expansion to

second order as, (Einstein summation over greek indices is assumed)

$$R(\vec{r}-\vec{c}_i,t) \approx R(\vec{r},t) - c_{i\alpha}\partial_\alpha R(\vec{r},t) + \frac{1}{2}c_{i\alpha}\partial_\alpha c_{i\beta}\partial_\beta R(\vec{r},t). \tag{2.22}$$

The moment propagation method according to Warren (1997) is

$$R(\vec{r},t+1) = \sum_i w_i \left[\left(\frac{f_i^+}{\rho} - \frac{\Delta^*}{b}\right) R\right]_{r-c_{i\alpha}} + \Delta^* R(\vec{r},t). \tag{2.23}$$

Assuming a uniform flow, the equilibrium distribution f^{eq} can be substituted and we can put $f_i(\vec{r}-c_i,t) = f_i(\vec{r},t)$. After subsequent substitution of Eq. 2.22 into Eq. 2.23 we get,

$$\begin{aligned} R(\vec{r},t+1) = \Bigg(\frac{1}{b}\sum_i w_i \Bigg(1 + \frac{u_\alpha c_{i\alpha}}{c_s^2} + \frac{u_\alpha u_\beta Q_{i\alpha\beta}}{2c_s^4} - \Delta^* + c_{i\gamma}\partial_\gamma \\ - \frac{u_\alpha c_{i\alpha}c_{i\gamma}\partial_\gamma}{c_s^2} - \frac{u_\alpha u_\beta Q_{i\alpha\beta}c_{i\gamma}\partial_\gamma}{2c_s^4} + c_{i\gamma}\partial_\gamma\Delta^* + \frac{1}{2}c_{i\gamma}\partial_\gamma c_{i\delta}\partial_\delta \\ + \frac{1}{2}\frac{u_\alpha c_{i\alpha}c_{i\gamma}\partial\gamma c_{i\delta}\partial_\delta}{c_s^2} + \frac{1}{2}\frac{u_\alpha u_\beta Q_{i\alpha\beta}c_{i\gamma}\partial_\gamma c_{i\delta}\partial_\delta}{2c_s^4} - \frac{1}{2}c_{i\gamma}\partial_\gamma c_{i\delta}\partial_\delta\Delta^*\Bigg) \\ + \Delta^*\Bigg) R(\vec{r},t), \end{aligned} \tag{2.24}$$

with $Q_i\alpha\beta = c_{i\alpha\beta} - c_s^2\delta_{\alpha\beta}$. Substituting Eqs. 1 and 2 of Warren (1997), we find

$$\begin{aligned} R(\vec{r},t+1) &\approx R(\vec{r},t) - u_\alpha\partial_\alpha R(\vec{r},t) + \frac{1}{2}u_\alpha u_\beta\partial_\alpha\partial_\beta R(\vec{r},t) \\ &\quad + \frac{1}{2}c_s^2(1-\Delta^*)\nabla^2 R(\vec{r},t) \\ &\approx R(\vec{r}-\vec{u}\Delta t,t) + \frac{1}{2}c_s^2(1-\Delta^*)\nabla^2 R(\vec{r},t), \end{aligned} \tag{2.25}$$

which agrees to Eq. 9 of Warren (1997).

The standard moment propagation method as it was used in conjunction with the lattice Boltzmann method in Lowe & Frenkel (1995) and Kaandorp *et al.* (1996) is,

$$R(\vec{r},t+1) = \sum_i \left[\frac{\left(f_i^+ - \frac{\Delta}{b}\right) R}{\rho}\right]_{\vec{r}-\vec{c}_i,t} + \Delta\frac{R(\vec{r},t)}{\rho(\vec{r},t)}, \tag{2.26}$$

with the whole quantity inside $[\ldots]$ evaluated at $(\vec{r}-\vec{c}_i,t)$. The assumption of uniform flow implies that $f_i^+ = f_i^{\mathrm{eq}}$ and that $f_i(\vec{r}-\vec{c}_i,t) = f(\vec{r},t)$. Substituting the second

order Taylor expansion for $R(\vec{r},t)$ and the equilibrium distribution f_i^{eq} we can write

$$R(\vec{r},t+1) \approx \frac{R(\vec{r},t)}{\rho}\left(\left(\sum_i\left(t_i\rho\left(1+\frac{c_{i\alpha}u_\alpha}{c_s^2}+\frac{u_\alpha u_\beta Q_{i\alpha\beta}}{2c_s^4}\right)-\Delta/b\right)\left(1-c_{i\gamma}\partial_\gamma+\frac{1}{2}c_{i\gamma}\partial_\gamma c_{i\delta}\partial_\delta\right)\right)+\Delta\right) \tag{2.27}$$

Working out the parentheses, and substituting the following equalities

$$\begin{aligned}
&\sum_i t_i c_{i\alpha} = 0, \sum_i t_i c_{i\alpha}c_{i\beta}c_{i\gamma} = 0, \sum_i t_i c_{i\alpha}c_{i\beta} = c_s^2\delta_{\alpha\beta},\\
&\sum_i t_i c_{i\alpha}c_{i\beta}c_{i\gamma}c_{i\delta} = c_s^4(\delta_{\alpha\beta}\delta_{\gamma\delta}+\delta_{\alpha\gamma}\delta_{\beta\delta}+\delta_{\alpha\delta}\delta_{\beta\gamma}),\\
&\sum_i t_i Q_{i\alpha\beta} = \sum_i t_i Q_{i\alpha\beta}c_{i\gamma} = 0, \sum_i t_u Q_{i\alpha\beta}c_{i\gamma}c_{i\delta} = c_s^4(\delta_{\alpha\gamma}\delta\beta\delta+\delta_{\alpha\delta}\delta_{\beta\gamma}),\\
&\sum_i t_i = 1, \sum_i \frac{1}{b} = 1,
\end{aligned} \tag{2.28}$$

we find

$$\begin{aligned}
R(\vec{r},t+1) \approx R(\vec{r},t) - u_\alpha\partial_\alpha R(\vec{r},t) + \frac{1}{2}u_\alpha u_\beta\partial_\alpha\partial_\beta R(\vec{r},t)\\
+\frac{1}{2}\left(c_s^2-\frac{1}{bd}\sum_i c_{i\alpha}c_{i\beta}\frac{\Delta}{\rho}\right)\nabla^2 R(\vec{r},t),
\end{aligned} \tag{2.29}$$

with d the dimension of the lattice and b the amount of lattice vectors. The diffusion coefficient D_m becomes (note that for all indices $\alpha \neq \beta$, $\sum_i c_{i\alpha}c_{i\beta} = 0$)

$$D_m = \frac{1}{2}\left(c_s^2-\frac{1}{bd}\sum_i \vec{c}_i.\vec{c}_i\frac{\Delta}{\rho}\right), \tag{2.30}$$

which is equal to Eq. 2.11.

CHAPTER

THREE

Particle Aggregation in Laminar Flows[1]

The study of environmental effects on abiotic growth processes may be helpful in interpreting the causes of morphologic plasticity in stony corals. In the diffusion-limited aggregation (DLA) model, pioneered by Witten Jr. & Sander (1981), diffusing particles irreversibly attach to a growing cluster which is initiated with a single solid seed. This process generates clusters with a branched morphology. Advection-diffusion limited aggregation (ADLA) is a straightforward extension to this model, where the transport of the aggregating particles not only depends on diffusion, but also on a fluid flow. Authors studying two-dimensional and three-dimensional ADLA in laminar flows, reported clusters preferentially growing against the flow direction. The internal structure of the clusters was mostly reported to remain unaffected, except by Kaandorp *et al.* (1996) who found compact clusters "as flow becomes more important". In the present chapter we present three-dimensional simulations of ADLA. We did not find significant effects of low Reynolds-number advection on the cluster structure. We discuss the causes of the contradicting results by Kaandorp *et al.* (1996).

3.1 Introduction

Before considering more detailed models of coral morphogenesis in Chapter 4 and Chapter 5, we study two physical metaphors of coral growth: diffusion-limited aggregation (DLA) and Laplacian growth. The study of abiotic growth processes may help us to get a detailed understanding of the mechanisms underlying resource flux driven branching, which is relevant for understanding coral growth. Moreover, the study of

[1]This chapter is based on: R. M. H. Merks, A. G. Hoekstra, J. A. Kaandorp & P. M. A. Sloot (2003). Diffusion Limited Growth in Laminar Flows, Submitted to *International Journal of Modern Physics C*.

environmental affects on abiotic growth may be helpful in interpreting the causes of morphologic plasticity in stony corals. In Section 1.3 we distinguished *adaptive* and *mechanistic* explanations of morphologic plasticity. Adaptive explanations emphasise the functional advantage of morphological changes (see e.g. Sebens *et al.*, 1997; Bruno & Edmunds, 1998), and assume that morphological plasticity is an *active, genetically fixed* response to environmental change. By contrast, mechanistic explanations consider plasticity a *passive* environmental effect on the growth process. Such mechanistic explanations focus mostly on resource transport. If such passive mechanisms of plasticity play a role in coral growth, they should also be found in abiotic growth processes in which passive resource transport is important.

The first step in studying such passive effects of water flow on coral growth is to determine the typical Reynolds-numbers and Péclet-numbers that characterise the transport of growth resources to the coral colony. Estimates of typical flow velocities in a coral reef range from about $\bar{u} \approx 10^{-2} ms^{-1}$ to $\bar{u} \approx 10^{-1} ms^{-1}$ (Lesser *et al.*, 1994; Kuffner, 2002), where the former estimate is considered "low" and the latter "high" (Kuffner, 2002). Estimating the typical thickness of a coral branch to $L \approx 10^{-2} m$, and taking the kinematic viscosity of water, $\nu \approx 10^{-6} m^2 s^{-1}$ we find Reynolds-numbers ($Re = \bar{u}L/\nu$) of $Re \approx 100$ (low flow velocity) to $Re \approx 1000$ (high flow velocity). A similar estimate can be made for the Péclet-number ($Pé = \bar{u}L/D$), which expresses the relative importance of advective and diffusive transport. Estimating relevant diffusion coefficients is difficult, since this depends largely on the growth resource which under consideration. A discussion of the diffusion coefficients relevant for coral growth will be given in Section 4.4.3. Based on this discussion, for actively moving food particles a typical Péclet-number would range from $Pé \approx 10$ ("low flow") to $Pé \approx 100$ ("high flow"). Considering ionic resources, as needed for calcification, the Péclet-numbers would be much higher, in the order of $Pé \approx 10^5$ to $Pé \approx 10^6$.

In this chapter we concentrate on the effects of fluid flow on the formation of solid particle aggregates by means of diffusion-limited aggregation (DLA). Since the pioneering paper by Witten Jr. & Sander (1981), DLA has been of continuous and extensive interest in studies using experimental (Trigueros *et al.*, 1991; Chambliss & Wilson, 1991), theoretical (Muthukumar, 1983; Halsey, 2000; Ball & Somfai, 2002), and computational (Witten Jr. & Sander, 1981; Castro *et al.*, 2000) approaches. In computational models of DLA an initial solid seed is placed in the middle of a domain. A particle is then released from a random position at some distance from the seed. The particle carries out a random walk until it hits the seed after which it is added to the developing cluster. This procedure, when iterated, produces aggregates "distinguished by their wispy appearance" (Witten Jr. & Sander, 1981). More recently, a number of authors (Toussaint *et al.*, 1992; Brémond & Jeulin, 1995; Warren *et al.*, 1995; Kaandorp *et al.*, 1996; Kovács & Bárdos, 1997) have studied this process under the influence of flow, where Warren *et al.* (1995) studied "growth by interception" with a growth probability determined by the fluid velocity. Such *advection-diffusion limited aggregation* (ADLA) has been studied in the context of coral growth modelling (Kaandorp *et al.*, 1996; Kaandorp, 2001), but also for understanding abiotic growth processes such as the growth of sedimenting clusters and the crystallisation of (falling) snowflakes (see Warren *et al.*, 1995 and references therein). In models of advection-

diffusion limited aggregation the aggregating particles are transported both by diffusion and by a fluid flow which interacts with the growing aggregate. Such systems should be distinguished from models of ballistic deposition (Vold, 1959; Meakin *et al.*, 1986; Nagatani & Sagues, 1991; Nagatani, 1991), where particles move straightly or according to a biased random walk and whose governing direction is unaffected by the growing aggregate.

These simulation studies of advection-diffusion limited aggregation all operated in the low Reynolds-number regime, with Reynolds-numbers $Re << 1$ where $L = 1$ lattice unit. Thus these studies seem of limited relevance for the study of morphologic plasticity of stony corals, and indeed in most of these studies the only effect of fluid flow was a preferential growth against the flow. The fractal structure of the clusters as expressed by the fractal dimension was hardly affected, because of the "screening of streamlines from the interior of (...) the clusters" (Warren *et al.*, 1995). These results contradict an experimental study on electrodeposition (López-Tomàs *et al.*, 1993) and a simulation study by Kaandorp *et al.* (1996), where it was found that under the influence of a governing flow the aggregates became more compact and the "wispy appearance" was suppressed. This observation parallels observations in stony corals, where specimens growing in fast flowing water were found to be more densely branched than specimens in slow flows (see discussion in Section 1.3). The fact that Kaandorp *et al.* (1996) found effects in the low Reynolds-number, low Péclet-number regime, may suggest a trend which also holds in higher, more realistic parameter regions. To further understand this trend, and to investigate the differences between the work of Kaandorp *et al.* (1996) and the other models of advection-diffusion limited aggregation, in this chapter we reinvestigate the effect of low Reynolds-number flows ($Re \approx 0.06$–0.3) on advection-diffusion limited aggregation. Furthermore, we aim to understand why Kaandorp *et al.* (1996) found an effect of flow on the fractal structure of the growing aggregates, whereas other authors did not.

3.2 Model and simulation methods

The model that we present here is based on the aggregation model by Kaandorp *et al.* (1996), which was originally developed to study the effect of flow on coral morphology. This model is a Meakin (1986) growth model with added advection. In these models, all possible biased random paths of the particles are ensemble averaged and approximated by a continuous advection-diffusion process where the growing cluster is a particle sink. The aggregation probabilities are then given by the fluxes into the cluster.

The simulation set-up is shown schematically in Fig. 3.1. We started with an initial solid seed on a solid ground plane. A flow field was calculated using the lattice Boltzmann BGK method (Qian *et al.*, 1992; see also Chapter 2). This method is well-suited for problems of complex geometry (Chen & Doolen, 1998; Succi, 2001) such as DLA clusters. It is resolved on a structured lattice, where we use eighteen velocities and a zero velocity (D_3Q_{19}). A no-slip ($u = 0$) boundary condition was applied at the aggregate and at the solid ground plane. We also applied a no-slip boundary condition

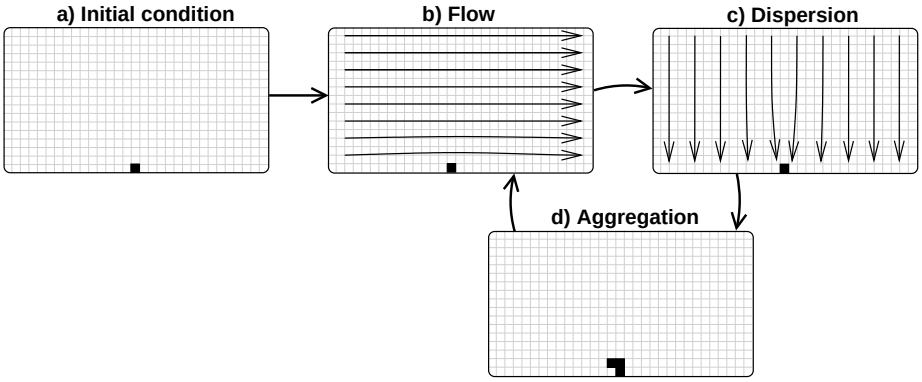

Fig. 3.1: Simulation set up. a) Initial condition, b) calculation of flow field, c) advection-diffusion of the growth resource, where the top plane is a source of resource and the ground plane and the solid particles are resource sinks and d) aggregation, the addition of particles. The sequence b), c) and d) is called a "growth cycle". All calculations were carried out in three dimensions.

at the top plane, following Kovács & Bárdos (1997). Hence the clusters were growing in a channel flow. The left, right, front and rear boundaries were periodic.

When the flow field had sufficiently approached stability (full convergence model, FC) or after a fixed number of time steps (partial convergence model, PC), the dispersion of particles through the fluid was simulated by numerically solving the advection-diffusion equation. The advection-diffusion equation was solved using the moment propagation method (Eq. 2.6; Lowe & Frenkel, 1995; Warren, 1997; Merks *et al.*, 2002; see Chapter 2 for explanation). The ratio between advective and diffusive transport is expressed by the Péclet number $Pé = \bar{u}L/D$, where $\bar{u}$ is the mean velocity and L is a characteristic length. Throughout this paper we exclusively use the *lattice* Péclet number $\overline{Pé}_{\mathrm{lat}}$, in which $L = 1$ l.u., the distance between two nodes of the lattice.

Following Kaandorp *et al.* (1996), the top plane was a source of growth resource and both the ground plane and the cluster were resource sinks. We have followed the Meakin (1986) convention by putting the resource sink *at* the developing cluster. For the advection-diffusion calculations, the front and rear boundaries were periodic, whereas at the left and right boundaries (i.e. in the flow direction) a no-flux (reflecting) boundary was applied, thus preventing effects of the periodic images of the growth forms.

In the Full Convergence model, the moment propagation equation was iterated until the influx of resources at the top plane balanced to certain extent the outflux of resource at the cluster and the ground plane, i.e. when the change of the total resource mass in the system fell below a threshold,

$$\left| \frac{\Delta(\sum_x R)}{\Delta t \ \sum_x R} \right| < \theta_{\mathrm{AD}}, \tag{3.1}$$

Number of possible positions (n)	Number of particles added
$n < 100$	1
$100 \leq n \leq 1000$	10
$1000 < n \leq 10000$	50
$n > 10000$	100

Table 3.1: Amount of new particles added to the cluster per growth step in the multi-particle model depending on the amount of available new positions (Kaandorp, *pers. comm.*)

where typically $\theta_{\mathrm{AD}} = 10^{-6}$. In the Partial Convergence model, the moment propagation equation was iterated for a fixed number of time steps; in this paper we typically applied 50 iterations per growth cycle, thus following Kaandorp *et al.* (1996). After a resource dispersion field was obtained, solid nodes were added to the cluster (Fig. 3.1d). Here we study two variants of this aggregation. In the *single particle model* during each growth cycle a single solid particle is added to the cluster. This follows the Witten Jr. & Sander (1981) model and the original Meakin (1986) model. In the *multiple particle model*, however, the number of particles added increased during the simulation, depending on the size of the cluster (Table 3.1). In order to compare our results to the results obtained previously by Kaandorp *et al.* (1996) we take diffusion coefficients as used in their simulations.

In order to decide which fluid sites should be added to the cluster, we first determined the set of "growth candidates"; this is the set of nearest (face-connected) neighbours of the cluster. In each of these candidates, the growth resource concentration $R(x_i)$ indicates the probability that a particle is present and adheres to the cluster. To enforce the addition of a fixed number of particles, these probabilities were normalised to sum up to 1. Hence the probability $P(x_i)$ that a new particle is added to the cluster at a face-connected neighbour was,

$$P_{\mathrm{aggr}}(x_k) = R(x_k) / \sum_j R(x_j), \tag{3.2}$$

where $\sum_j$ sums over all nearest neighbours.

The ADLA clusters were characterised using the fractal dimension, which we measured using the radius of gyration R_g (see Meakin, 1983a), where

$$R_g = \frac{1}{n} \sum_i |(\frac{1}{n} \sum_i \vec{x}_i) - \vec{x}_i| \tag{3.3}$$

with $\vec{x}_i$ the coordinates of the particles in the cluster. The fractal dimension can be obtained by keeping track of the radius of gyration during the growth of the cluster. For large DLA-clusters, the radius of gyration gets a power-law dependence of the number of particles N, $R_g \sim N^{\beta}$, where the fractal dimension $F_r = \frac{1}{\beta}$. The clusters were further characterised using the *compactness* C, which we define as the fraction of

solid material inside the convex hull[2] of the cluster,

$$C \equiv \frac{V_{\mathrm{object}}}{V_{\mathrm{hull}}}, \tag{3.4}$$

where V_{object} is the volume of the object, and V_{hull} is the volume of the convex hull, which was determined using the quickhull algorithm (Barber *et al.*, 1996)[3]. Hypothesis testing was carried out using one-way analyses of variance (ANOVA[4]). The simulations were carried out on clusters of workstations, the DAS-2 (Bal *et al.*, 2000) and a Beowulf cluster (Sterling *et al.*, 1995) on which a typical simulation presented here took around 15 hours (partial convergence) to 50 hours (full convergence). Further details regarding the performance of our simulation code on these machines will be presented in Chapter 6.

3.3 Results

In Fig. 3.2 we show two typical clusters developed with the Full Convergence, Single Particle model. In Fig. 3.2a. the resource was exclusively transported by means of diffusion, whereas in Fig. 3.2b. transport was by diffusion and by advection, where the mean flow velocity was 0.05 l.u. The diffusion coefficient was set to 0.166, giving lattice Péclet numbers of 0 and 0.30, respectively. Since the internal structure of these three-dimensional pictures is difficult to interpret, we only show cross-sections in the remainder of the paper. In Fig. 3.3 we present an overview of the results of the advection-diffusion limited aggregation models. In these figures the grey scale indicates the particle concentration, and the flow direction is always along the x-axis. In Fig. 3.3a. and 3.3b. we show the clusters of Fig 3.2 in cross-section. The applied flow did not affect the compactness nor the fractal dimension (see Table 3.2). We also tried to increase the Péclet-number further, by using a smaller diffusion constant. However, this led to extremely high computation times (150 growth cycles with $D = 0.083$ took four days of computer time on 32 processors of the DAS-2), which made the model computationally intractable.

In order to keep the simulation times feasible, we compared the results of the full convergence model to a model where a fixed amount of moment propagation iterations was applied per aggregation step. In Figs. 3.3c. and 3.3d. we show two results of this model, in which we applied 50 moment propagation iterations and 10 lattice Boltzmann iterations per aggregation step. In both simulations, the mean flow velocity was set to $\bar{u} = 0.01$. For these parameter settings, the results of the partial convergence model did not differ from the full convergence model: neither the compactness nor the fractal dimension differed significantly. When we increased the Péclet-number, by decreasing the diffusion coefficient to 0.001, we found a "wake" behind the cluster, and the cluster tended to grow into the direction of the flow. The clusters' internal structure was how-

[2] Think of the convex hull as the surface given by the tightest gift wrapping around the object.

[3] see `http://www.geom.umn.edu/software/qhull/`

[4] See `http://mathworld.wolfram.com/ANOVA.html`

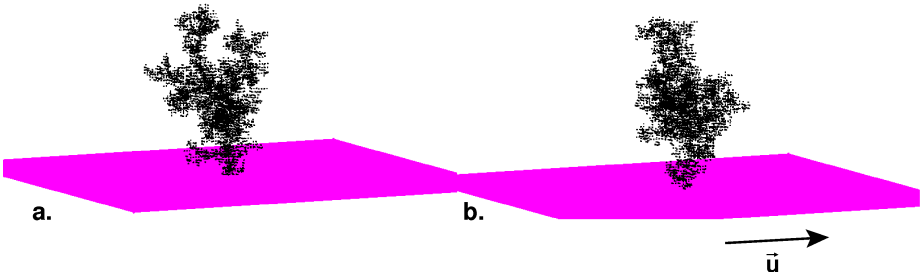

Fig. 3.2: Typical three-dimensional clusters developed with the fully converged advection-diffusion limited aggregation model. a) Diffusion limited growth. $\bar{u} = 0$, $D = 0.166$. b) Advection-diffusion limited aggregation $\bar{u} = 0.05$ (from left to right), $D = 0.166$; both clusters contain 4500 particles.

ever hardly affected; the compactness was found to be slightly, though significantly different (Table 3.2), but the fractal dimension showed no significant difference.

In Fig. 3.3e. and Fig. 3.3f. we present results of the multiparticle model. Both simulations were carried out under the influence of a flow of velocity $\bar{u} = 0.01$. When we used a large diffusion coefficient ($D = 0.167$) we found open, DLA-like clusters (see Fig. 3.3e). When the diffusion coefficient was decreased (Fig. 3.3f), the clusters became more dense (Table 3.2). However, when we applied 250 rather than 50 moment propagation iterations per growth cycle, less dense clusters developed (with $C = 0.17 \pm 0.0$), indicating that the advection-diffusion diffusion fields had not equilibrated after 50 iterations (data not shown). This suggests that the amount of diffusion (Dt), rather than the Péclet-number, is an important factor in determining the compactness of the cluster.

The clusters that developed in the *multiple particle model* did not become as dense as the clusters reported previously (Kaandorp *et al.*, 1996; Kaandorp, 2001). In fact, Kaandorp *et al.* used an alternative model for the aggregation probability (Kaandorp, *pers. comm.*). In this model, the aggregation probability is the normalised probability that a particle collides with a solid-fluid interface after propagation,

$$P_{\text{aggr}}(x_k) = \frac{R(x_k,t)\sum_i f_i(x_k,t)\delta(x_k+\vec{c}_i,t)}{\sum_j R(x_j,t)\sum_i f_i(x_j,t)\delta(x_j+\vec{c}_i,t)}, \tag{3.5}$$

where $\sum_i$ sums over the 19 velocities of the lattice and where $\delta(x_i,t) = 1$ when x_i is a solid node and $\delta(x_i,t) = 0$ when it is fluid. Note that this aggregation function favours the addition of nodes enclosed by several solid nodes.

The clusters shown in Fig. 3.4 were developed using this growth function. With a high diffusion coefficient of $D = 0.17$, these clusters became a bit more dense (Fig. 3.4a; Table 3.2) than the clusters that were developed with the standard growth function (Fig. 3.3e). The clusters were significantly more dense than with the standard growth function when a smaller diffusion coefficient was used (Fig. 3.4b). Note that the clusters are somewhat more dense away from the flow. This effect becomes stronger if

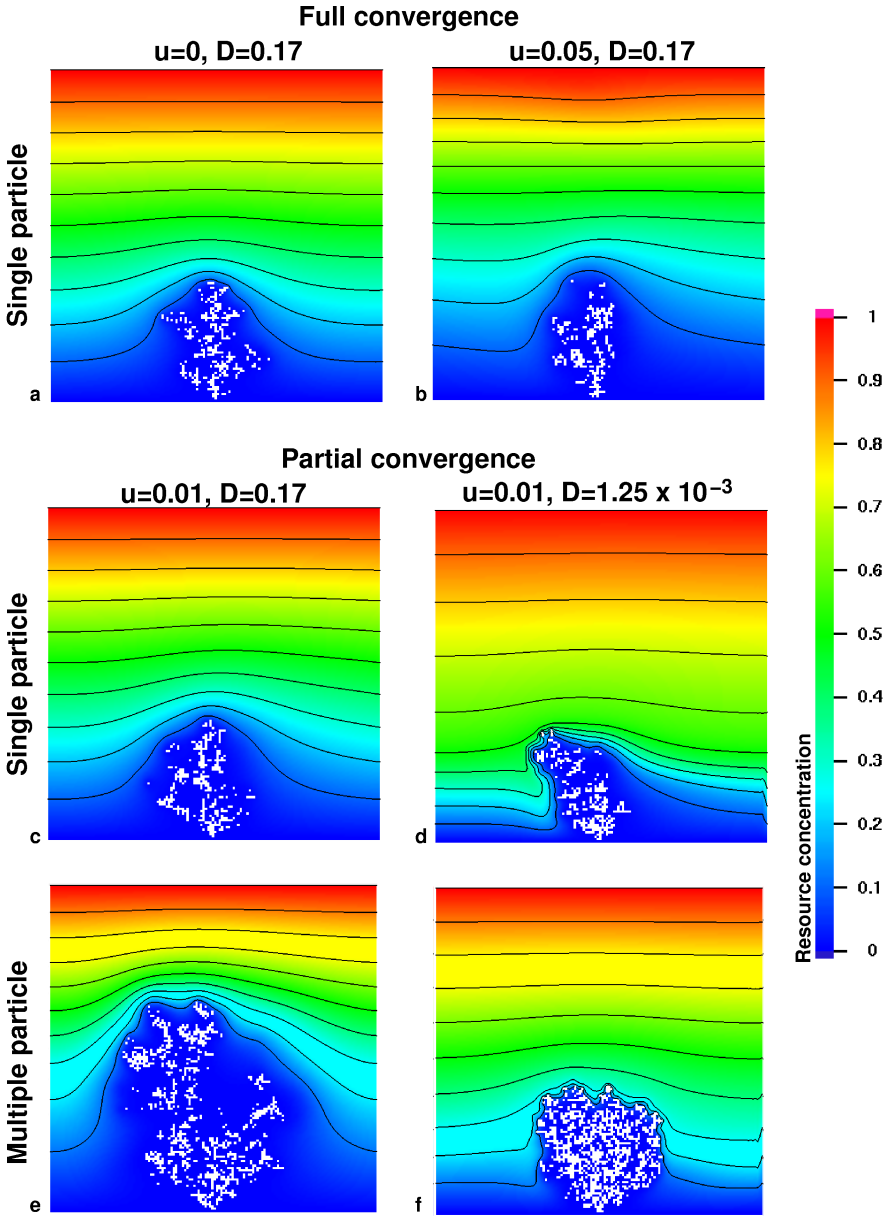

Fig. 3.3: Cross-sections through 3D resource fields and clusters developed with the advection-diffusion limited aggregation model. The single particle clusters were grown for 4700 (top) and 6150 (middle) growth cycles. The multiple particle clusters were grown for 450 growth cycles. Flows (when applicable) are directed from left to right

Model	Figure	$\bar{u}$	D	$\overline{Pé}_{\mathrm{lat}}$	Compactness	F_r
SADLA, FC	3.2a, 3.3a	0.0	0.167	0.0	0.12 ± 0.01	2.62 ± 0.36
SADLA, FC	3.2b, 3.3b	0.05	0.167	0.3	0.12 ± 0.01	2.60 ± 0.21
SADLA, PC	3.3c	0.01	0.167	0.06	0.12 ± 0.01	2.61 ± 0.07
SADLA, PC	3.3d	0.01	0.00125	8	0.14 ± 0.01	2.67 ± 0.34
MADLA	3.3e	0.01	0.167	0.06	0.10 ± 0.00	2.59 ± 0.11
MADLA	3.3f	0.01	0.00125	8	0.26 ± 0.00	3.03 ± 0.07
MADLA II	3.4a	0.01	0.167	0.06	0.18 ± 0.00	2.58 ± 0.11
MADLA II	3.4b	0.01	0.00125	8	0.38 ± 0.01	2.99 ± 0.09

Table 3.2: Compactness and fractal dimension. Abbreviations used are, SADLA: Single particle advection-diffusion limited aggregation, FC: full convergence, PC: partial convergence, MADLA: Multiple particle advection-diffusion limited aggregation, MADLA II: MADLA with growth function as in Eq. 3.5, D: diffusion coefficient, $\overline{Pé}_{\mathrm{lat}}$: lattice Péclet-number, F_r: fractal dimension. Mean and standard deviation of compactness and fractal dimension calculated over five simulations.

the ground plane is removed from the simulation, resulting in a higher velocity around the cluster (data not shown).

3.4 Discussion

In this chapter we studied three-dimensional advection-diffusion limited aggregation (ADLA) under the influence of a laminar flow. In this straightforward extension of the diffusion-limited aggregation (DLA) model (Witten Jr. & Sander, 1981), particles are transported by a diffusive process which is biased by a governing flow. We studied two variants of this model, the single particle model and the multiple particle model. In the single particle model one particle is added in a growth cycle. In the multiple particle model, during a growth cycle one or several particles are added, depending on the current size of the cluster. Apart from several complications, which we will discuss below, this model could be seen as a hybrid between the diffusion limited aggregation model and models of Laplacian growth, where growth occurs over the full surface of the cluster in parallel.

We studied two variants of the single particle ADLA model. These variants differ in the way the flow and dispersion fields are relaxed. In the first variant, we relax the advection-diffusion field until the change per unit time of the total mass falls below a threshold (Eq. 3.1). Although this full convergence model would be preferred when studying advection-diffusion limited aggregation in a Meakin model, these simulations quickly became computationally intractable when small diffusion coefficients were used. After adding a new particle to the cluster, it often took hundreds to thousands of time steps before the resource field had sufficiently stabilised, in particular for high Péclet-numbers. Note that this indicates a major caveat of our simulation methods, because it shows that the assumption that the flow and resource fields are in equilibrium

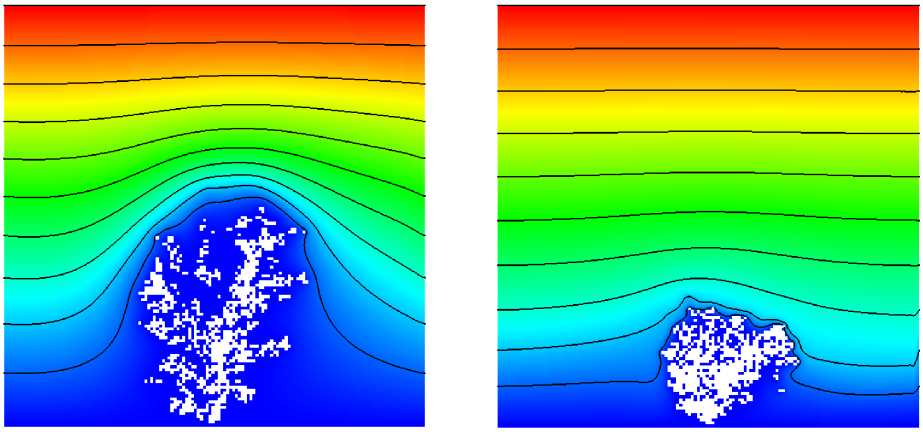

Fig. 3.4: Advection-diffusion limited aggregation model with the alternative aggregation function as used by Kaandorp *et al.* (1996). Flow is directed from left to right, $\bar{u} = 0.01$

cannot always be met.

Being aware of this caveat, we also studied an alternative model in which the tracer field was relaxed for a fixed number of time steps (50 per growth cycle). In both cases, the cluster tended to grow slightly into the direction of the governing flow, but the overall structure of the clusters was unaffected by flow, as expressed by the fractal dimension and the compactness. When we used a higher Péclet-number by decreasing the diffusion coefficient (Fig. 3.3d), the cluster became slightly more compact. However, this small effect is most likely unphysical, because we use a fixed advection-diffusion time and because the used Péclet-number is well over the upper-limit above which the moment propagation method no longer produces physical results (Chapter 2; Merks *et al.*, 2002).

To keep the computations tractable, we only studied the partial convergence variant of the multiparticle model, which is more closely related to the model studied previously in our group (Kaandorp *et al.*, 1996). For small Péclet-numbers, the resulting clusters were indistinguishable from the clusters developing with the single particle model, based on the fractal dimension and on the compactness of the clusters. However, when we decreased the diffusion coefficient, keeping the flow velocity constant (as in Kaandorp *et al.*, 1996), the clusters compactified. In the context of accretion models, which are related to models of Laplacian growth, we have observed that growth forms become more compact (Merks *et al.*, 2003; see also Chapter 4) when the time scales of growth and resource transport come closer together. In the ADLA model the growth rate may not be large enough to reach this region of parameter space. However, when the growth rate is increased as in the multiple particle model, this region will be reached when the resource transport is slowed down by decreasing the diffusion coefficient.

In the single particle models the laminar flow did not affect the internal structures of the clusters. In these models, the highest flow velocity is found at a large distance

from the clusters, whereas the flow velocity close to the clusters is very low. Thus in close vicinity of the cluster, resource transport is dominated by diffusion, resulting in the DLA-like growth dynamics. Note that the diffusion coefficients for which compact clusters were obtained were extremely low. In fact, the moment propagation method that we have used in this chapter becomes invalid for such low values (Chapter 2; Merks *et al.*, 2002), since in that case negative values are propagated through the lattice. The probability of this becomes larger as the flow velocity increases. In our simulations the clusters grow along the flow for such incorrect parameter settings, which may be explained by extremely low or even negative tracer concentrations occuring at the front where the flow velocity is highest (data not shown).

With these results, it becomes necessary to reinterpret results of Kaandorp *et al.* (1996, 2001), who claimed that DLA clusters become more compact under the influence of advection. Our results suggest that this compactification occurs only in the multiparticle model, that compactification only results when the net diffusion per growth cycle (Dt) is small and that it occurs preferentially at parameter setting where the moment propagation method no longer produces physical results. Applying the methods described in Chapter 2, it is easily shown that in the simulations by Kaandorp *et al.* (1996), who used a 24-velocity model on a FCHC-lattice, the lattice Péclet-number may never exceed a value of 2. However, the Péclet-numbers up to 3 as reported by Kaandorp *et al.* (1996) were based on the mean velocity. Optimistically estimating $u_{\max} = 2 * \bar{u}$, the lattice Péclet-numbers reported previously should be multiplied by a factor of two to get the maximum Péclet-numbers. Hence, we estimate that negative amounts of tracer may be transported in simulations with reported $P\acute{e}_{\mathrm{lat}} > 1.0$.

A further difference between our results and those presented earlier is the growth direction of the clusters. We found clusters growing mainly towards the source plane, where the clusters may slightly deviate towards the flow, or even away from the flow. Kaandorp *et al.* (1996) reported that the clusters had the strong tendency to grow towards the flow; this tendency became stronger when the diffusion coefficient was decreased. This difference may be attributed to the following. In the simulations presented here, the initial condition was a linear concentration field, the stable solution for a system with a source and a sink plane. (Kaandorp *et al.*, 1996) started with all concentrations set to 1.0. (*pers. comm.*) From the analytic, time dependent solution of the diffusion equation, the time to relax from this initial condition to the stable linear solution is estimated as $t \approx L^2/D$, where L is the height of the simulation box in lattice units. Already for the highest diffusion coefficient that they used ($D = 0.25$), this time exceeds the total advection-diffusion time available in a simulation of 1000 growth cycles with 50 tracer iterations in total. Hence the initial shape of the tracer field affects the growing clusters throughout the time of the simulation. When the diffusion coefficient is decreased, this effect becomes even stronger. In an empty simulation box and with the lowest diffusion coefficient ($D = 0.00125$), at the end of the total simulation time the concentration would follow a sharp gradient from the sink plane to about one fifth of the simulation box; everywhere else the concentration would be close to 1. The absence of a full top-to-bottom resource gradient removes the tendency of the clusters to grow towards the source plane. This may well explain why the growth forms by Kaandorp *et al.* (1996) bent more strongly against the flow when the diffusion

coefficient was decreased.

The moment propagation method that we use in this thesis seems not very well suited for the simulation of ADLA. It is computationally very intensive to reach stable flow and resource fields. Moreover, we can only reach moderate Péclet-numbers (see Chapter 2). Particle tracking methods (Maier *et al.*, 1998) may be better suited for this purpose. Such methods simulate off-lattice random walks biased by the flow field, and would result in a model more closely related to the Witten Jr. & Sander (1981) model. In such a discrete model one would need to track only the single particle to be added to the aggregate, making it computationally much less demanding than the continuous methods which were applied here and in the previous work.

In conclusion, we could not confirm the observation that DLG-clusters compactify as "the flow becomes more important (Pé increases)" (Kaandorp *et al.*, 1996). This finding is in agreement with previous two-dimensional studies of advection-diffusion limited aggregation (Toussaint *et al.*, 1992; Brémond & Jeulin, 1995; Warren *et al.*, 1995; Kovács & Bárdos, 1997). Its explanation may be given by the fact that the flow velocity is very low in close vicinity and inside of the cluster, resulting in diffusion-limited resource transport. We expect, however, that the higher Reynolds-number flows which are found in coral reefs may affect the aggregation process, since they may lead to recirculations inside the cluster. Such effects may have been important as well in the experimental study on flow-driven electrodeposition by López-Tomàs *et al.* (1993). Advective transport was found to affect the compactness in a model of bacterial plaques (Picioreanu *et al.*, 2000), caused by increased nutrient transport towards the plaque. However, in this model some biomass spreading was allowed, which distributed the extra growth over a small area of the plaque. In diffusion-limited aggregation models, attachment is irreversible and immediately affects the flow and diffusion fields which may explain why we did not find a flow effect.

CHAPTER

FOUR

Physical Metaphors of Branching and Compactification[1]

In stony corals it is often observed that specimens collected from a sheltered growth site have more open and more thinly branched growth forms than specimens of the same species from more exposed growth sites, where stronger water currents are found. This observation was explained using a computational model, in which the growth velocity depended locally on the absorption of a resource dispersed by advection and diffusion (Kaandorp & Sloot, 2001). In that model, more compact and spherical growth forms were found when advective transport became more important relative to diffusive transport. Two unsatisfactory items have remained however, which we address in the present chapter. First, an explicit curvature rule was responsible for branching. We show that this rule is not needed: the model exhibits spontaneous branching, provided that the resource field is computed with enough precision. Second, previously no explanation was given for the effects of advective transport observed in the model. In this chapter we explain the observations by the conditions under which spontaneous branching occurs in our model. Our results suggest that the computational evidence that hydrodynamics influences the compactness of corals in *laminar* flows may not be conclusive.

4.1 Introduction

One of the main questions in the study of the morphogenesis of branching corals is the branching mechanism. The branching pattern of many stony corals is thought to be tightly genetically regulated, since branches in many corals are added according to typical, species specific architectural rules (Dauget, 1991). In *Stylophora pistillata*, for

[1] This chapter is based on: Roeland M.H. Merks, Alfons G. Hoekstra, Jaap A. Kaandorp and Peter M.A. Sloot (2003). Models of coral growth: Spontaneous branching, compactification and the Laplacian growth assumption, Journal of Theoretical Biology, *in press*.

example, such architectural rules generate a nearly spherical colony shape, that regenerates when damaged (Loya, 1976; Rinkevich, 2001; Rinkevich, 2002). This regulation of the growth form is sometimes thought to be mediated by chemical signals excreted into the water, the *isomones* (Rinkevich & Loya, 1985). Branching patterns also often arise in abiotic growth processes, such as viscous fingering (Bensimon *et al.*, 1986; Arnéodo *et al.*, 1989; Lajeunesse & Couder, 2000), electric discharge (see e.g. Pasko *et al.*, 2002; Arrayás *et al.*, 2002 and references therein) and crystallisation (see e.g. Plapp & Karma, 2000a; Plapp & Karma, 2000b; Al-Rawahi & Tryggvason, 2002). The development of such patterns is explained with models of diffusion-limited aggregation (DLA) (Witten Jr. & Sander, 1981) and Laplacian growth (see for example Bensimon *et al.*, 1986; Mineev-Weinstein & Dawson, 1994; Magdaleno & Casademunt, 1998; Arrayás *et al.*, 2002 and references therein). In such models, the growth of the pattern depends locally on the value of an external field that may either describe the concentration of aggregating particles, as in the case of DLA, or a pressure or electric field, as in the case of viscous fingering or electric discharge. The branching patterns that arise from such abiotic growth processes are often similar in appearance to the patterns that arise in biotic growth processes, such as coral growth. This similarity suggests the possibility that in these biotic growth processes a comparable Laplacian growth mechanism may be at work.

Abiotic growth models for coral growth may help in understanding for which aspects of coral morphogenesis abiotic processes may provide *sufficient* explanation (this does *not* imply that these processes provide *all* the explanation), and for which aspects genetic regulation is necessarily responsible. In these models the basic assumption is that the growth rate directly depends on the local availability of organic or inorganic resources. Evidence for this so called *resource dependent growth* is indirect. The availability of dissolved inorganic carbon has been shown to limit the rate of photosynthesis in *Pocillopora damicornis* (Lesser *et al.*, 1994), which is a limiting factor for calcification (Barnes & Chalker, 1990; Gattuso *et al.*, 1999). The calcification rate of a coral community was found to depend linearly on the saturation state of calcium carbonate (Langdon *et al.*, 2000). Organic nutrients, such as zooplankton and fine particulate matter are crucial for coral growth (see Sebens *et al.* (1997), Anthony (1999) and references therein).

Two models of resource dependent growth have been proposed by Kaandorp *et al.* In their *aggregation* model (Kaandorp *et al.*, 1996; Kaandorp, 2001; see also Chapter 3) coral growth was modelled as an advection-diffusion limited Meakin growth process (Meakin, 1986), which is closely related to diffusion-limited aggregation (Witten Jr. & Sander, 1981). A model that is more similar to Laplacian growth is the hydrodynamically influenced radiate accretive growth model (HIRAG model) (Kaandorp & Sloot, 2001; Kaandorp, 2001), in which the growth of the simulated coral proceeds by the iterative accretion of growth layers whose thickness is dependent on the local flux over the coral surface of a resource transported by advection and diffusion. Using that model, the observation that corals growing at exposed growth sites have more compact growth forms than corals growing at sheltered growth sites (see for example Kaandorp, 1999) was assessed. When resource transport was primarily driven by diffusion, thinly branched growth forms developed in the model. As the diffusion coefficient was low-

ered and advective transport became relatively more important, more compact growth forms developed in the HIRAG model.

In this chapter we address two previously unresolved issues regarding the HIRAG model. Firstly, the splitting of branches was previously driven by a heuristic curvature rule, that *enforced* the branches to split as soon as a pre-set minimum curvature was reached. This curvature rule estimated "the amount of contact with the environment [...] by measuring the local radius of curvature [...] on the triangulated surface of the object" (Kaandorp & Sloot, 2001). In the same work it was shown that growth forms developing without the curvature rule did not branch spontaneously. For this reason only the regulation of the overall branching *pattern* by the nutrient field, and not the mechanism of branch *splitting* could be assessed. From the Laplacian growth literature, however, it is known that branch splitting can occur spontaneously under the influence of a branching instability (see for example Mineev-Weinstein & Dawson, 1994; Magdaleno & Casademunt, 1998 and references therein). Since the HIRAG model without the curvature rule is structurally similar to a three-dimensional Laplacian growth model, we expected that such spontaneous branch splitting can also occur in the HIRAG model. In this chapter we investigate whether branch splitting can occur spontaneously in the HIRAG model. The second issue that we address in this chapter is the mechanism behind flow induced compactification. In agreement with observations on real corals (such as Kaandorp, 1999), in the original HIRAG model more compact growth forms developed when advective transport became relatively more important. However, the mechanism behind this phenomenon was not understood. In the present chapter we aim to explain the mechanism which generates this advection induced compactification.

These topics will be dealt with in the remainder of this chapter, which is organised as follows. In Section 4.2 we introduce the hydrodynamically influenced radiate accretive growth (HIRAG) model, of which several aspects have been improved relative to the original model (Kaandorp & Sloot, 2001). In Section 4.3.1 we present the appearance of spontaneous branch splitting in the HIRAG model and discuss under which conditions it appears. Using this observation, we explain in Section 4.3.2 why in the original model more compact growth forms are found as the influence of advective transport becomes more important. Finally, in Section 4.4 we discuss the relevance of these results for understanding the mechanism of branching coral growth.

4.2 Methods

The work presented in this chapter is based on the advection-diffusion limited accretive growth model by Kaandorp *et al.* (Kaandorp, 1995; Kaandorp & Sloot, 2001). In this model, coral growth is modelled as a resource dependent accretive growth process (Kaandorp, 1994a), where the dispersion of resource in the surrounding water is modelled by numerically solving the equations of fluid flow and advection-diffusion. The outer boundary of the coral tissue is represented by a curved surface. The periodic retreat of the tissue from the skeleton, after which a dissepiment is left behind, is modelled by constructing a new outer surface over and parallel to the previous one. The

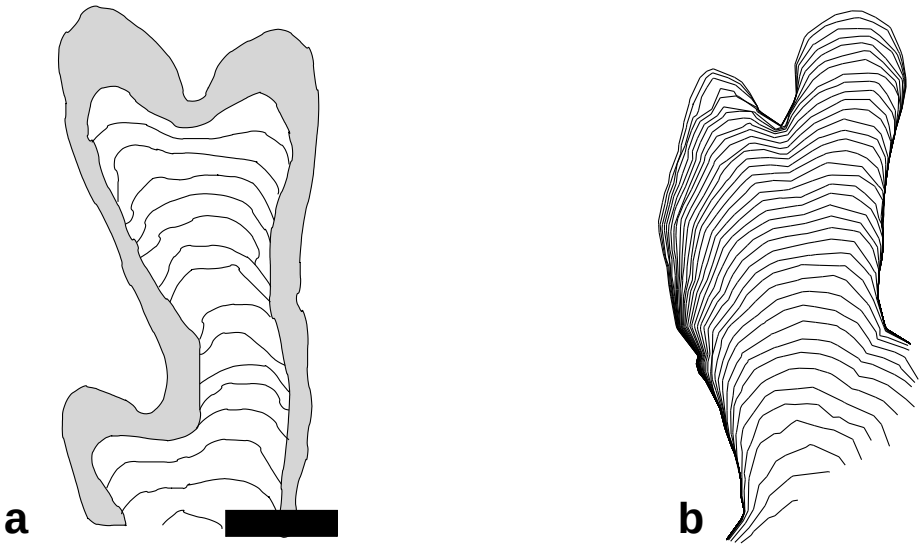

Fig. 4.1: Modelling accretive growth. (a) Redrawn after Fig. 9(d) of Le Tissier *et al.* (1994). The position of dissepiments in a cross section *Porites porites*. The grey area was formerly occupied by tissue. Scale bar = 1cm. (b) Cross section of a branch of a simulated object, the lines indicate the successive surfaces.

local extension of skeleton is determined by a *growth function*, which is dependent on the availability of a resource dispersed by the surrounding simulated fluid. This process generates a growth form whose inner structure resembles the pattern formed by the dissepiments in real corals. This is exemplified in Fig. 4.1, where a cross section of a branch of a simulated coral (Fig. 4.1b.) is compared to the position of the dissepiments in a skeletal slice of *Porites porites* (Fig 4.1a., redrawn after Le Tissier *et al.*, 1994).

More formally, the growth model is described as follows. The coral surface is conceptually modelled as a curved, continuous surface that is approximated by a triangular mesh. The mesh consists of vertices v_i and intervertex links $\vec{\Lambda}_{ij}$ (Fig. 4.2). Each vertex v_i consists of a coordinate x_i, y_i, z_i and of a vector of locally measured growth parameters $\vec{\mu}_i$, for example the flux of growth resource. The advective and diffusive transport of resources is modelled on a cubic lattice using numerical simulations of the Navier-Stokes and advection-diffusion equations. The simulation proceeds as follows (see Fig. 4.3). The initial geometry is a triangulised hemisphere, that contains 81 vertices (Fig. 4.3a). The hemisphere is mapped onto the cubic lattice, for which we use a triangle voxelisation method (Huang *et al.*, 1998), after which the resulting hollow shell is filled using a fast, heuristic three-dimensional seed fill algorithm (Fig. 4.3b). The fluid flow around the voxelised geometry can then be calculated (Fig. 4.3c) by numerically solving the Navier-Stokes equations of (incompressible) fluid flow,

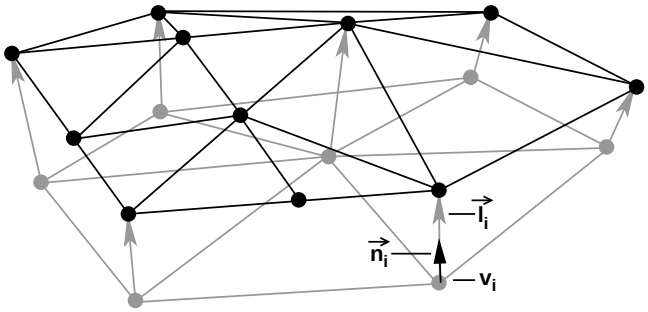

Fig. 4.2: Diagram of an accretive growth step. Vertical extension of the skeleton is simulated by building an element $\vec{l}_i$ (shown as grey arrows) on top of the vertices (grey disks), in the direction of the local surface normal vector $\vec{n}_i$. The length of the element $\vec{l}_i$ depends on the local measurements $\vec{\mu}_i$ and on the growth function g. After the construction of a new layer, it is refined by inserting and removing vertices. The new, refined layer is shown in black.

$$\vec{\nabla}.\vec{u} = 0$$
$$\frac{\partial \vec{u}}{\partial t} = -(\vec{u}.\vec{\nabla})\vec{u} - \vec{\nabla}p + \nu\vec{\nabla}^2\vec{u}, \tag{4.1}$$

where $\vec{u}$ is the velocity, t is the time, p is the pressure and ν is the kinematic viscosity. We do not solve the Navier-Stokes equations directly; instead we use the lattice Boltzmann method (Chen & Doolen, 1998; Succi, 2001), which was briefly introduced in section 2.2.1. The flow is driven by imposing a constant velocity at the top plane. The ground plane and the coral are treated as solids with a no-slip boundary condition, i.e. the fluid velocity is zero, whereas the lateral boundaries are periodic. In this thesis we only consider stable flow fields (i.e. laminar and time-independent). The flow field is iteratively solved until the change per unit time of the mean velocity $\langle|\vec{u}|\rangle$ falls below a convergence threshold,

$$\left|\frac{\Delta\langle|\vec{u}|\rangle}{\Delta t}\right| < \theta_{\mathrm{NS}}, \tag{4.2}$$

with θ_{NS} some small number. As soon as the flow has stabilised according to Eq. 4.2, the transport of the resource R by advection and diffusion and the uptake of resources by the growing coral colony is simulated by numerically solving the advection-diffusion equation (Fig. 4.3d),

$$\frac{\partial R}{\partial t} + \vec{u}.\vec{\nabla}R = D\vec{\nabla}^2R, \tag{4.3}$$

where R is the resource concentration and D is the diffusion coefficient and the velocity $\vec{u}$ is taken from the stabilised flow field. The top plane is kept at a fixed concentration

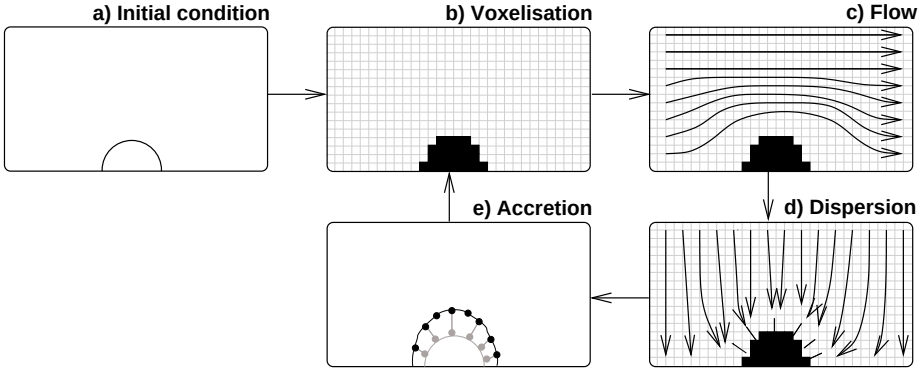

Fig. 4.3: Schematic flowchart of the simulation. The initial sphere, represented by a triangular mesh containing 162 vertices, is voxelised in a cubic lattice (b), after which the fluid flow (c) and resource dispersion (d) are calculated until stability. The resource flux ϕ_i is measured using a "probe" (shown as a black line in d) at each vertex of the coral surface. In the accretion step (e), a new triangular mesh is built on top of the previous mesh, where the growth rate depends on a function g of the resource flux. This mesh is voxelised (b), initiating a new growth cycle.

$R = 1.0$. At the side, front and back planes a periodic boundary condition is applied, whereas the ground plane is kept at a concentration of $R = 0$, hence assuming that resources reaching the sea floor are taken up by competing sessile organisms such as hydrozoans, coralline algae and other corals. These boundary conditions generate concentration gradients over the simulation box. Indeed, such concentration gradients of zooplankton occur at night in coral reefs of the Red Sea, with high concentrations of plankton near the sea surface and much lower concentrations close to the sea floor (R. Horzman and A. Genin, personal communication). As in Chapter 3, the advection-diffusion equation is solved using the moment propagation method (Lowe & Frenkel, 1995; Warren, 1997; Merks *et al.*, 2002), which is introduced and validated in Chapter 2. The advection-diffusion equation is iteratively solved until the change per unit time of the total resource mass falls below a convergence threshold,

$$\left| \frac{\Delta(\sum_x R)}{\Delta t \ \sum_x R} \right| < \theta_{\mathrm{AD}}. \tag{4.4}$$

The relative importance of advective versus diffusive transport processes is expressed by the dimensionless Péclet-number,

$$P\acute{e} = \frac{\langle |\vec{u}| \rangle L}{D}, \tag{4.5}$$

where $P\acute{e}$ is the Péclet number, $\langle |\vec{u}| \rangle$ is the mean flow velocity and L is a characteristic length. In this thesis, we mostly consider the *lattice Péclet number* $\overline{P\acute{e}}_{\mathrm{lat}}$ with the characteristic length set to $L = 1$ lattice unit (l.u.), the distance between two neighbouring

nodes in the computational grid.

As soon as the resource influx at the top plane balances the absorption of resources by the ground plane and the coral, we measure the resource flux ϕ_i at each vertex of the mesh by probing the resource concentration R_i at a distance $l = 1$ l.u. from the vertex v_i along the surface normal (the probes are shown as black lines in Fig. 3.1d). Since $R = 0$ at the coral surface, the resource gradient ∇R at the surface can be approximated as R/l. According to Fick's law, the flux per unit area $\phi_i = D\nabla R = DR/l$.

After the resource fluxes have been measured, we move back to the triangular mesh representation and carry out an *accretive growth* step (Fig. 4.3e). On top of the previous layer, a new layer of skeleton is built, whose local thickness depends on (amongst others) the resource flux ϕ_i. In each accretion step, the vertical extension of the skeleton is simulated by placing an element $\vec{l_i}$ on top of each vertex v_i along the surface normal vector $\vec{n}_i$ at vertex v_i, according to

$$\vec{l_i} = g(\vec{\mu_i})\vec{n}_i, \tag{4.6}$$

where $g(\vec{\mu}_i)$ is a *growth function* which takes the local measurement vector $\vec{\mu}_i$ which returns a (scalar) growth velocity. We do not explicitly model the secondary thickening of the skeleton. We have used several growth functions for the experiments carried out in this thesis. These are described in Chapters 4 and 5. The vertex v_i is moved to the end of the element $\vec{l_i}$, as if the coral surface is pushed upwards by excreting calcium skeleton. In this process, the value of $\vec{\mu}_i$ is retained. As a result of this accretion, the surface locally expands or contracts, depending on the local surface curvature.

In the simulations presented in this thesis, the measurement vector $\vec{\mu}_i$ contains at least the local nutrient flux ϕ_i. As the object grows towards source planes, the resource fluxes ϕ_i increase; hence the growth rate would increase during the simulation. In order to fix the growth rate, the value of the growth function is normalised against its maximum value occurring in the simulation, $g(\vec{\mu_i}) \mapsto g(\vec{\mu_i})/\max(g(\vec{\mu_i}))$. Note that due to this normalisation, the value of the resource fluxes ϕ_i becomes independent of D/l, so we can simply set $\phi_i = R_i/R_{\max}$. We have also carried out simulations without this normalisation; these results do not differ qualitatively from the ones reported in this thesis (data not shown). Using this normalisation of the resource fluxes we fix the thickness of the boundary layer between the growing coral colony and the rest of the sea water, in which the nutrient concentration is assumed constant and constantly mixed. An alternative interpretation is the following.

Above we assumed that coral growth proceeds by the addition of layers. Indeed, in cross sections of coral skeleton annual growth bands caused by seasonal variations in growth rates are observed (Knutson *et al.*, 1972). However, coral polyps excrete skeleton continuously and it is thus more natural to model accretive growth as a time continuous process. Hence the present model can be interpreted either as a discrete time model, in which growth proceeds by discrete time steps, or as a continuous time model, in which the accretion steps simply reflect the discretisation of a continuous process. In the latter interpretation, the displacement of a vertex v_i can be described by

$$\frac{dz_i}{dt} = \phi_i k, \tag{4.7}$$

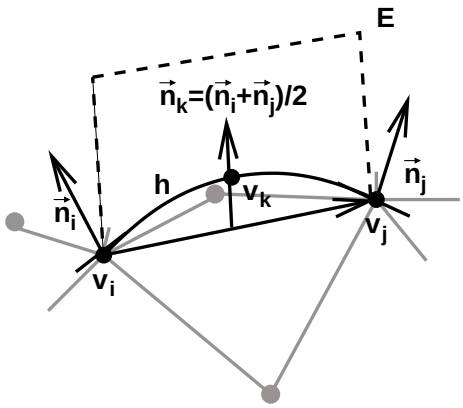

Fig. 4.4: Interpolation of the coral surface for vertex insertion. A third order polynomial h is constructed, perpendicular to the surface normals $\vec{n}_i$ and $\vec{n}_j$ at v_i and v_j. The new vertex v_k is constructed at $v_k = (\frac{1}{2}, h(\frac{1}{2}), 0)$, relative to an orthonormal basis where $v_i = (0,0,0)$, $v_j = (1,0,0)$ and $z = 0$ at plane E. The gray lines indicate a newly constructed part of the coral surface, before vertex insertion.

in which dz_i/dt is the growth velocity at vertex v_i along the local coral surface normal, and k is a constant linking resource flux to the growth velocity. After discretising Eq. 4.7,

$$z_{i,t+1} = z_{i,t} + \Delta t \frac{dz_i}{dt}(t) = z_t + k\Delta t \phi_i(t), \tag{4.8}$$

it becomes clear that a parameter s, coupling the nutrient flux to the local layer thickness, can be expressed in units of the continuous model, $s = k\Delta t$. Using the continuous time interpretation, one does not need our biological explanation to justify the normalisation of nutrient fluxes that we carry out to keep the subsequent layer thicknesses equal. In this normalisation we scale the nutrient fluxes to the maximum food flux $\phi_{\max}(t)$ occurring in the simulation at time step t. The discretised form is

$$z_{i,t+1} = z_{i,t} + \Delta t k \frac{\phi_i(t)}{\phi_{\max}(t)}, \tag{4.9}$$

which can be rewritten as

$$z_{i,t+1} = z_{i,t} + \Delta t^* k \phi_i(t), \tag{4.10}$$

in which $\Delta t^* = \Delta t/\phi_{\max}(t)$. Hence the time step Δt^* is scaled relative to the maximum nutrient flux $\phi_{\max(t)}$ and decreases as the coral colony approaches the nutrient source.

In order to keep a correct and concise triangular mesh describing the coral surface, vertices are inserted and removed. Such mesh refinement is carried out according to the following rules. Two vertices fuse, if their link length $|\vec{\Lambda}_{ij}| < \theta_{\mathrm{FUSE}}$, where

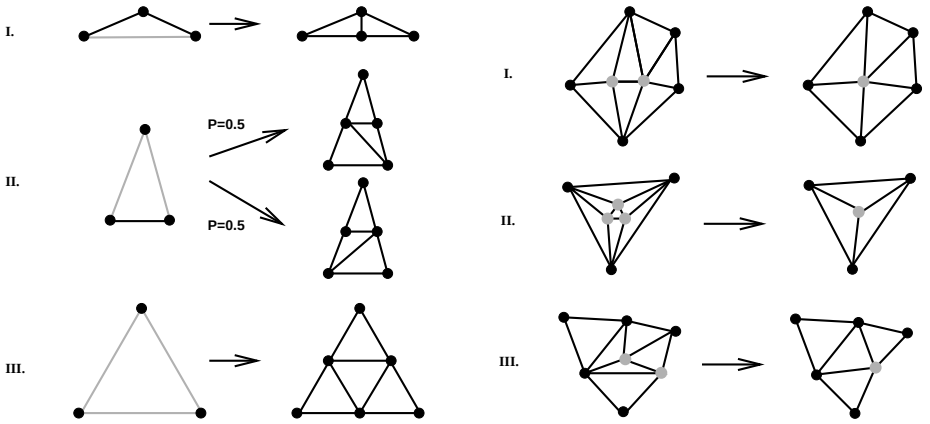

Fig. 4.5: Triangle insertion (left) and deletion (right) rules. Gray links are divided and gray nodes are fused. Insertion rule I: a vertex is inserted in one of the sides of the triangle. Insertion rule II: a vertex is inserted in two sides of the triangle, one of the two possible configuration is chosen at random. Insertion rule III: a vertex is inserted in all sides of the triangle. Deletion rule I: Two vertices are fused; note the expansion of the surrounding triangles. Deletion rule II: all vertices fuse. Deletion rule III: the area of the triangle is smaller than $\theta_{\rm AREA} = .1\langle A_{\rm Tri}\rangle_{\rm init}$, although all the edges of the triangle are larger than the fusion threshold. The triangle is removed by fusing the vertices of the shortest side.

$\theta_{\rm FUSE}$ is the fusion threshold. A new, fused vertex v_k is placed at the middle of the intervertex link, and the value of $\vec{\mu}_k$ is set equal to the mean $\vec{\mu}_k = (\vec{\mu}_i + \vec{\mu}_j)/2$. Then, the vertices v_i and v_j are deleted. A new vertex is inserted between vertex v_i and v_j, if the link length $|\vec{\Lambda}_{ij}| > \theta_{\rm INS}$, where $\theta_{\rm INS}$ is the insertion threshold. The position of the new vertex on the continuous curved surface is determined using a third order interpolation (see Fig. 4.4). The insertion and fusion thresholds are set relative to the initial mean distance between the vertices $\langle|\vec{\Lambda}_{ij}|\rangle_{\rm init}$. Insertion occurs if the distance between two vertices has grown by 50% to $\theta_{\rm INS} = \frac{3}{2}\langle|\vec{\Lambda}_{ij}|\rangle_{\rm init}$. The vertices fuse if their distance becomes less than half of the minimal intervertex distance directly after insertion, $\theta_{\rm FUSE} = \frac{3}{4}\langle|\vec{\Lambda}_{ij}|\rangle_{\rm init}$. As vertices are inserted and deleted from the simulation, new intervertex connections are created and old ones are removed. In this way triangles are inserted and deleted from the mesh, according to the triangle insertion and deletion rules. These rules are summarised in Fig. 4.5.

This method of mesh refinement has a few advantages relative to the method introduced by Kaandorp (1994a). Firstly, unlike the previously used method where subdivided triangles occurred next to undivided triangles, this refinement method generates a standard triangular mesh so that standard algorithms for triangular meshes apply. Secondly, the insertion and deletion algorithms are carried out locally to the triangles, which simplifies them relative to the previous, non-local algorithms. Thirdly, we have solved a problem in the previous mesh refinement algorithm, where always a few elon-

gated triangles remained that were not removed by the deletion rules.

To characterise the morphologies we used the compactness C, which we have defined in Chapter 3 as the fraction of solid material inside the convex hull (Eq. 3.4)[2] of the object. The convex hull was determined using the quickhull algorithm (Barber *et al.*, 1996) and the volumes enclosed by the meshes were calculated according to the method described in Jülicher (1996). Our definition of compactness is dimensionless, making it size invariant and exclusively dependent on the morphology. It would be easily measured in the field, by dividing the displaced volume of the coral by the displaced volume of the same coral, tightly wrapped in plastic.

The objects were visualised using the General Mesh Viewer (GMV), developed at Los Alamos National Laboratory[3]. Colour images, three-dimensional images in VRML format and movies of the developmental sequences can be found on the CD-ROM accompanying this thesis. The simulations were carried out on a Linux Beowulf cluster of 58 AMD Athlon processors running at 700 Mhz, with 256 MByte or 512 MByte internal memory per processor. The accretive growth algorithm was executed on a single processor, while the numerical methods for the Navier-Stokes (Eq. 4.1) and advection-diffusion (Eq. 4.3) equations have been parallelised (Kandhai *et al.*, 1998; see Chapter 6). The simulations of the HIRAG model without curvature rule in Section 4.3.1 were carried out on 16 processors. The flow and advection-diffusion calculations were the main bottleneck. The CPU time needed for the objects shown in Fig. 4.6 was 1:30 hours for $\theta_{AD} = 10^{-4}$ and 9 days for $\theta_{AD} = 10^{-6}$. Note that in these simulations no flow field was calculated. The calculation of each of the objects shown in Fig. 4.8 took 40 days of computer time on 16 processors. A major fraction of this time was used for the flow calculations. The simulations of the model of Section 4.3.2 were considerably less demanding, for which reason we needed only 6 to 12 processors per simulation. These took on the order of 3 up to 12 hours each, depending on the amount of processors used for the flow and advection-diffusion calculations, and on the amount of triangles needed to describe the accretive growth layers (for performance analysis, see Chapter 6).

4.3 Results

4.3.1 Spontaneous branch splitting

In the original HIRAG model (Kaandorp & Sloot, 2001) it was not possible to assess the mechanism of branch splitting in coral growth, since a *curvature rule* enforced the branches to split. Without this heuristic, no branch splitting occurred and so-called "lobed" growth forms developed, that have a folded surface and no second order branches. In this section we show that spontaneous branch splitting *does* occur in the HIRAG model, depending on the convergence threshold θ_{AD} (Eq. 4.4). The original "lobed" growth forms arise if this threshold is relatively high, giving imprecise solutions of the resource field. If the advection-diffusion equation is iterated until a

[2]Think of the convex hull as the space enclosed by the tightest possible gift wrapping around the object.

[3]GMV can be obtained from `http://www-xdiv.lanl.gov/XCM/gmv/`

lower convergence threshold has been reached, branching growth forms are found. We have used the original formulation of the curvature-independent HIRAG model (Kaandorp & Sloot, 2001). Aiming to keep the model as simple as possible, the growth is exclusively driven by the local resource flux as in the linear growth function,

$$g(\vec{\mu}) = s\mu_1 \tag{4.11}$$

where $\mu_1 = \phi_i/\phi_{\max}$. ϕ_i is the resource flux at vertex v_i and $\phi_{\max}$ is the maximum resource flux occurring during the growth cycle. s is the maximum thickness of a growth layer and is set to 1.25 l.u. for the simulations in this section. This setting ensures that in the computational grid the object grows by steps of at most one solid node thick. This growth function is nearly identical to the growth function in which "only the influence of the local availability of simulated nutrient is included" (Kaandorp & Sloot, 2001), except for the omission of a minimal growth velocity threshold tr. The dynamic stopping criteria (Eqs. 4.2 and 4.4) are used and a computational grid of 200^3 is used.

In Fig. 4.6 we have shown four realisations of the HIRAG model with the growth function given by Eq. 4.11 in the diffusion-limited regime (that is, $\langle|\vec{u}|\rangle = 0$) for strict and loose resource convergence thresholds θ_{AD}. For loose convergence thresholds ($\theta_{\mathrm{AD}} = 10^{-4}$) we found very compact, nearly spherical non-branching objects (Fig. 4.6c), agreeing to the results obtained by Kaandorp & Sloot (2001). However, for strict convergences ($\theta_{\mathrm{AD}} = 10^{-6}$) we found branched, open structures (Fig. 4.6a). Thus spontaneous branch splitting *does* occur in the HIRAG model, provided that the resource field has converged well enough. The initial condition also has an effect on the growth form. An initial sphere of radius $r = 8$ l.u. and $r = 16$ l.u. was used for the objects in the left and right column, respectively. The initial radius determines the initial mean link length $|\langle\vec{\Lambda}_{ij}\rangle|_{\mathrm{init}}$, which dictates the spacing of the vertices over the coral surface (see Section 4.2).

In Fig. 4.7 we have studied the convergence of the resource field of the object of Fig. 4.6a by measuring the relative change in the resource field as defined in Eq. 4.4. Slices of the resource field at a convergence of $\theta_{\mathrm{AD}} = 10^{-4}$, 5×10^{-5} and 5×10^{-5} are shown as well. For this figure the convergence was started from a linear resource field. Note that in the growth simulations we start with the last resource field of the previous growth cycle. The field converges progressively more slowly as the solution approaches stability. After about 10^4 iterations we observe a slight speed-up of the resource field convergence. We have not investigated this effect. Only after the strict convergence criterion of $\theta_{AD} = 5 \times 10^{-5}$ is met, a depletion zone with very small resource concentrations has formed between the branches and around the coral. Apparently such detail in the resource field is important for spontaneous branch splitting.

Growth forms with Eq. 4.11 were also developed in a low velocity flow. The velocity at the top plane was set to $\vec{u}_{\max} = 0.04$ l.u., where the flow was directed parallel to the top plane and the flow field was iterated until a convergence of $\theta_{\mathrm{NS}} = 10^{-8}$ was reached. The flow field convergence typically took on the order of 100 to 5000 lattice Boltzmann iterations, depending on the complexity of the growing object.

In Fig. 4.8 two of the resulting objects are shown. In both cases a resource field convergence of $\theta_{\mathrm{AD}} = 10^{-6}$ was used. The objects slightly bent towards the flow, but

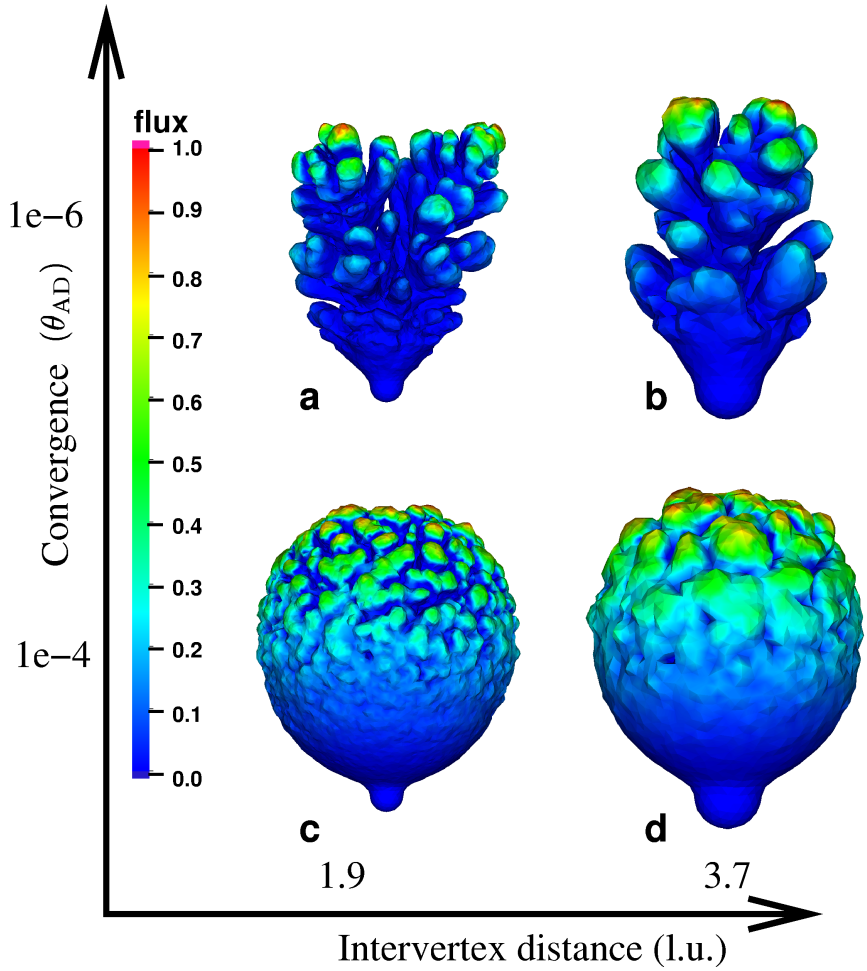

Fig. 4.6: Results of the resource flux driven HIRAG model (growth function 4.11) for increasing resource field convergence (vertical axis) and increasing intervertex distance (horizontal axis); 83 accretive growth cycles; computational grid has size 200^3; No flow ($\langle|\vec{u}|\rangle = 0, Pé = 0$); a) $C = 0.39$ b) $C = 0.55$ c) $C = 0.89$ d) $C = 0.91$.

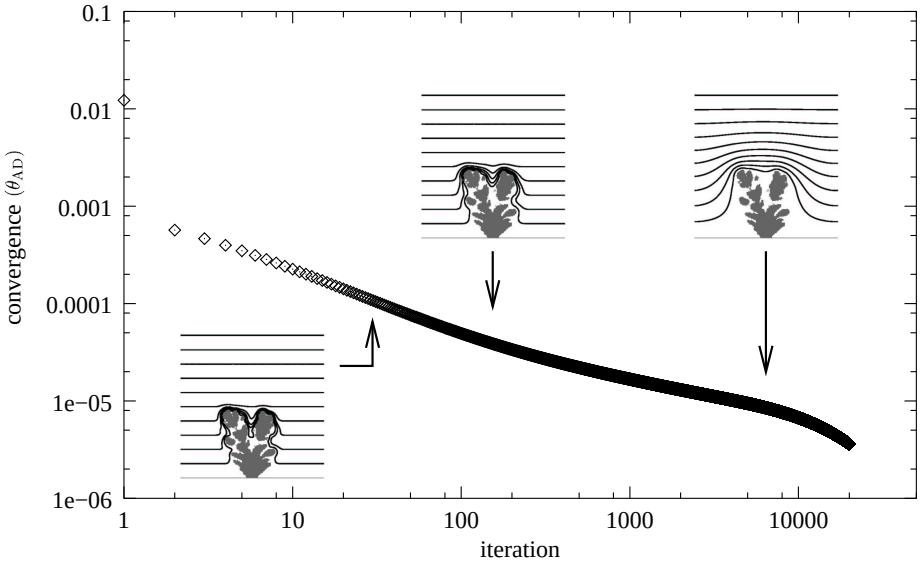

Fig. 4.7: Convergence of the resource field as a function of the iteration number, starting from a linear initial resource field. Insets: resource fields on an xz-section ($y = 100$ l.u.) of the upper left object of Fig. 4.6 for a convergence of $\theta_{\mathrm{AD}} = 10^{-4}$ (left), $\theta_{\mathrm{AD}} = 5 \times 10^{-5}$ (middle) and $\theta_{\mathrm{AD}} = 10^{-5}$. Isolines indicate concentrations of $R = 0.1$ (bottom) to $R = 1.0$ (top) with increments of 0.1

we did *not* find apparent effects of the laminar flow field on the compactness of the growth forms (Table 4.1). When we increased the Péclet-number by using a smaller diffusion coefficient (Fig. 4.8, right), the growth form did not compactify. However, when we used a smaller degree of resource field convergence (i.e. $\theta_{\mathrm{AD}} = 10^{-4}$), the growth form did compactify (data not shown) like in the diffusion-limited case of Fig. 4.6. Thus we did not find an apparent effect of the flow velocity on the compactness of the growth forms, suggesting that in the present model stable laminar fluid flows do not affect the growth form. The compactness remained unchanged even for Péclet-numbers at which flow effects were reported in previous studies (Kaandorp & Sloot, 2001).

4.3.2 Resource field convergence and compactification

In the previous section we showed that spontaneous branch splitting can occur in the HIRAG model, provided that the resource fields are allowed to converge well enough. If not enough advection-diffusion time is allowed (i.e. if the number of iterations is kept too low) zones depleted of nutrients cannot form which precludes the formation of branches. The formation of depletion zones is also important for the formation of a branching *pattern*, where nutrient depletion by one branch suppresses the growth of the neighbouring branches. This phenomenon is well known from the literature of Lapla-

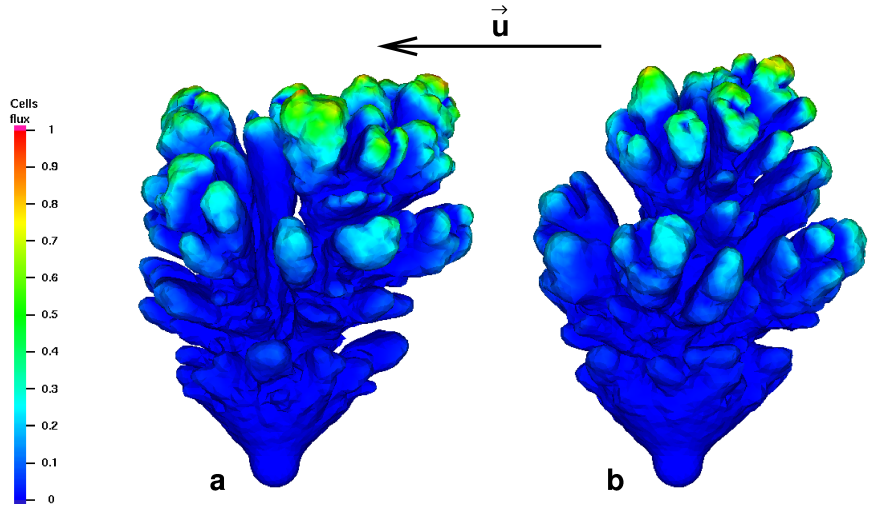

Fig. 4.8: Branching objects grown with the resource flux driven HIRAG model (growth function given by 4.11) in a monodirectional flow directed from right to left. Intervertex distance was 1.9 (compare Figs. 4.6a and b). a) 84 growth cycles, $\vec{u}_{\max} = 0.04$, $D = 0.17$, $\overline{Pé}_{\text{lat}} = 0.24$, $C = 0.39$ b) 84 growth cycles, $\vec{u}_{\max} = 0.04$, $D = .07$, $\overline{Pé}_{\text{lat}} = 0.60$, $C = 0.43$.

cian growth (Mineev-Weinstein & Dawson, 1994; Magdaleno & Casademunt, 1998 and references therein). The formation of such depletion zones may be important in explaining the observation that corals growing in exposed growth sites often have more compact, robust growth forms than corals growing under more sheltered environmental conditions. If no depletion zones would develop, or if they would be disturbed by (unstable, possibly turbulent) water currents, we would expect the branches to approach each other more closely than when clear depletion zones have developed. In this section, we test this hypothesis and study whether the suppression of depletion zones by hydrodynamics can explain the flow induced compactification of the growth forms that was previously observed in the HIRAG model (Kaandorp & Sloot, 2001). In order to correctly compare the results of the present HIRAG simulations to the previous work, we reintroduced the *curvature rule* (Kaandorp & Sloot, 2001) in the growth function,

$$\begin{aligned} g(\vec{\mu}_i) &= s\mu_{i,1}\mu_{i,2} \qquad \forall \mu_{i,1}\mu_{i,2} > \text{tr} \\ &= 0 \qquad\qquad\quad \forall \mu_{i,1}\mu_{i,2} \leq \text{tr}, \end{aligned} \tag{4.12}$$

where $\text{tr} = 0.0001$ and s is the maximum thickness of a layer, which was set to $s = \langle|\vec{\Lambda}|\rangle$, the mean length of the links in the initial condition. Following Kaandorp & Sloot (2001), the measurements $\mu_{i,1} = \phi_i/\phi_{\max}$ and $\mu_{i,2} = h2_i$ contained the normalised local resource flux and an estimation of "the amount of contact with the environment",

$\bar{u}$	D	$\overline{Pé}_{\mathrm{lat}}$	Compactness (n=1)	Fig.
0.0	0.167	0	0.39	4.6a
0.0	0.167	0	0.55	4.6b
0.0	0.167	0	0.89	4.6c
0.0	0.167	0	0.91	4.6d
0.0	0.167	0.24	0.39	4.8a
0.0	0.067	0.60	0.43	4.8b

Table 4.1: Compactness of the simulated growth forms developed with the growth function of Eq. 4.11. Only one object could be simulated for each parameter setting due to the very long simulation times

$h2_i$. In this chapter the value of $h2_i$ was calculated from the two principal curvatures κ_1 and κ_2 at vertex v_i,

$$h2_i = \texttt{low\_norm\_curv} \times \bar{\kappa} \tag{4.13}$$

where

$$\texttt{low\_norm\_curv} = \Theta_1(1-(\Theta_2(\frac{1}{\kappa_2})-\texttt{min\_curv})/(\texttt{max\_curv}-\texttt{min\_curv}))) \tag{4.14}$$

in which $\kappa_2 < \kappa_1$ and $\bar{\kappa} = \frac{1}{2}(\kappa_1 + \kappa_2)$ is the mean curvature. The threshold function $\Theta_1(x)$ sets all negative values to 0 and all values greater than 1 to 1; $\Theta_2(x)$ sets all negative values to 0. The principal curvatures κ_1 and κ_2 were measured with the method by Meyer *et al.* (2002). $\texttt{min\_curv} = 2s$ is the radius of curvature below which the growth is maximal; $\texttt{max\_curv} = 20s$ is the radius of curvature above which the growth is set to 0. Note that, following their original definition (Kaandorp, 1994a; Kaandorp, 1995; Kaandorp & Sloot, 2001), these parameters are defined in terms of the *radius of curvature* instead of the *curvature*. Instead of using the field convergence stopping conditions as in eqs. 4.2 and 4.4, the simulations in this section were stopped after a fixed number of lattice Boltzmann and moment propagation iterations, thus following the simulation set-up by Kaandorp & Sloot (2001). According to that work, we used a cubic lattice of size 144^3 and 50 advection-diffusion iterations per growth cycle (Kaandorp, personal communication). Note that with 50 iterations a stable resource field is not reached (see Fig. 4.7). The radius of the initial sphere was $r = 8$ l.u.

In Fig. 4.9 we show two realisations of this model in a non moving fluid. In the left panel $D = 0.167$, in the right panel $D = 0.017$. In both cases the flow was $\langle|\vec{u}|\rangle = 0$, such that $Pé = 0$. For $D = 0.167$ we found relatively thinly branched growth forms (Fig. 4.9a.). This finding reproduces the observations in the previous work. Note that this growth form is slightly asymmetric, despite the absence of flow. When we used a smaller diffusion coefficient ($D = 0.017$), the growth forms obtained more branches and were better centred (Fig. 4.9b.) This finding violates the original assumption that the flow and resource fields are in equilibrium, in which case the resource field, and

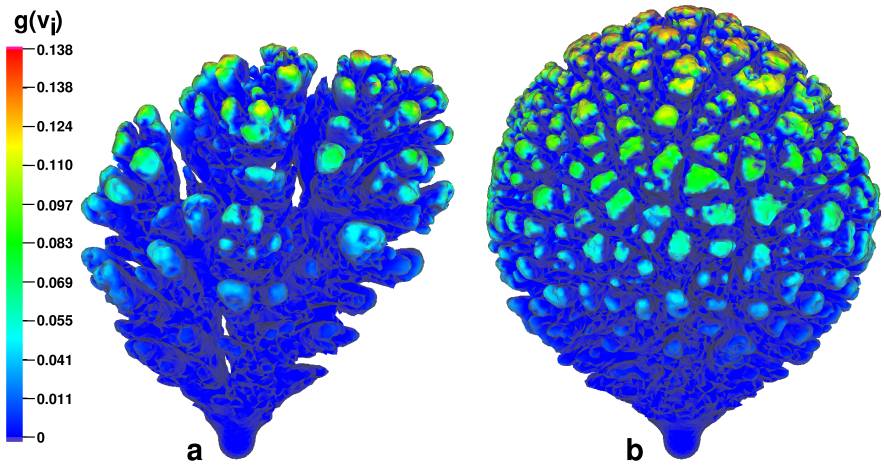

Fig. 4.9: Results of the diffusion-limited HIRAG-model with *curvature rule*. 85 accretive growth cycles were applied in both panels. The size of the simulation box was 144^3, the radius of the initial sphere was 8 l.u.. a) $D = 0.167, Pé = 0$ b) $D = 0.017, Pé = 0$.

consequently the growth form, should be independent of the diffusion coefficient. In the original work by Kaandorp & Sloot (2001), the Péclet-number was varied by exclusively changing the diffusion coefficient, while the same flow velocity was used for all simulations. For large Péclet-numbers, that were obtained by lowering the diffusion coefficient keeping the flow velocity unchanged, the growth forms were found to be more compact and more spherical. Our results agree to this observation, although here we did not apply any fluid flow ($\langle|\vec{u}|\rangle = 0, Pé = 0$): for lower diffusion coefficients, we found more compact and more spherical growth forms. This suggests that the compactification as it was observed in the original simulations is not a Péclet-number effect; instead, the compactness appears to depend directly on the diffusion coefficient.

This conclusion is further supported by the results shown in Fig. 4.10. Objects a. and b. were grown in a monodirectional flow (right to left) with $\langle|\vec{u}|\rangle = 0.05$ l.u. The velocity at the top plane was set to $\vec{u}_{\max} = 0.1$ l.u., a velocity which is close to the upper limits of applicability of the used lattice Boltzmann method. We used velocities close to those used in Kaandorp & Sloot (2001). Following that work, we applied 10 iterations of the lattice Boltzmann method (see Chapter 2) per growth cycle (Kaandorp, personal communication), which — given the 100 to 5000 iterations per growth cycle that were needed to obtain a convergence of $\theta_{\mathrm{NS}} = 10^{-8}$ in Section 4.3.1 — is not sufficient to obtain a stable flow field. The resulting morphologies were not strongly affected by the fluid flow. We only observed a slight asymmetry, directed against the fluid flow. The diffusion coefficient for the object shown in Fig. 4.10a. was $D = 0.167$, for which $\overline{Pé}_{\mathrm{lat}} = 0.3$. Its compactness did not differ from Fig. 4.9a.

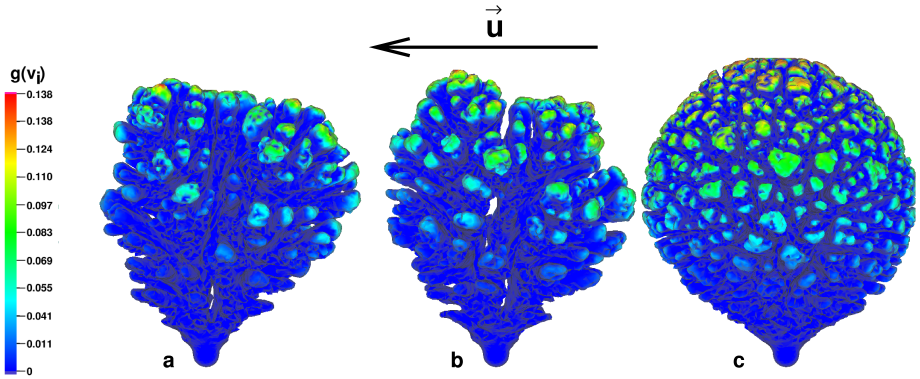

Fig. 4.10: Objects grown in a monodirectional flow (right to left) with the curvature rule. The size of the LBGK-lattice is 144^3, the size of the initial sphere is 8 l.u.. a) $\overline{Pé}_{\mathrm{lat}} = 0.3$, $u = 0.05$, $D = 0.167$. b) $\overline{Pé}_{\mathrm{lat}} = 0.75$, $u = 0.05$, $D = 0.067$. c) $\overline{Pé}_{\mathrm{lat}} = 0.75$, $u = 0.0125$. Other instantiations of these objects can be found on the CD accompanying this thesis.

(see Table 4.2), where no flow was applied. Thus, also in this experiment we observed no effect of the laminar flow on the compactness. A smaller diffusion coefficient led to compactification and stronger branching (Fig. 4.10b.) like in the absence of flow as in Fig. 4.9. The diffusion coefficient was set to $D = 0.067$, which is the minimum diffusion coefficient for which the advection-diffusion-method gives correct results at $\bar{u} = 0.05$ (see Chapter 4; Merks *et al.*, 2002). For these parameters, $\overline{Pé}_{\mathrm{lat}} = 0.75$. When the diffusion coefficient was further lowered to $D = 0.017$ keeping the Péclet-number constant by using a smaller flow velocity ($\bar{u} = 0.0125$), we found even more compact growth forms (Fig. 4.10c.). Statistical testing (ANOVA[4]) revealed that the compactness measurements (Table 4.2) were not significantly different from the values of Fig. 4.9b., where the same diffusion coefficient was used in a still-standing fluid. The compactness of these objects thus directly depends on the diffusion coefficient, and not on the Péclet number.

The present results do not support the conclusion that for "(...) an increasing influence of hydrodynamics, the simulated morphologies (are) gradually transformed from thin-branching ones into more spherical and compact morphologies" (Kaandorp & Sloot, 2001). The limited number of iterations in solving the resource and flow fields in their simulations was responsible for the observed dependence of the compactness on the diffusion coefficient. For the final, stable solution of the diffusion equations, the value of the diffusion coefficient is of course irrelevant. But if the advection-diffusion equations are solved numerically for a fixed, small number of iterations this stable solution is not reached. In fact, for smaller diffusion coefficients the solution remains even further from stability, because the time to reach the stable solution becomes longer. In such a case depletion zones around the branches may not form sufficiently which

[4]See `http://mathworld.wolfram.com/ANOVA.html`

$\bar{u}$	D	$\overline{Pé}_{\mathrm{lat}}$	Compactness (n=5)	Fig.
0.0	0.167	0	0.290 ± 0.008	4.9a
0.0	0.017	0	0.416 ± 0.002	4.9b
0.050	0.167	0.3	0.288 ± 0.003	4.10a
0.050	0.067	0.75	0.325 ± 0.003	4.10b
0.012	0.017	0.75	0.418 ± 0.004	4.10c

Table 4.2: Compactness of the simulated growth forms developed with the growth function of Eq. 4.12

results in more compact growth forms and more branches as in Fig. 4.9b and 4.10c. With the dynamic stopping criterion that was used in Section 4.3.1, the deviation from the stable solution does no longer depend on the diffusion coefficient, but only on the stopping criterion. Indeed, there the compactness depended on the stopping criterion and not on the diffusion coefficient (Figs. 4.6 and 4.8). According to the original assumption of the HIRAG model, resource transport is a much faster process than coral growth. The results presented here suggest that the fact that these timescales were not well separated in the original simulations, resulted in an incorrect interpretation of the compactification effect. In the next section the assumption of time scale separation is further analysed, based on the time scales that are expected in real life coral growth. Hence we come to a biological reinterpretation of the simulation results.

4.4 Discussion

We have studied the hydrodynamically influenced radiate accretive growth model (HIRAG model) (Kaandorp & Sloot, 2001). The HIRAG model is an abiotic growth model that is inspired by coral growth. Rather than to model the morphogenesis of a specific coral species, the aim of such a model is to understand for which aspects of coral growth abiotic mechanisms provide a *sufficient* explanation, and for which aspects biotic effects, such as genetic regulation and differential tissue and skeletal growth, must be responsible.

In the present chapter we have focused exclusively on abiotic mechanisms that are sufficient to reproduce aspects of coral growth. The model of these abiotic mechanisms was deliberately kept as simple as possible. For example, we have used a linear growth function, whereas it would biologically be more plausible to use a saturated growth function. We think, however, that only through a prior thorough understanding of the simplified model the effect of such more complicated assumptions can be understood. For the same reason we have refrained from including a number of biological mechanisms that do play an important role in coral morphogenesis. The inclusion of such mechanisms would extend the range of morphologies produced by the HIRAG model. For example, we could include genetic regulation in the HIRAG model by having the coral surface excrete growth suppressing “isomones” (Rinkevich & Loya, 1985; Kaandorp, 2001), or by allowing for interpolypal communication by introducing signalling

chemicals diffusing over the coral surface. Also, we have ignored the fact that many modular cnidarians transfer resources through the gastrovascular cavity (Rinkevich & Loya, 1983; Oren *et al.*, 1997; Gateno *et al.*, 1998), which we could model by allowing the resources to diffuse over the coral surface. Polyps subject to high flow velocities become flattened, making it impossible for them to catch food particles (Sebens *et al.*, 1997). Including such flow dependent resource uptake would certainly affect the simulation results. Currently we have also ignored the fact that in real corals the rates of tissue growth and skeletal growth can be controlled by different environmental factors (Barnes & Lough, 1992; Darke & Barnes, 1993). In the present model the rate of "tissue growth", as given by the rate of extension of the coral surface, is directly linked to the rate of "skeletal growth". We could model such differential tissue and skeletal growth by decoupling the rates of vertex insertion and skeletal accretion and making those processes dependent on different resources. Although these biotic factors would all affect the results of our model, we have not included them in the present model. This enables us to study for which facets of coral growth abiotic growth processes provide *sufficient* explanation. Moreover, the future one-by-one inclusion of these biotic processes may provide a clear picture of the role of each of these additional processes in coral morphogenesis.

In this chapter we addressed two issues of the HIRAG model: the mechanism of branch splitting and the mechanism of compactification under the influence of water flow. In Kaandorp & Sloot (2001) the splitting of branches was enforced by a *curvature* rule. Thus, it was not possible to study the mechanism of branch splitting in the original HIRAG model. In Section 4.3.1, we demonstrated that branch splitting can also occur in the HIRAG model if no such *curvature rule* is used, provided that the resource field is solved until near stability. Such branch splitting occurred only if the time-scales of growth and resource dispersion were well separated. Such *Laplacian growth* is discussed below in Section 4.4.1. In Section 4.3.2 it was argued that this observation suggests that the simulation results reported in Kaandorp & Sloot (2001) and in Kaandorp (2001) were wrongly interpreted as the effect of hydrodynamics. This conclusion is discussed in Section 4.4.2. In Section 4.4.3, finally, it is discussed whether and under which conditions it is correct to separate the time-scales of skeletal growth and resource dispersion in corals.

4.4.1 Laplacian growth

The assumption that resource diffusion is a much faster process than growth puts the diffusion-limited HIRAG model in the class of Laplacian growth models (like viscous fingering). It will be discussed below whether that assumption is correct for coral growth. These growth forms have a few dominating branches that absorb more resources than the smaller ones thus creating a zone of resource depletion around them, which sets off a branching instability, where the growth of smaller branches is suppressed by the larger branches. Such stagnation points are well known from theoretical, numerical and experimental studies of Laplacian growth (see for example Mineev-Weinstein & Dawson, 1994; Magdaleno & Casademunt, 1998 and references therein). If the resource field is not well converged, the depletion zone around a slightly larger

branch does not extend very far and the instability does not occur. The surface grows out at a uniform rate creating spherical, compact growth forms. Branching morphologies occur if the time scales of resource diffusion and of coral accretion are sufficiently separated, whereas more compact morphologies are generated if growth and diffusion occur in the same time scale. Interestingly, this observation agrees to studies of diffusional growth in the limit of small anisotropy, for example solidification. Here dense *compact* morphologies occur for quickly growing solid-fluid interfaces, whereas for slowly growing interfaces a more thinly branching *fractal* morphology occurs (Ihle & Müller-Krumbhaar, 1994; Brener *et al.*, 1998).

It is well known that branching instabilities do also occur in Laplacian growth systems in which the local curvature is not an explicit variable. For example, it was shown numerically and theoretically that in the absence of surface tension (which is a stabilising curvature dependent effect) tip splitting, stagnation points and other features of viscous fingering occur (Mineev-Weinstein & Dawson, 1994; Magdaleno & Casademunt, 1998). Although in the HIRAG model the curvature rule is not a necessary condition for branching to occur (Section 4.3.1), we do not think that it is free of curvature dependent effects. In the HIRAG model we observe a positive correlation between the resolution of the surface discretisation and the size of the branches (Fig. 4.6). The surface discretisation, which may reflect the density of polyps, appears to determine how strongly the surface can be bent. We may therefore interpret it as an implicit surface tension effect, which has the effect of smoothening out high frequency irregularities on the surface. The precise embedding of the HIRAG model into the field of Laplacian growth is the subject of ongoing research.

4.4.2 The effect of hydrodynamics

The conditions under which spontaneous branching occurs, suggest the explanation for the observations in the original simulations of the curvature dependent model (Kaandorp & Sloot, 2001), where a positive correlation was found between the object's compactness and the Péclet-number. In these simulations only the diffusion coefficient was changed to vary the Péclet number, keeping the flow velocity unchanged in all simulations. Also, the developing morphologies were not compared to morphologies that develop in the absence of flow. Here we obtained the same result (Fig. 4.9) if we changed the diffusion coefficient in a stationary fluid ($\langle|\vec{u}|\rangle = 0$ and $P\acute{e} = 0$) with a fixed number of iterations as in the work by Kaandorp & Sloot (2001). Moreover, when we imposed a flow with a velocity near the limits of applicability of the used lattice Boltzmann method, the growth forms did not change (Fig. 4.10a.). The growth forms compactified when we increased the Péclet-number by lowering the diffusion coefficient, keeping the flow velocity at the same high level (Fig. 4.10b.). If the diffusion coefficient was further lowered, concurrently lowering the flow velocity in order to keep the Péclet number constant, we found strong compactification (Fig. 4.10c.). The probable explanation of the mechanism of compactification is given by these results. In the simulations by Kaandorp & Sloot (2001) and those in Section 4.3.2 a small and fixed number of advection-diffusion iterations was used. A stable solution of the advection-diffusion equation was not reached when the next growth cycle started. If

a smaller diffusion coefficient was used, the solution was even further from the stable equilibrium when the next growth cycle was started. Hence in these simulations the diffusion coefficient probably directly determined the degree of resource field convergence, which, as we have seen above, governs the compactness of the objects. The results presented here strongly suggest that the compactification as previously observed in the HIRAG model was wrongly interpreted to be caused by hydrodynamics. It resulted from the insufficient separation of the time scales of growth and resource dispersion: by lowering the diffusion coefficient in combination with the use of a fixed number of advection-diffusion iterations, these time scales approached each other resulting in increased compactification. Therefore, the present computational evidence that hydrodynamics influences the compactness of corals in laminar flows (Kaandorp & Sloot, 2001) is inconclusive.

In future work we plan to include unstable and turbulent flows in our simulations. Under such flow conditions we expect that recirculations between the branches or turbulence will occur. Such effects may carry nutrients more quickly into the crevices between the branches, which may affect the resulting coral morphologies. A more elaborate discussion on this topic is given in Chapter 7.

4.4.3 Separation of time-scales of growth and transport

So far we have have demonstrated that the growth forms produced by the HIRAG model are strongly influenced by the convergence of the resource field. It was assumed that resource transport is a much faster process than the growth process. For this reason, we waited until the resource field had stabilised before starting a new accretive growth cycle. Doing so, we approximated the HIRAG process by a discretised Laplacian growth process in which the resource field, called "driving force" in Laplacian growth terminology, converges instantaneously. The correctness of this Laplacian growth assumption depends on the correctness of the assumption that the time scales of growth and transport are sufficiently separated. Assuming a transport mechanism that can be approximated by diffusion, the time needed to transport a resource over a distance Δx is estimated as

$$t_D \approx \frac{(\Delta x)^2}{D}. \tag{4.15}$$

The time scales of growth and transport are compared by estimating the time needed to diffuse over the yearly skeletal extension rate (i.e. the growth caused by extension of vertical skeletal elements, ignoring secondary thickening). The skeletal extension rate varies between coral species and on environmental parameters such as the sea surface temperature (Lough & Barnes, 2000). A short overview of skeletal extension rates reported in the literature is given in Table 4.3, from which we derive a typical yearly extension rate for branching corals of $17\ \mathrm{mm\ yr}^{-1}$. The value for *Acropora* was not included in this estimate, since in this genus branches are led by an enlarged axial polyp, which is a branching mechanism not covered by the HIRAG model.

The typical diameter of particles captured by colonies of *Madracis mirabilis* is about $1\ mm$ (Kaandorp & Sloot, 2001). A typical passive diffusion coefficient in wa-

Species	Growth form	Ext. rate ($\frac{mm}{yr}$) (Mean)
Porites spp.	massive	12.0 ± 4.9 [a]
Porites spp.	branching, columnar	2 to 48 (10)[b]
Pocillopora damicornis	branching	9 to 57 (28)[b]
Acropora spp.	branching	21 to 172 (77)[b]
Montastrea annularis	massive	5 to 25 (11)[c]
Pocillopora damicornis	branching	1.6 to 35.9 (19)[c]

[a] Lough & Barnes (1997)
[b] Harriott (1999)
[c] Buddemeier & Kinzie III (1976)

Table 4.3: Brief overview of skeletal extension rates as reported in review papers.

ter of such particles is $5.10^{-16} m^2 s^{-1}$ (Weast *et al.*, 2000). Using Eq. 4.15 we have estimated that the time needed for a fair amount of these particles to diffuse $17\ mm$ is about 18000 years. Hence it is not correct to approximate coral growth with a Laplacian growth process based on such passive particle diffusion alone. The diffusion coefficients of food particles increase substantially by assuming additional mechanisms. Many organic food particles display active, random movement. For example, a guess of the diffusion coefficient of the unicellular alga *Chlamydomonas nivalis*, based on mean free path calculations, ranges from 5.0×10^{-9} to $5.0 \times 10^{-7}\ m^2 s^{-1}$ (Kessler, 1986), for which the diffusion times are in the order of eight hours to five minutes. Kaandorp & Sloot (2001) estimated the diffusion coefficient of actively moving food particles of about $1\ mm$ in diameter at $3.5 \times 10^{-5}\ m^2 s^{-1}$; hence such particles diffuse over a distance of $17\ mm$ in about $8\ s$. Using $D \approx \frac{1}{3} V_c \delta$ as in Kessler (1986), this estimate was based on an average swimming distance of $\delta = 10^{-2}\ m$ covered without changing direction and an average swimming speed of $V_c = 10^{-2}\ ms^{-1}$ (Sloot, personal communication). Thus, assuming direct dependence of the growth rate on the availability of actively moving food particles and assuming that the polyps take up all the food that reaches them, the Laplacian growth assumption may be correct.

An interesting situation arises if we hypothesise a growth limiting resource with a lower diffusion coefficient than the ones estimated above. Examples of such slowly diffusing resources would be dissolved inorganic material, such as phosphate, nitrate or inorganic carbon (Lesser *et al.*, 1994), whose diffusion coefficients are on the order of $10^{-9}\ \mathrm{m^2 s^{-1}}$ (Weast *et al.*, 2000). Assume a resource which diffuses just quickly enough to sufficiently separate the time scales of growth and resource diffusion for a slowly growing coral. In such a case the HIRAG model would predict the growth of a widely spaced morphology and a strong degree of branch dominance. If the object would grow more quickly, according in our model the resource field would never completely stabilise, resulting in more compact and dense growth forms. Such a dependence of the morphology on the growth velocity agrees to observation and theory on diffusional growth, such as solidification. Here, a shift from a "*fractal*" to a "*compact*" morphology occurs as the growth velocities increases, thus bringing the time scales of

diffusion and growth closer together (Ihle & Müller-Krumbhaar, 1994; Brener *et al.*, 1998).

The growth velocity in physical units can be estimated for the simulations with a fixed number of advection-diffusion (AD) iterations n_{AD}. The length of a single AD time step in physical units is estimated as

$$\Delta t = \frac{D_{\mathrm{sim}}}{D_{\mathrm{real}}}(\Delta x)^2, \tag{4.16}$$

where Δx (m $(\mathrm{l.u})^{-1}$) is the size of a lattice unit in physical units, D_{real} is the diffusion coefficient in physical units and D_{sim} is the diffusion coefficient in simulation units. The growth velocity is then estimated as $v_{\mathrm{growth}} = (s\Delta x)/(n_{\mathrm{AD}}\Delta t)$, where s is the maximum layer thickness (see Eq. 4.12) in lattice units. Assuming the size of the simulation box to be 50 cm, for the simulations in Section 4.3.2 $\Delta x = 0.5m/144$ l.u. $= 3.5 \times 10^{-3}m$ $(\mathrm{l.u})^{-1}$. For these simulations $n_{\mathrm{AD}} = 50$, and the D_{sim} varies from $D_{\mathrm{sim}} = 0.167$ to $D_{\mathrm{sim}} = 0.017$. Taking an estimate of the diffusion coefficient of *Chlamydomonas* cells of $D_{\mathrm{real}} \approx 5 \times 10^{-8}$ $m^2 s^{-1}$, a growth cycle takes 40 seconds ($D_{\mathrm{sim}} = 0.167$) to 4 seconds ($D_{\mathrm{sim}} = 0.017$). Throughout Section 4.3.2 $s = 1.8$ l.u. $= 6.3 \times 10^{-3}m$, giving growth velocities of 3×10^{-6} ms^{-1} to 3×10^{-5} ms^{-1}, which is about 100 m to one km per year! Taking the estimate of $D_{\mathrm{real}} = 3.5 \times 10^{-5}$ from Kaandorp & Sloot (2001) we even find growth rates of 70 to 700 km y^{-1}. If we interpret the diffusing resource as calcium ions, we still find growth rates in order of a meter per year, which is still two orders of magnitude larger than the real growth velocities of 2 to 57 mm y^{-1}.

Likewise, the maximum number of advection-diffusion time steps n_{AD} corresponding to a natural growth velocity of 17 mm per year can be estimated, with $n_{\mathrm{AD}} = (s\Delta x)/(v_{\mathrm{growth}}\Delta t)$. These estimates range from $n_{\mathrm{AD}} \approx 10^{18}$ for $D_{\mathrm{real}} = 5 \times 10^{-8}$ $m^2 s^{-1}$, to $n_{\mathrm{AD}} \approx 10^{15}$ for $D_{\mathrm{real}} = 3.5 \times 10^{-5}$.

Above we have assumed pure diffusive transport of the resource or active random walks that we model as diffusion. At the length- and time scales at which coral morphogenesis takes place however, convective transport and advection is likely to be of much greater importance than diffusion. If even in a glass of water convection must be put to a rest with gelatin to study pure diffusion (Vogel, 1988), it is clearly unrealistic to assume that in a dynamic environment as the ocean no other means of transport would be of importance. We must therefore be careful in interpreting our results, and realise that we have lumped together a variety of transport processes such as convection and turbulent mixing that we have modelled as advection and diffusion. The diffusion coefficients that are associated with these mixing processes and the realistic interaction of these processes with our flow obstacle — the growing coral — are the subjects of future study.

4.5 Acknowledgements

We are grateful for the very useful comments of two anonymous referees.

CHAPTER

FIVE

Polyp oriented modelling of coral growth[1].

The morphogenesis of colonial stony corals is the result of the collective behaviour of many coral polyps depositing coral skeleton on top of the old skeleton on which they live. Yet, in models of coral morphogenesis the polyps are often approximated by a single, continuous growing surface. In the present work, the polyps are modelled individually, where each polyp takes up resources, deposits skeleton, buds off new polyps and dies. In this polyp oriented model spontaneous branching is more robust to disturbances of the resource field, than the Laplacian growth mechanism that we discussed in Section 4. We argue that branching is caused by a so called "polyp fanning effect" by which polyps on a convex surface have a competitive advantage relative to polyps on a flat or concave surface. We discuss the application of the polyp oriented model to the study of environmentally driven morphological plasticity in stony corals. In a few examples we show how the properties of the individual polyps influence the whole colony morphology.

5.1 Introduction

In Chapter 3 and Chapter 4 we considered physical processes, such as diffusion-limited aggregation and Laplacian growth, and discussed whether coral growth can be understood by comparing it to these physical metaphors. We concluded that certain aspects of coral growth, such as the branching mechanism, resemble physical branching processes, but only under restricted conditions. We discussed that spontaneous branching in the Laplacian growth mechanism occurs only when resource transport is a much

[1]This chapter is based on: R. M. H. Merks, A. G. Hoekstra, J. A. Kaandorp and P. M. A. Sloot. Polyp oriented modelling of coral growth, Submitted to *Journal of Theoretical Biology* and on: R. Merks, A. Hoekstra, J. Kaandorp and P. Sloot (2002). Spontaneous Branching in a Polyp Oriented Model of Coral Growth. ICCS 2002. *LCNS* **2329**, 88–96

faster process than coral growth, in which case depletion zones around the branches can be formed.

A coral reef, however, is a very dynamic environment, with continuous water movement caused by waves and fishes. Thus the stable conditions, necessary for the Laplacian growth mechanism to work, do not occur in coral reefs. In this chapter we add more biological detail to the accretive growth models. By explicitly modelling the coral polyps, the models become more robust against disturbances. Moreover, it becomes possible to study the effect of the polyp's biological — possibly environmentally dependent — properties on the morphogenetic process.

In the present study, we attempt to take a first step in bridging the gap between adaptive and mechanistic approaches, as introduced in Section 1.3, for understanding morphogenesis and morphologic plasticity in stony corals. In contrast to previous models, we use a *polyp oriented approach*. In this approach, coral growth is seen as the collective result of a growth process taking place in the polyps. The polyps are modelled as separate entities in our model; each of these model polyps takes up resources, deposits skeleton, buds off new model polyps and dies.

Since coral morphologies are ultimately generated by the polyps that build the skeleton, adaptive genetic factors can only affect coral morphology indirectly, by setting the properties of the individual polyp. Of course inter-polyp signalling and feedback mechanisms via the environment may also play a role. In order to understand environmentally driven morphological plasticity it is thus important to understand how the individual polyps are influenced by the environmental parameters that control morphological plasticity, such as light, food availability and water flow. The polyp oriented approach may enable us to study how the interplay between genetic and environmental effects on the polyp properties affect the coral morphology. As a first step in this approach, we investigate whether branching growth can be obtained by exclusively describing the behaviour of the individual polyps. Also we study whether, and how, genetic or environmental variability of the micromorphological traits of the individual polyps and the skeleton may affect the colony's macromorphology.

The remainder of this chapter is organised as follows. In the next section, the polyp oriented accretive growth model is introduced. Thereafter we present two variants of the model, that we consider as two limits of a continuous range of growth mechanisms. In the one extreme, the skeletal extension rate is directly determined by the resource uptake rate, giving skeletal porosity that varies over the calyces. In the other extreme, we consider the growth of a skeleton of uniform porosity. We present parameter studies of these models, that cover a small part of the morphospace that can be spanned by the models. In the last section we discuss our model and its present and future applicability in the study of morphological plasticity in stony corals.

5.2 The Model

The polyp oriented radiate accretive growth model (PORAG model) was based on the accretive growth model described in Chapter 4. The PORAG model is a variation of this model, where we model the polyps individually, rather than treating the coral surface

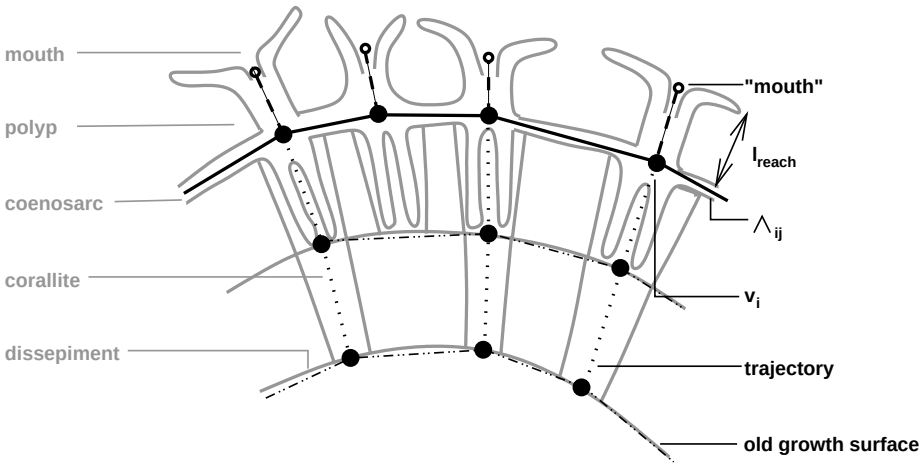

Fig. 5.1: Derivation of the polyp oriented radiate accretive growth (PORAG) model. A diagrammatic cross section of a small portion of a stony coral with a newly inserted polyp is shown in grey. The overlay in black shows the corresponding model entities.

as a continuum. Each vertex v_i of the triangular mesh was considered a polyp in this model (see Fig. 5.1). The intervertex links $\tilde{\Lambda}_{ij}$ represent the coenosarc, the connective tissue bridges between the polyps. Each of the "polyps" v_i absorbs its growth resources R from a cell in the cubic lattice at a small distance l_{reach} along the surface normal from its position on the mesh; this was motivated by the fact that coral polyps are slightly elevated above the coral surface, take up food particles through the mouth (Sebens *et al.*, 1997) and actively transport inorganic resources needed for skeletal accretion across the oral epithelium into the coelenteron (Gattuso *et al.*, 1999). Throughout this chapter we fixed $l_{\mathrm{reach}} = 3$ lattice units (l.u.), which approximately agrees to polyp elevations found in real corals (see Section 5.4.1).

In Chapter 4 we concluded that low Péclet-number, low velocity laminar flows have little effect on the accretive growth process. Therefore we did not include such flow effects in the simulations presented in this chapter[2]. For the advection-diffusion equation, the boundary conditions were as follows. The top plane was kept at a fixed concentration of resource $R = 1.0$, thus acting as a source; the "polyps mouths" distributed over the "coral" surface at a distance of l_{reach} from the "polyps" were resource sinks (i.e. $R = 0.0$) according to the procedure described above. In contrast to the HIRAG model, in the PORAG model the surface of the "coral" colony was made impenetrable to the diffusion resource by applying a bounce back boundary condition in the moment propagation method (Chapter 2; Warren, 1997; Merks *et al.*, 2002). The ground plane may be either a resource sink or an impenetrable plane. Unless otherwise stated, a periodic boundary condition was applied on the side planes.

The moment propagation algorithm was iterated until the change per unit time and

[2]Indeed we have not found any flow effects on the PORAG model (data not shown).

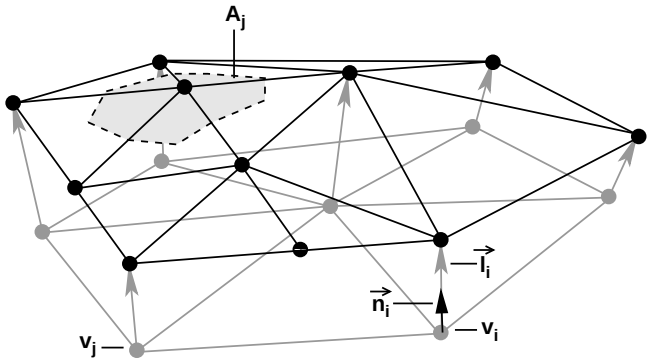

Fig. 5.2: Diagram of an accretive growth step. On top of the "polyps" (grey disks) an element $\vec{l}_i$ is built (shown as grey arrows), in the direction of the local surface normal vector $\vec{n}_i$. The length of the element $\vec{l}_i$ depends on the local measurements $\vec{\mu}_i$. The new positions of the "polyps" are shown as black disks. New "polyps" are inserted where the length of the links $\vec{\Lambda}_{ij}$ (shown as grey and black lines for old and new links respectively) exceeds the threshold θ_{INS}. The "polyp" area A_j (see section 5.3) is shown in gray for one of the "polyps" (top left).

unit mass of the resource mass dropped below a small convergence threshold θ_{AD} (Eq 4.4), up to a maximum of 1000 time steps (which was never reached in the simulations shown here). Throughout this chapter we set $\theta_{\mathrm{AD}} = 10^{-5}$. At this convergence the influx of resources through the top plane sufficiently balanced the outflux into the "polyps" and the ground plane. After convergence the resource uptake rate ϕ_i was measured for each "polyp" v_i, as the rate of resource removal from the lattice node representing the polyp mouth.

The exact form of the growth function (See Eq. 4.6) is hard to derive a priori, since it depends on what growth resource is represented by the diffusing resource in the model. If we interpret it as an energy source, the availability of resource affects the accretion rate more indirectly, than when the diffusing resource is interpreted as a skeletal building block. The form of g influences the resulting morphology, as will be shown in the next section.

In this chapter we interpret the diffusing resource as a material whose availability directly limits the generation of skeletal material. Even in this case the derivation of the growth function is not straightforward. Coral skeleton is a porous material consisting of the individual calices in which the polyps reside. The calices consists of a central cylinder, the columella, from which radial septa project onto a surrounding wall (see Fig. 1.5b). This wall is shared between neighbouring calices in cerioid corals, while in plocoid corals the calices have their own wall, that are separated by a more solid skeletal area called the coenosteum (see for example Barnes, 1973 and Bruno & Edmunds, 1997 and references therein). The porosity of the columella is variable. In some species it is a solid, central cylinder, whereas in other species it may be more porous or completely absent. The porosity of the skeleton shows seasonal variation (Knutson

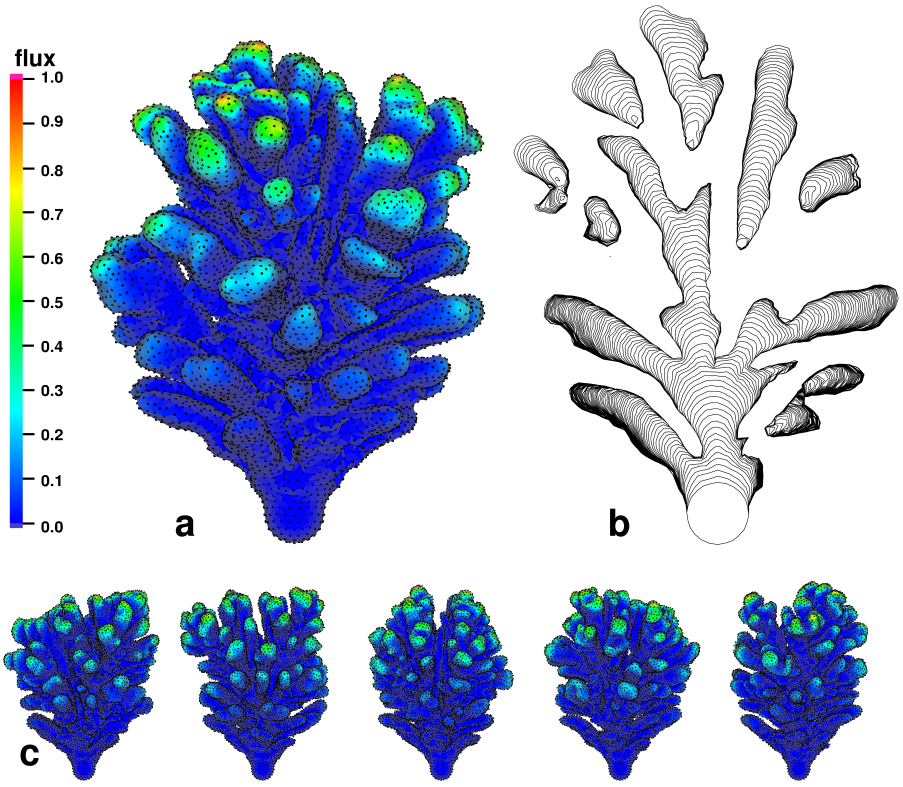

Fig. 5.3: Simulated branching “coral” after 84 growth steps. The size of the cubic grid is 200^3. The “coral” contains 18006 “polyps”, that are shown as black dots. The mean “inter-polyp” distance is 1.8 l.u. (a) outside view, colour scale: normalised resource flux. (b) cross section, in which the successive growth layers are visible. (c) A range of alternative realisations.

et al., 1972); also it varies between calices on the same colony and it is influenced by the environment (Foster, 1980). Hence, due to the variable skeletal density, it is not possible to directly relate the mass flux of skeletal building blocks to an increase of skeletal volume. For this reason, we studied two limits in a range of biologically motivated growth functions. These growth functions differ in the structure of the newly deposited skeleton. In the one extreme, the skeletal extension rate is directly related to the resource uptake rate, as

$$g(\vec{\mu}) = \vec{n}\mu_i, \text{with } \mu_i = \theta\widehat{R_i}, \tag{5.1}$$

where θ is the maximum size of a growth step and $\widehat{R_i}$ is the normalised net resource flux into the "polyp". This growth function implies that the mean porosity of the calix is proportional to its area, because the resource taken up by the "polyp" is redistributed over the "polyp's" area. A coral species with large calices and little coenosteal skeleton would be close to this limit. Throughout this chapter, this function is referred to as *growth function I*.

In the other extreme of our range of growth functions, we considered a coral skeleton of uniform skeletal density; a coral with small calices relative to the amount of coenosteal skeleton, or a coral with calices of equal porosity to the coenosteal skeleton would be close to this extreme. In this growth function the amount of resource taken up through the "polyp's" mouth is redistributed over the "area of influence" of the "polyp", according to

$$g(\vec{\mu}) = \vec{n}\mu_i, \text{with } \mu_i = \theta\widehat{\frac{1}{A_i}R_i}, \tag{5.2}$$

where A_i is the "area of influence" of "polyp" v_i. $A_i = \frac{1}{3}\sum_j A(T_j)$, where the summation is over all the triangles surrounding v_i and $A(T_j)$ is the area of triangle T_j (see Fig. 5.2). In the rest of this chapter, this growth function is called the *growth function II*.

In our model, we assumed that new polyps are formed as soon as space becomes available. A new "polyp" was inserted between "polyps" v_i and v_j, if the link length $|\vec{\Lambda}_{ij}| > \theta_{\mathrm{INS}}$. The position of the new "polyp" was determined using a third order interpolation of the "coral" surface. Two "polyps" fused, if their link length $|\vec{\Lambda}_{ij}| < \theta_{\mathrm{FUSE}}$. The settings of the insertion and fusion thresholds determine the mean and variance of the "inter-polyp" distances later during the growth process. The "inter-polyp" distances had a large effect on the growth form, as we will show in section 5.3.1. Therefore, insertion and deletion thresholds were chosen, for which the variance of the "polyp" spacing is minimised. The insertion threshold was set to $\theta_{\mathrm{INS}} = \frac{3}{2}\langle|\vec{\Lambda}_{ij}|\rangle_{\mathrm{init}}$, where $\langle|\vec{\Lambda}_{ij}|\rangle_{\mathrm{init}}$ is the initial mean distance between the "polyps". In this way, a new "polyp" was inserted when the distance between the two "polyps" had grown by 50% of the initial distance. The fusion threshold was set to $\theta_{\mathrm{FUSE}} = \frac{3}{4}\langle|\vec{\Lambda}_{ij}|\rangle_{\mathrm{init}}$. With this setting two "polyps" fused if their distance became less than half of the minimal "inter-polyp" distance directly after insertion.

All the simulations presented here were carried out on a grid of 200^3 lattice units (l.u.). The initial hemisphere was positioned at the ground plane, with its centre located at $(x, y, z) = (100, 100, 0)$. The radius of the initial hemisphere, which by setting θ_{INS} and θ_{FUSE} determines the initial and later spacing of the "polyps", varied over the presented simulations between 6.25 l.u. and 12.5 l.u.

The simulations were carried out on a Linux Beowulf cluster, using 16 AMD Athlon processors running at 700 Mhz with 256 MByte to 512 MByte of internal memory each. On this setup typical run-times reached from 18 hours to 36 hours, depending on the complexity of the emerging geometries (see Chapter 6 for performance analysis). Animations and three-dimensional images of the corals shown in this chapter have been made available on the CD-ROM.

5.3 Simulations and Results

5.3.1 Growth function I

In figure 5.3 a possible outcome after 84 growth cycles with growth function I (Eq. 5.1) is shown. This "coral" was grown upon an initial hemisphere of radius 6.25 l.u., giving a mean initial "inter-polyp" distance of 1.9 l.u. The top plane was kept at a concentration of $R = 1.0$, whereas the ground plane was set to $R = 0.0$, thus reflecting the active take-up of resources by competing sessile organisms in the sea-floor, such as hydrozoans, coralline algae and other corals. These boundary conditions created a vertical concentration gradient over the simulation box; indeed such concentration gradients of zooplankton have been observed at night in coral reefs of the Red Sea (Horzman & Genin, 2002). The resulting growth forms were strongly branched, and they were robust against the noise that was added in the "polyp" insertion rules (see Chapter 4), as demonstrated by the alternative realisations shown in Fig. 5.3c. These growth forms have a similar appearance and the same compactness (see error bar in Fig. 5.4i).

Note that in this model branching growth occurred spontaneously for much lower values of θ_{AD} than in the HIRAG model (Chapter 4), although we did not use an explicit curvature rule. Yet, it may be possible to explain branching by a similar process. Absorption took place at a distance $l_{\mathrm{reach}} = 3$ l.u. from the skeleton, corresponding to real coral polyps, where the mouth and tentacles are located at a small distance from the coral surface. This causes the "polyps" to fan out at convex locations, giving them better access to the resources than "polyps" located at flat or concave parts of the "coral" surface. At concave sites the resources may thus be more quickly depleted, because many "polyps" absorb resources from the same location and resource replenishment to concavities is poor. This suggests that the resource flux into the "polyps" correlates positively to the local curvature. Indeed in Fig. 5.3 the resource flux is highest at the tips of the "coral" branches. Hence the local deposition rate correlates positively to the local curvature. A curvature effect, caused by the "polyps" fanning out at convex sites, may thus enhance the underlying Laplacian growth mechanism in generating branching growth forms. The more the absorbing "mouths" of the "polyps" fan out, the quicker

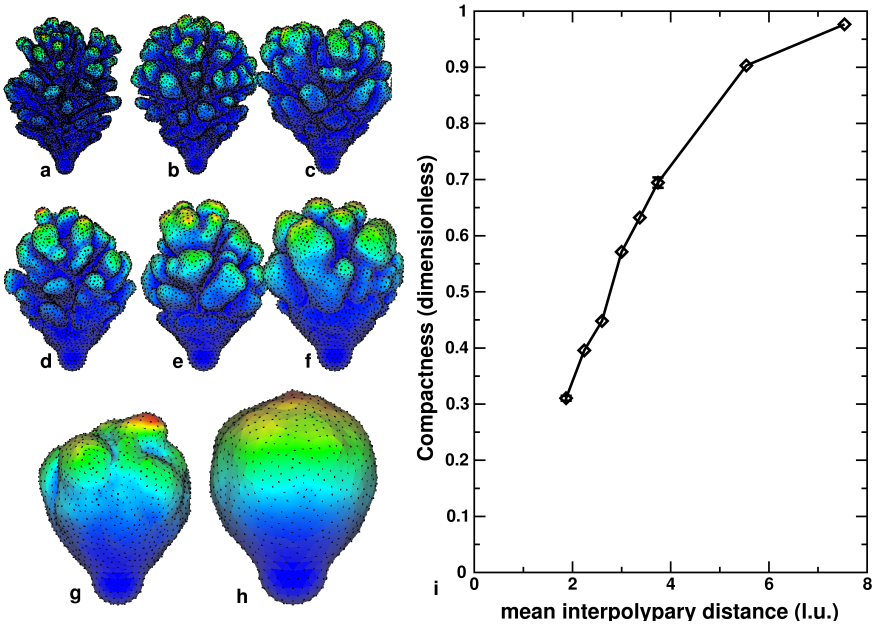

Fig. 5.4: Range of "coral" morphologies with increasing mean "inter-polyp distance. 85 growth cycles. Initial sphere has 181 "polyps". (a) "Inter-polyp" distance is 1.9 l.u. (b-f) Mean "inter-polyp" distance increases with regular intervals to 3.7 l.u. (g) "Inter-polyp" distance 5.5 (h) "Inter-polyp" distance 7.5 (i) Compactness (Eq. 3.4) after 85 growth cycles as a function of the mean "inter-polyp" distance. Error bars are given for first and sixth value (n=10). Colour scale: resource flux

the resource is taken up by the "polyps". One would therefore expect, that the mean "polyp" spacing modulates the curvature effect, which in turn affects the growth form. We have tested this hypothesis by starting with initial hemispheres of increasing radius, each of them having 81 "polyps". The initial spacing of the "polyps" dictates the mean "inter-polyp" distance in the growth form, because the insertion and fusion threshold θ_{INS} and θ_{FUSE} are set relative to the initial mean "inter-polyp" distance.

In Fig. 5.4 a range of growth forms obtained after 84 accretive growth cycles is shown. In Fig. 5.4a, the mean "inter-polyp" distance was 1.8 l.u., increasing to 7.5 l.u. in Fig. 5.4h. In these experiments the size of the "polyps" did not change, since in both cases the resources were absorbed from a single lattice node. With increasingly wide "polyp" spacing, the branches became thicker and less numerous, as expressed by the compactness shown in Fig. 5.4i. Also, the branches split less quickly; the branch grew for a longer time before splitting up. It would of course be possible that this morphology change was caused by a finite size effect, in which case the far right "lobed coral" would become a scaled up version of the far left morphology when grown for another 85 growth cycles. In order to exclude this possibility we continued the growth of the

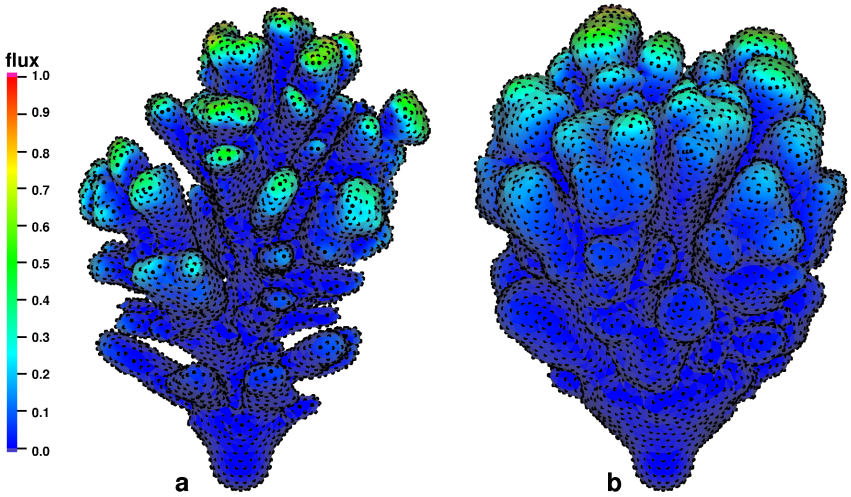

Fig. 5.5: (a) Coral with initial "inter-polyp" distance of 1.9 l.u. (Fig. 5.4f.) after 150 half growth steps, C=0.32 (b) Coral with initial "inter-polyp" distance of 3.7 l.u. (Fig. 5.4a.) with 150 growth steps. C=0.59

"coral" in Fig. 5.3 until we obtained 150 growth layers[3] (see Fig. 5.5b). Indeed, the resulting morphology was quite different from the "thinly branched" morphology that developed with a "inter-polyp"distance of 1.8 l.u. Another possible explanation for the morphology change would be that in a "lobed" morphology (such as Fig. 5.4f.) — relative to the "polyp" spacing — smaller growth steps were taken than in a "thinly branched coral" (Fig. 5.4a.). In order to exclude this possibility, we halved the growth steps of the "thinly branched coral" and left the other parameters unchanged. After 150 growth cycles we obtained the morphology as shown in Fig. 5.5, where all dimensions were scaled up by a factor 2 for comparison. This morphology has a similar compactness to that of Fig. 5.4a, but it is somewhat more thinly branched. This could be attributed to the more frequent calculation of the resource fields, as we will discuss later in this section. We conclude that the "polyp" spacing is the most probable explanation for the shown morphology change.

In Fig. 5.6 we reconstructed the trajectories of the "polyps" of the objects shown in Fig. 5.4a and 5.4f. These trajectories are constructed by connecting the "polyp" centres v_i in the subsequent growth layers. They are built up from many subtrajectories, since the "polyps" move through the plane of intersection during the growth process. This figure allows us to get an impression of the "polyp" trajectories similar to the impression one can get from the study of X-ray skeleton slices of real corals (Fig. 5.6c).

Above we assumed that the top plane was a nutrient source and the ground plane was a nutrient sink. In order to test the effect of these boundary conditions on the devel-

[3] Shortly hereafter the object grows into the boundaries after which further simulation is not sensible.

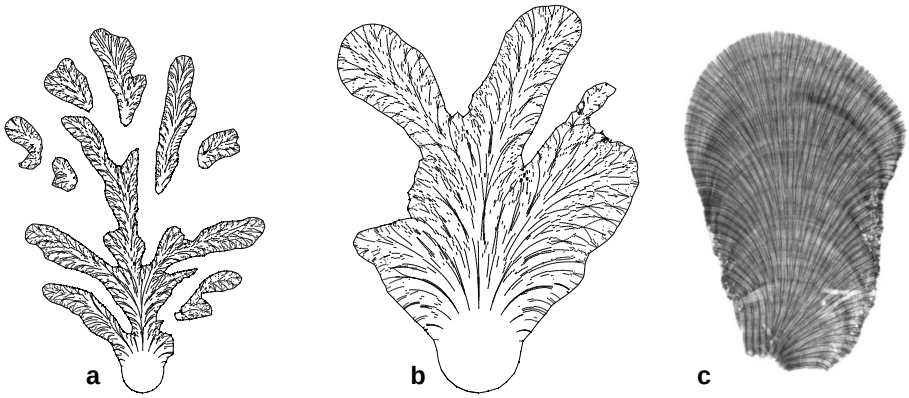

Fig. 5.6: "Polyp" trajectories in cross sections of (a) Fig. 5.4a. and (b) Fig. 5.4f. (c) Radiograph of a slice of *Montastrea annularis*

oping morphologies, alternative boundary conditions were applied. In Fig. 5.7 we have shown two results of the PORAG model with a simulation box in which the ground plane was made impenetrable to the diffusing resource, as if there were no competing organisms in the sea floor. This influenced the shape of the resource field. When the ground plane absorbed resources, the coral grew in a top to bottom resource gradient, but when the ground plane was made impenetrable to the resource, initially the simulation box was filled with a uniform resource concentration. In this case, the growth form attained a more hemispherical shape, and was flattened against the ground plane. The branching structure and the dependence on the "inter-polyp" distance, however, were probably not affected by the boundary conditions, as expressed by the compactnesses of the objects that were close to those in Fig. 5.4a. and in Fig. 5.4f.

The periodic boundaries also affected the growth forms. If we would consider an isolated coral growing outside a reef, resources would diffuse in equally from the top plane and the side planes. We tested this growth situation in Fig. 5.8, where the ground plane was a resource sink, and all four side planes and the top plane were sources. We obtained a more hemispherical growth form, that is slightly elevated from the ground plane. Again, the branching structure is not strongly affected by the changed boundary conditions, as indicated by the compactness values.

Like in the HIRAG model as described in Chapter 4, the convergence of the resource field θ_{MP} is an important parameter in determining the growth form. In agreement to the results obtained with the HIRAG model, we found compact growth forms when the resource field had insufficiently converged at the onset of a new growth step, and we found forms with a wider branch spacing when the resource field was closer to equilibrium at the onset of a new growth step (Fig. 5.9). With these results it becomes possible to understand why the growth form developed with half size accretion steps (see Fig. 5.5a.) was more thinly branched. The double amount of growth cycles results in better converged resource fields. Note that in the PORAG model branching also occurs for a convergence of $\theta_{\mathrm{MP}} = 10^{-4}$ Fig. 5.9c. For such a low convergence in the HIRAG model branching did not occur spontaneously. Thus the "polyp fanning" effect

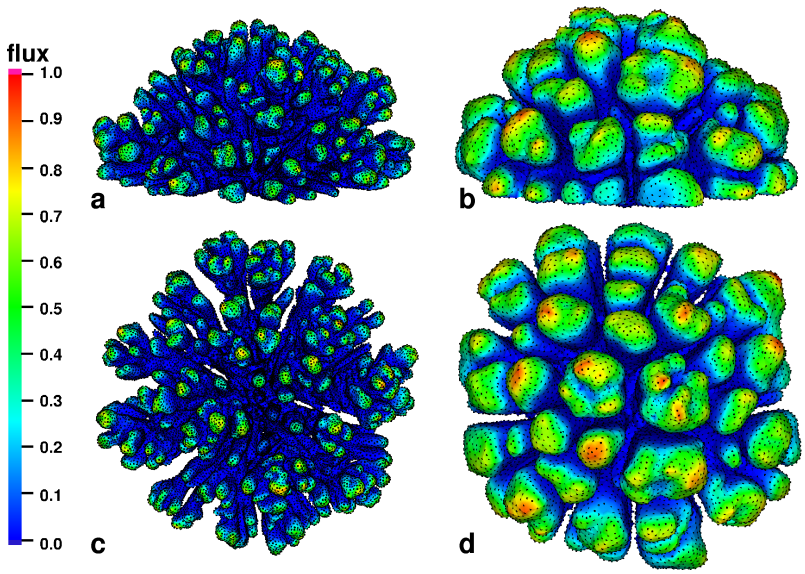

Fig. 5.7: Simulation of the growth function I PORAG model with a non-absorbing ground plane. Morphology after 80 growth cycles. Side view (a. and b.), 10° elevation) and top view (c. and d.), 90° elevation). "polyp" mouths are shown as black dots. The "polyp" spacing in a. and c. is 1.8 l.u. and $C = 0.24$. (compare Fig. 5.4(a)). In b. and d. it is 3.7 l.u. and $C = 0.56$ (compare Fig. 5.4f). The other parameters are as in Fig. 5.3.

is a more robust branching mechanism than the Laplacian growth mechanism that we have described in chapter 4.

5.3.2 Growth function II

In this section growth with growth function II (Eq. 5.2) is studied. In this extreme of the range of growth functions we assume a coenosteal skeleton that is dense and voluminous relative to the skeleton deposited in the calices. Thus we approximate this process by assuming the growth of a skeleton of uniform density. As a first approach we assumed strict boundaries between the areas of influence of the "polyps". The resource taken up by the "polyp" was uniformly distributed over its area of influence and no transport of resource over the coral surface was allowed. In figure 5.10 we show two of the resulting morphologies, with an "inter-polyp" distance of 1.8 l.u. (Fig. 5.10a) and an "inter-polyp" distance of 3.7 l.u. (Fig. 5.10b). We found the same trend as with growth function I: higher "inter-polyp" distances result in thicker and more lobed growth forms. However, the branches are more rugged than with growth function I. The

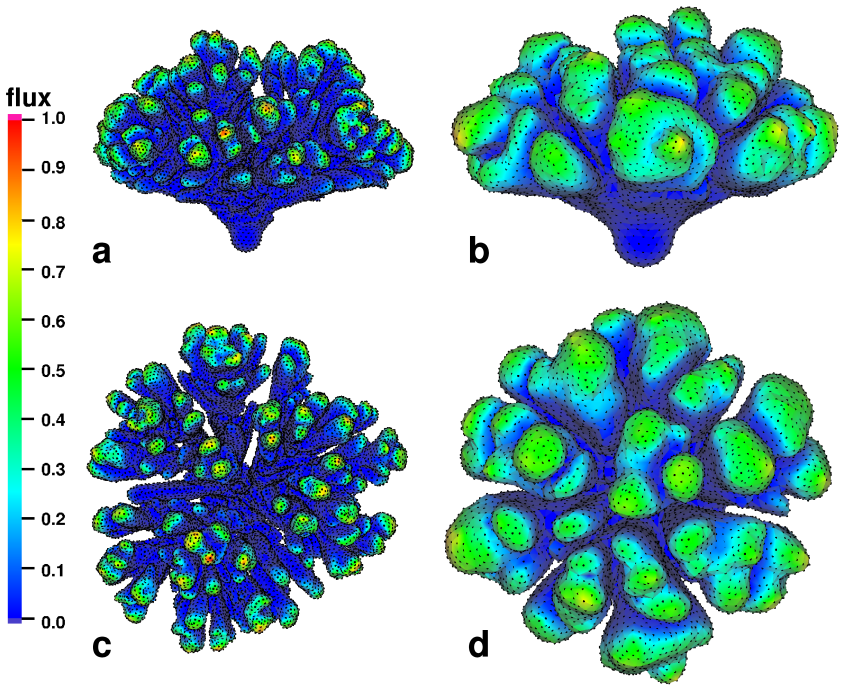

Fig. 5.8: Simulation of the growth function I PORAG model; sources at side- and top-planes, absorbing boundary at the ground plane. Morphology after 75 growth cycles. Side view ((a) and (b), 10° elevation); top view ((c) and (d), 90° elevation). "Polyp" mouths are shown as black dots. The "polyp" spacing in (a) and (c) is 1.8 l.u. and $C = 0.26$ (compare Fig. 5.4a). For (b) and (d) it is 3.7 l.u. and $C = 0.58$ (compare Fig. 5.4f). Other parameters as in Fig. 5.3.

area of influence of the "polyps" is highly variable, leading to a highly variable intra-polyp resource concentration. This causes the skeletal growth rate to vary from one "polyp" to its neighbours, which results in the irregular growth forms of the "corals" shown in figure 5.10.

It may however be unrealistic to assume that the "intra-polyp" resource concentrations vary so much from one polyp to the other. Translocation of nutrients has been shown to occur in the branching scleractinian *Stylophora pistillata* (Rinkevich & Loya, 1983) and in the massive scleractinians *Favia favus* and *Platygyra lamellina* (Oren *et al.*, 1997), presumably through the coenosarc, the tissue covering the coenosteum. Including such nutrient translocation in the PORAG model would result in a more gradual change of resource concentration between "polyps". In the extreme case where no lateral resource translocation would take place, the "intra-polyp" resource concentra-

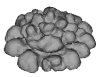

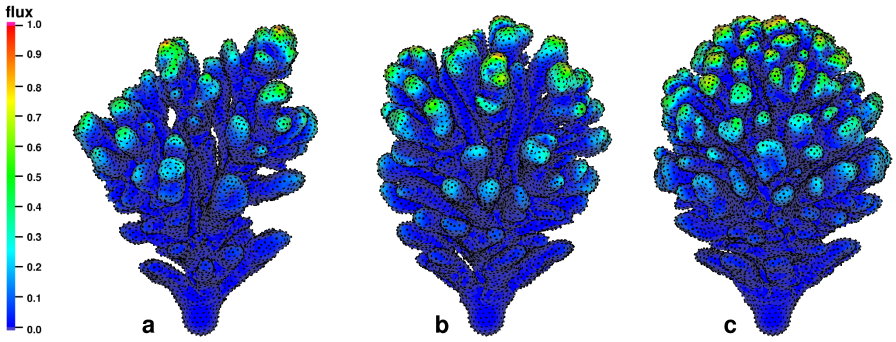

Fig. 5.9: Effect of resource field convergence in the PORAG model. (a) $\theta_{\mathrm{MP}} = 10^{-6}$, $C = 0.29$ (b) $\theta_{\mathrm{MP}} = 10^{-5}$, $C = 0.30$ (c) $\theta_{\mathrm{MP}} = 10^{-4}$, $C = 0.39$. All parameters are set as in Fig. 5.3.

tion would be fully determined by the resource flux and the "polyp" area, and we would obtain the situation as shown in figure 5.10. In the other extreme case where extensive lateral resource transport would take place, uniform growth would occur, resulting in hemispherical growth forms. We modelled the intermediate cases by allowing for some diffusion of resources over the coral surface using a method for surface diffusion on triangulised manifolds (Zemlin, 2000). Depending on the amount of surface diffusion that we allowed, more smoothened, regular morphologies were found (Fig. 5.11). As we increased the amount of surface diffusion, we found increasingly thick branches.

5.4 Conclusions and discussion

In this chapter we introduced the polyp oriented approach to modelling coral growth. In this approach, we consider coral growth as the collective behaviour of many individual coral polyps, where genetics and the environment can only affect the morphology through their effect on each of the coral polyps.

We have tested two extremes of a range of growth functions. In the one extreme, growth function I, the skeletal extension rate was directly proportional to the resource uptake rate. The morphologies that developed in this model sometimes resemble natural coral morphologies surprisingly well, which can for instance be seen by comparing the morphologies in Fig. 5.3 and in Fig. 5.7 to the colonies of *Madracis mirabilis* shown in Fig. 1.6. For further visual comparison, the real corals were scanned with a CT-scanner (Kaandorp & Kübler, 2001). A triangulised surface was constructed from the resulting 3D-dataset; the surface was simplified to obtain a surface described with approximately the same amount of triangles as the simulated objects. The resulting datasets are shown in Fig. 5.12 together with the simulated objects of Fig. 5.3 and Figs. 5.7b. and 5.7d. respectively. By showing natural morphology through such a "filter" of computer visualisation, one obtains a "Turing-test" (Turing, 1950) for sim-

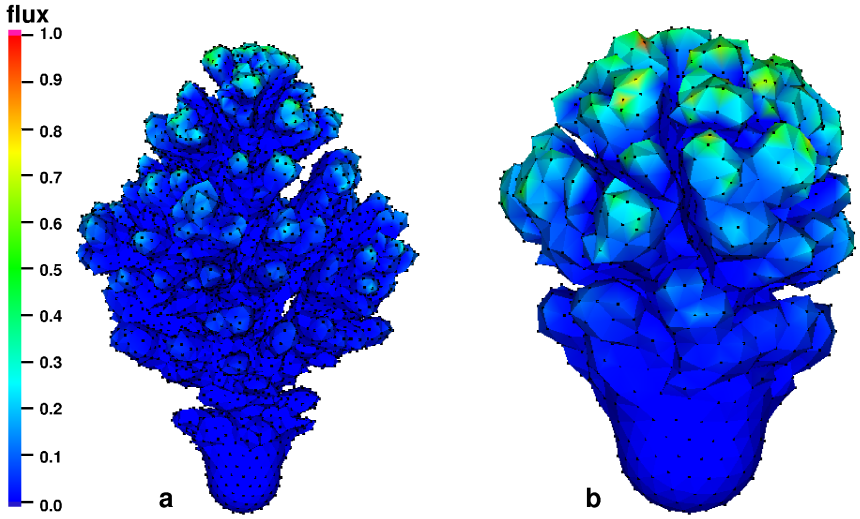

Fig. 5.10: "Coral" morphologies generated by the growth function II model (Eq. 5.2). The colour scale gives the normalised value of the growth function. (a) "inter-polyp" distance is 1.8 l.u., $C = 0.30$(b) "inter-polyp" distance is 3.7 l.u., $C = 0.63$

ulated morphology. A small, non-representative survey among colleagues revealed that most of them easily distinguished the simulated from the natural morphology in Fig. 5.12a, while many of them confused them in Fig. 5.12b[4]. Indeed, according to coral biologists working in the field, the hemispherical morphologies in Fig. 5.7 show more resemblance to real coral colonies, such as *Madracis mirabilis* (Fig. 5.7a.) and *Madracis decactis* or possibly *Montastrea annularis* (Fig. 5.7b.), than the upwardly growing morphologies in Fig. 5.3 (Mark Vermeij, personal communication). Note that to attain such similarity, we have not included any specific assumptions in our model. One should however be extremely careful when interpreting such visual similarity, since morphological similarity does not imply a similar growth process. Extensive morphometry would be necessary to better compare simulated and natural morphologies, for which recently developed tools could be used (García Leiva, 2001; Kaandorp & Kübler, 2001). As a start of such comparisons, we measured the compactness of the simulated objects and found that the objects in Fig. 5.12a were of similar compactness, while the compactnesses of the objects shown in Fig. 5.12b were quite different. It would be easy, but not necessarily informative, to attain more similar compactnesses by tuning model parameters such as the polyp spacing. In order to compare the simulated growth process to natural coral growth, correlations between model parameters and morphologies should be compared to such correlations in natural morphology.

In the other extreme of the range of growth functions, in growth function II, we

[4]Please do try out the "Turing-test" in 3D; it has been made available on the CD-ROM accompanying this thesis.

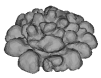

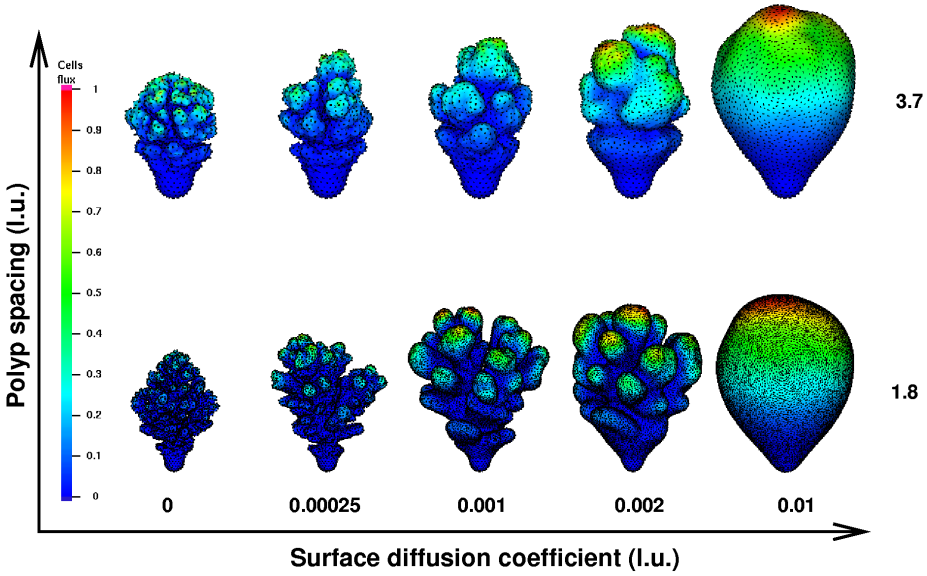

Fig. 5.11: A morphospace of "coral" morphologies generated by the growth function II model of coral growth, with 85 growth cycles. A small amount of resource diffusion along the surface was applied (1000 surface diffusion iterations with $\Delta t = 0.01$). The colour scale gives the normalised value of the growth function (Eq. 5.1).

assumed that the accreted *volume* of skeleton was directly proportional to the resource uptake rate. The morphologies produced under this assumption (Fig. 5.10) do not resemble real coral colonies. They are more irregular and rugged, because variations in polyp spacing caused variations in resource concentrations in the polyps, resulting in variable skeletal accretion rates. In this model the polyps were strictly isolated from each other, which may be an unrealistic assumption, because the gastrovascular cavities of coral polyps are connected through the coenosarc. Moreover, there is evidence that resources are translocated in corals and in other colonial cnidarians (Rinkevich & Loya, 1983; Oren *et al.*, 1997; Gateno *et al.*, 1998). In Fig. 5.11, we allowed some resource transport. This caused the growth forms to become more regular and more similar to real corals.

In both of these model variants, the morphologies branched spontaneously. The mechanism through which such branching occurs suggests a hypothesis on branching growth in stony corals, which we discuss in Section 5.4.1. We believe that the polyp oriented modelling approach could be used in studying the effects of environmental and genetically influenced polyp traits on the colony morphology. As a first attempt of such studies, we have assessed the effect of resource translocation and polyp spacing on coral morphology. This approach is discussed in Section 5.4.2. The presentation of the polyp oriented approach in coral growth modelling is concluded in Section 5.4.3.

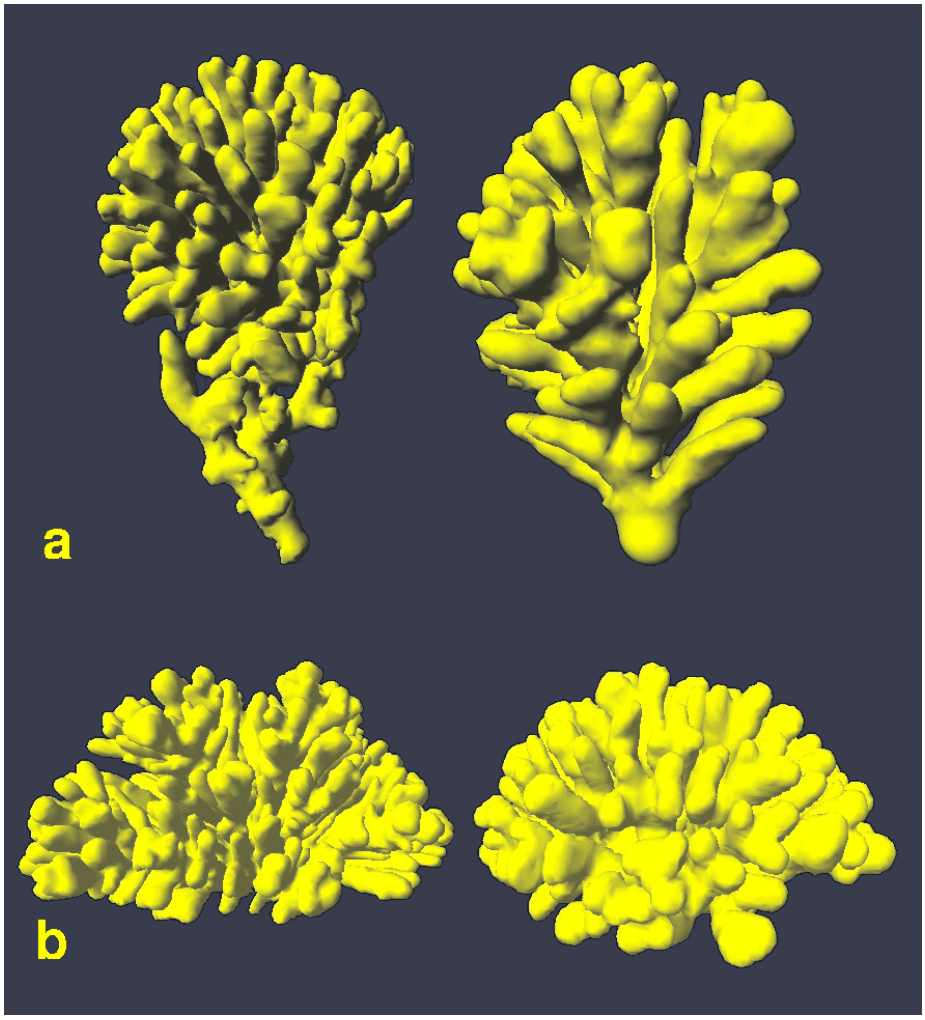

Fig. 5.12: Turing test for simulated coral morphogenesis. a) left: scanned growth form of *Madracis mirabilis* ($C = 0.29$); right: simulated growth form of Fig. 5.3 ($C = 0.30$). b) left: simulated growth form of Fig. 5.7b,d ($C = 0.24$); right: scanned growth form of *Madracis mirabilis* ($C = 0.41$)

5.4.1 Branching: the Polyp Competition Hypothesis

In the polyp oriented approach, branching occurs as an emergent property of our model. This finding and the occurrence of branching growth in the HIRAG model (see Chapter 4) contrast previous models of branching coral growth, where an explicit curvature rule was introduced to enforce branching growth(Kaandorp, 1995; Kaandorp & Sloot, 1997; Kaandorp, 2001; Kaandorp & Sloot, 2001).

The polyp oriented model suggests a biological explanation for branching growth in stony corals. At convex sites, the polyps fan out, thus getting better access to the diffusing resources. At concave sites, the polyps point towards each other, thus interfering in the uptake of resources. In this way, a curvature effect comes out as a natural consequence of the competition between the polyps to take up resources from the water. Indeed, in many coral species the polyps protrude above the coenosteum. Gardella & Edmunds (2001) cite a polyp protrusion of $2.6 \pm 0.1\ mm$ for the branching coral *Dichocoenia stokesii* and a protrusion of $9.6 \pm 0.5\ \mu m$ (sic) for *Stephanocoenia michilini*. Assuming that the width of the simulation box is $0.3\ m$, for which the height of the growth form in Fig. 5.3 is $0.167\ m$, the "polyps" in our model protrude $4.5 \times 10^{-3}\ m$ above the coenosteum, which is in the same order as the protrusion length given for *Dichocoenia stokesii*. Note that the actual protrusion length is a bit lower in our model, since the given protrusion length is measured from the triangular mesh, and not from the voxelised surface in the lattice Boltzmann grid. We have also tested longer and shorter protrusion lengths. The "polyp" protrusion parameter (l_{reach}) does not have a large influence on the branching pattern in the PORAG model (results not shown).

As the mean "inter-polyp" distance increased (Fig. 5.4), the model "corals" branched less strongly. This observation fits well within the "polyp competition hypothesis" that we proposed above. The competition for resources becomes less strong for larger mean "inter-polyp" distances. This conclusion is further supported by a geometric analysis in which we relate the fraction of the "coral" surface area that belongs to an absorbing "polyp mouth" to the local curvature. For this analysis, consider the two-dimensional diagram of the coral surface shown in Fig. 5.13a. The curvature of this surface is given by $\kappa = 1/r$, while the ratio between the "absorbing" area of the coral surface (i.e. the voxels of the "polyps" from which the growth resources are absorbed) and the total non-absorbing area between the "polyps" is expressed as follows. The total "absorbing length" d_2 is given by $d_2 = (1+\kappa l_{\mathrm{reach}})d_1$, where d_1 is the "inter-polyp"-distance. Assuming resource absorbance in a single, spherical voxel (indicated by the black circles) with $r = 0.5$ l.u., the "absorbance-ratio" a is expressed by

$$a(\kappa, d_1) = 1/(1 + \kappa\ l_{\mathrm{reach}})d_1 \tag{5.3}$$

Studying the partial derivative to κ of this function,

$$\frac{\partial a(\kappa, d_1)}{\partial \kappa} = -\frac{l_{\mathrm{reach}}}{d_1(1 + \kappa\ l_{\mathrm{reach}})^2}, \tag{5.4}$$

for $l_{\mathrm{reach}} = 3$ (as used in this Chapter) and $\kappa = 0$ (i.e. $\frac{\partial a}{\partial \kappa} = -3/d_1$) we can see that a small change of the curvature, due to a growth step, more strongly affects this

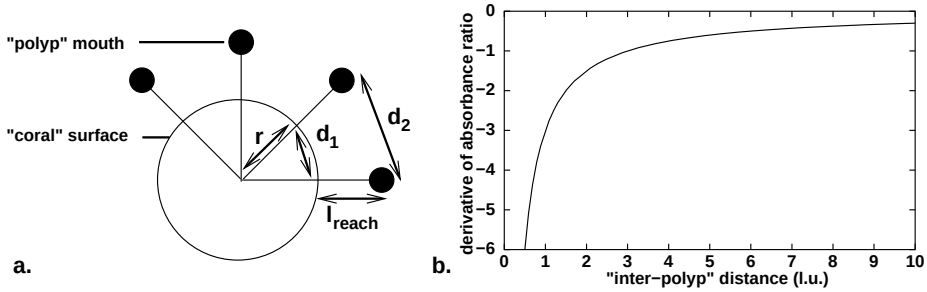

Fig. 5.13: Geometric analysis of the "polyp"-fanning effect. a) Two dimensional diagram of the coral surface. r, radius of curvature; d_1, "inter-polyp" distance; d_2, distance between "polyp"-mouths. b) Derivative at $\kappa = 0$ of the ratio between non-absorbing area and total area of the coral surface as a function of the "inter-polyp" distance d_1. $l_{\mathrm{reach}=3}$ and the polyps absorb resource from a single voxel

absorbing surface fraction if the "polyps" are more densely spaced (Fig. 5.13b). For large "inter-polyp"-distances, the curvature effect saturates to 0, which agrees well with the resulting non-branching morphologies as shown in Fig. 5.4.

The "polyp fanning" mechanism of coral branching that we suggest here, is a more robust putative mechanism of coral branching that the Laplacian growth mechanism that we have discussed in Chapter 4. There we showed that spontaneous branching can also occur in the hydrodynamically influenced radiate accretive growth (HIRAG) model. We treated the coral surface as a fully absorbing discretised continuous surface, instead of modelling the polyps individually as we did here. In the HIRAG model, branching only occurred when the resource field was computed until near stability ($\theta_{\mathrm{MP}} = 10^{-6}$), whereas here a much less strict convergence criterion ($\theta_{\mathrm{MP}} = 10^{-5}$) was sufficient. Hence the polyp fanning effect seems to promote branching even if the resource field is not in complete equilibrium. We have discussed in Chapter 4 that it is not likely that resource fields reach full equilibrium in real coral reefs, because the diffusion coefficients of the relevant resources are too low.

In the PORAG model, the polyp fanning effect promotes branch splitting despite insufficient resource field convergence. This may render the PORAG model a more likely and robust explanation of branching growth in corals than the HIRAG model. In the HIRAG model any disturbance of the resource fields had a strong impact on the growth forms, whereas the PORAG model appears not to be that sensitive to disturbances.

5.4.2 Morphologic plasticity

In Fig. 5.4 we demonstrated that the growth forms in the PORAG model becomes less thinly branched and more compact with increasing "inter-polyp" distance. Correlations between the polyp distance and the morphology are also found in natural corals, for example along an environmental gradient in *Madracis mirabilis* (Bruno & Edmunds,

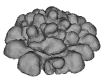

1997). At lagoon habitats up to $10\ m$ the branches of this species are more bulbous, and have a larger diameter than branches of colonies growing in fore reef habitats at depths of $10\ m$ to $20\ m$. Transplantation experiments showed that these traits are largely determined by environmental differences between the lagoon and fore reef habitats. Both the branch tip diameter and the calix spacing varies significantly between the two habitats. In the fore reef habitats the calix spacing is somewhat higher than in the lagoon habitats, while the branch tip diameter was found to be a bit smaller in the fore reef habitats(Bruno & Edmunds, 1997). Hence the trend in *Madracis mirabilis* seems to be opposite to the trend found in the PORAG model. Note however, that this study did not provide evidence for a causal relation between branch thickness and polyp spacing; due to the many environmental differences between the two habitats studied, such causality would be indistinguishable effects of other environmental parameters.

The relation between calix spacing and colony morphology might be more consistent to the PORAG model in *Montastrea annularis*. In this species three — genetically distinct — morphotypes are distinguished, a *bumpy*, *massive* and *columnar* type (Van Veghel & Bak, 1993); the columnar type forms parallel upright "branches", whereas the massive and bumpy types have more hemispherical and encrusting morphologies. The calices are often more widely spaced in *bumpy* morphologies than in *massive* and *columnar* morphologies (Van Veghel & Bak, 1993; Graus & Macintyre, 1982). In *Porites sillimaniani* Muko *et al.* (2000) found branched colonies under bright conditions and flat morphology under dark growth conditions. However, here no difference in calix spacing was found between the morphologies (Muko, personal communication). Unfortunately, not enough data is available to conclude whether a relation between calix spacing and colony morphology is found in the real world. Systematic measurements on preserved coral specimens would be necessary to settle this issue.

In the above mentioned field studies the correlation between calix spacing and colony morphology is often hard to distinguish from other factors that may influence the morphology. The experimental knowledge on the controlling parameters of morphological plasticity is sometimes fragmentary. Transplantation experiments are mostly carried out in natural environments due to the difficulty of culturing corals in controlled conditions (see for example Becker & Müller, 2001; note that much progress has been made by aquarists the last decenniums, see for a review Carlson, 1999). It is therefore hardly possible with experiments alone to distinguish possible environmental effects on coral morphology.

The polyp oriented modelling approach may help to provide insight in how single environmental parameters control coral morphogenesis. It is often possible to study the effects of single environmental parameters on single, young polyps under controlled conditions. For example, in a recent paper (Meroz *et al.*, 2002) the effect of gravity on skeletal deposition by young polyps was studied. The polyp oriented modelling approach would make it possible to study and understand how such plasticity on the level of the individual polyp can affect the morphology of the whole colony; one could generate morphospace which would relate the measured behaviour of the individual polyp to changes at the level of the coral colony.

5.4.3 Polyp Oriented Modelling

We have developed a polyp oriented approach to modelling coral growth. In this polyp oriented approach, morphogenesis is the natural consequence of the behaviour of the individual polyps at the coral surface. Despite the myriads of unanswered questions, of which some were touched in the previous sections, we believe that with the polyp oriented model of accretive coral growth we have made a start in bridging the gap between the "mechanistic" explanations of morphologic plasticity and the "adaptive" explanations of morphologic plasticity. The genetically and environmentally driven properties of the individual polyps ultimately determine the outcome of the growth process. For example in our example of the effect of "polyp" spacing, we see that the spacing of "polyps" determines the size and spacing of "coral" branches. Polyp spacing may be a trait that is influenced either adaptively, as a genetically fixed reaction to the environment, or a trait that is "passively" determined by the environment. Thus the polyp oriented approach will be useful in understanding how genetic and environmental information drives the morphogenesis of coral colonies. Genetics affects coral morphology indirectly, by setting the properties of the individual coral polyps. The environment may influence the coral morphology either on the level of the individual polyp or on the level of the whole colony.

Finally note that the polyp oriented modelling could also be used to study the feedback of the coral morphology on the fate of individual polyps. Cross sections of the simulated corals (Fig. 5.6) give an indication of the trajectories of the "polyps". These figures suggest that the "polyps" move away from each other at convex sites, allowing for the insertion of new polyps, whereas the "polyps" approach each other at surface concavities, resulting in frequent "polyp" fusions. Such concave regions of "polyp" fusion appear to occur often between branches, while at other places they may indicate the onset of branching. Preliminary results suggest that in our model the "polyps" in finely branched morphologies had a shorter life-time than the polyps in the more compact morphologies, possibly because the probability of reaching a concavity is higher in finely branched morphologies (results not shown). Such a relation between coral morphology and the life-time of polyps was also found in massive *Porites* colonies (Darke & Barnes, 1993). To further understand this phenomenon, in future studies we plan to follow the growth trajectories of the "polyps" through time and to compare these to polyp trajectories in real corals.

5.5 Acknowledgements

We thank Christian Zemlin (Humboldt Universität Berlin) for his kind permission to make use of his unpublished method for diffusion on triangulised manifolds, Mark Vermeij (Cooperative Institute for Marine and Atmospheric Studies), Rolf Bak (Netherlands Institute for Sea Research) for making available the corals in Fig. 1.6 and Leo E. H. Lampmann (St. Elisabeth Hospital, Tilburg) for CT-scanning the corals.

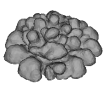

CHAPTER

SIX

Towards a Problem Solving Environment for Morphogenesis[1]

Apart from experimental and theoretical approaches, computer simulation is an important tool in testing hypotheses about biological morphogenesis. However, the construction and use of such simulation tools needs extensive computational skills and knowledge that is not available to most research biologists. Problem solving environments (PSEs) aim to provide a framework that hides implementation details and allows the user to formulate and analyse a problem in the language of the subject area. We have developed a prototypical PSE which enables computationally untrained researchers to experiment with the simulation models presented in this thesis. In this chapter we discuss its design and implementation, and present a performance analysis on two parallel systems. We discuss the relevance of our results for the future development of PSEs for studying morphogenesis and development.

6.1 Introduction

During its development, the three-dimensional shape of an organism is unfolded, guided by the genetic information stored in the DNA. To understand this process, called morphogenesis, it is very important to unravel the physical mechanisms underlying it (see for example Newman, 2002. Apart from experimental and theoretical approaches, during the last decenniums computational approaches have become more and more important in the study of morphogenesis. For example, a computational model was

[1]This chapter is based on: R. M. H. Merks, A. G. Hoekstra, J. A. Kaandorp and P. M. A. Sloot. Towards a problem solving environment for morphogenesis, Submitted and R. M. H. Merks, A. G. Hoekstra, J. A. Kaandorp and P. M. A. Sloot (2003). A Problem Solving Environment for Morphogenesis. To be published in the proceedings of ICCS 2003, *Lecture Notes of Computer Science*, St. Petersburg, Russia.

used to study the formation of lateral branches in the unicellular alga *Acetabularia acetabulum* (Mermaid's Cap) in terms of the interaction between turgor and cell wall strength (Brière & Goodwin, 1988; Goodwin, 1994). In the study of the life cycle of the cellular slime mould *Dictyostelium discoideum* experimental, theoretical and computational approaches are becoming equally important (see e.g. Segel, 2001; Marée & Hogeweg, 2001; Vasiev & Weijer, 1999). We have applied computational models to understand the morphogenesis and environmental plasticity of stony corals (see e.g. Kaandorp *et al.*, 1996; Kaandorp & Sloot, 1997; Kaandorp & Sloot, 2001; and this thesis). In these models, a computational model of the growing coral was combined with a model of the physical environment.

Developing and using the tools needed for such computational studies needs extensive training and knowledge that is not widely available to research biologists. Computational studies are therefore often carried out by mathematicians, physicists, computer scientists or computationally trained biologists, who inevitably spend a major part of their time in code and algorithm development. Problem solving environments (PSEs) (Gallopoulos *et al.*, 1994; Rice & Boisvert, 1996) are software systems aiming to alleviate this issue. They hide the implementation details of a simulation code and allow the user to formulate the problem at a higher abstraction level, in the language of the problem being studied. The low-level software engineering of numerical methods and algorithms is carried out by technical and mathematical specialists, while the biological researcher can consider these methods as a "black box" and concentrate on the biological problem. To do so safely, PSEs should contain some knowledge about the simulation system, in order to be able to advise the user about the chosen parameters and warn him or her when necessary. For example, a modeller who uses partial differential equations (PDEs) should be concerned only about the equation itself and not about the huge amount of mathematical and computational literature about their efficient, and correct numerical solution. The PSE ideally contains a set of ready made PDE solvers and advises the user on which one to use[2]. Problem Solving Environments also often aim to facilitate interfacing to new technologies for distributed and parallel computing, such as Grid (Foster *et al.*, 2001) middleware, for example the storage resource broker (SRB) [3]. The SRB provides transparent access to geographically distributed data storages. To do so, PSEs often have a modular architecture where the simulation codes and possible legacy codes communicate through a software layer, enabling easy and transparent migration to new architecture (Marinescu & Boloni, 2000; Iskra *et al.*, 2002). Thus, PSEs should make it possible to separate the technical work on the simulation codes, numerical methods and the mapping on the computing architecture from the conceptual computational experimentation and analysis.

In this chapter we describe a prototypical PSE which allows computationally untrained marine biologists to experiment with the simulation models discussed in this thesis. In this PSE the problem can be formulated in high-level terminology. Boundary conditions and initial conditions are made available as independent modules, enabling easy specification of the simulation set-up. The modular architecture encourages a

[2] See for a PSE for certain classes of PDE applications: `http://www.webpdelab.org/`

[3] `http://www.npaci.edu/DICE/SRB/`

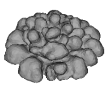

multi-model approach, were different models and solving methods can easily be tested and compared. In Section 6.2 the problem set covered by the PSE will be shortly described. In Section 6.3 we will describe the software architecture of the PSE. The performance of the PSE was evaluated on two parallel systems, which we discuss in Section 6.4. Finally, in Section 6.5 we will discuss the relevance of our results for the simulation of morphogenesis.

6.2 Model and Methods Covered by the PSE

The coral growth PSE enables experimentation with several models of coral morphogenesis. These models can be roughly divided into two classes, the *aggregation* models and the *accretion* models. The aggregation models (see also Chapter 3) are based on a Meakin growth model (Meakin, 1986), which is a generalisation of the diffusion-limited aggregation (DLA) model as introduced by Witten and Sander (Witten Jr. & Sander, 1981). In the DLA model an initial solid seed is placed in an (n-dimensional) simulation box. A particle, carrying out a random walk, is released until it hits a solid particle to which it attaches irreversibly. This procedure is iterated until an aggregate has formed. In the Meakin model (Meakin, 1986) the random walks are ensemble averaged and approximated by the diffusion equation, which is solved on a structured lattice. The solidified particles are sinks and a source is placed at a certain distance from the cluster. The probability that a nearest neighbour of the cluster solidifies is then given by the particle concentration. In an extension of this model, the particles are transported both by advection and by diffusion (*advection-diffusion limited aggregation*: ADLA). This model was studied by Kaandorp *et al.* (Kaandorp *et al.*, 1996; Kaandorp & Kübler, 2001) and in Chapter 3 as a model of coral growth under the influence of fluid flow.

In the accretion models (see Chapters 4-5) growth occurs due to the iterative construction of layers, represented by triangular meshes. In contrast to the aggregation models, in these models growth occurs in parallel all over the surface. This iterative accretive construction can be considered either a discrete (e.g. seasonal) process or the discretisation of a continuous growth process (see Section 4.2). The local thickness of the accreted layers can depend on a number of factors. In the first accretive growth models, it depended on the local curvature of the surface and on a "growth axis" (Kaandorp, 1994a; Kaandorp, 1995). In later models, the availability of a nutrient in the surrounding water was also taken into account. This nutrient was transported by diffusion (Kaandorp & Sloot, 1997) or by advection and diffusion (Kaandorp & Sloot, 2001). The latter model is called the *hydrodynamically influence radiate accretive growth* (HIRAG) in this chapter. The influence of advection-diffusion on accretive growth was reassessed in Chapter 4. In the *polyp oriented radiate accretive growth* (PORAG) model, the individual polyps contributing to the growth process are explicitly taken into account (Merks *et al.*, 2002a; Merks *et al.*, 2002b; Chapter 5). Both the HIRAG and PORAG models have been included into the coral growth PSE.

In Fig. 6.1 we present a flow diagram of these accretive coral growth models. The simulations are carried partly in parallel, as indicated by the decomposed computa-

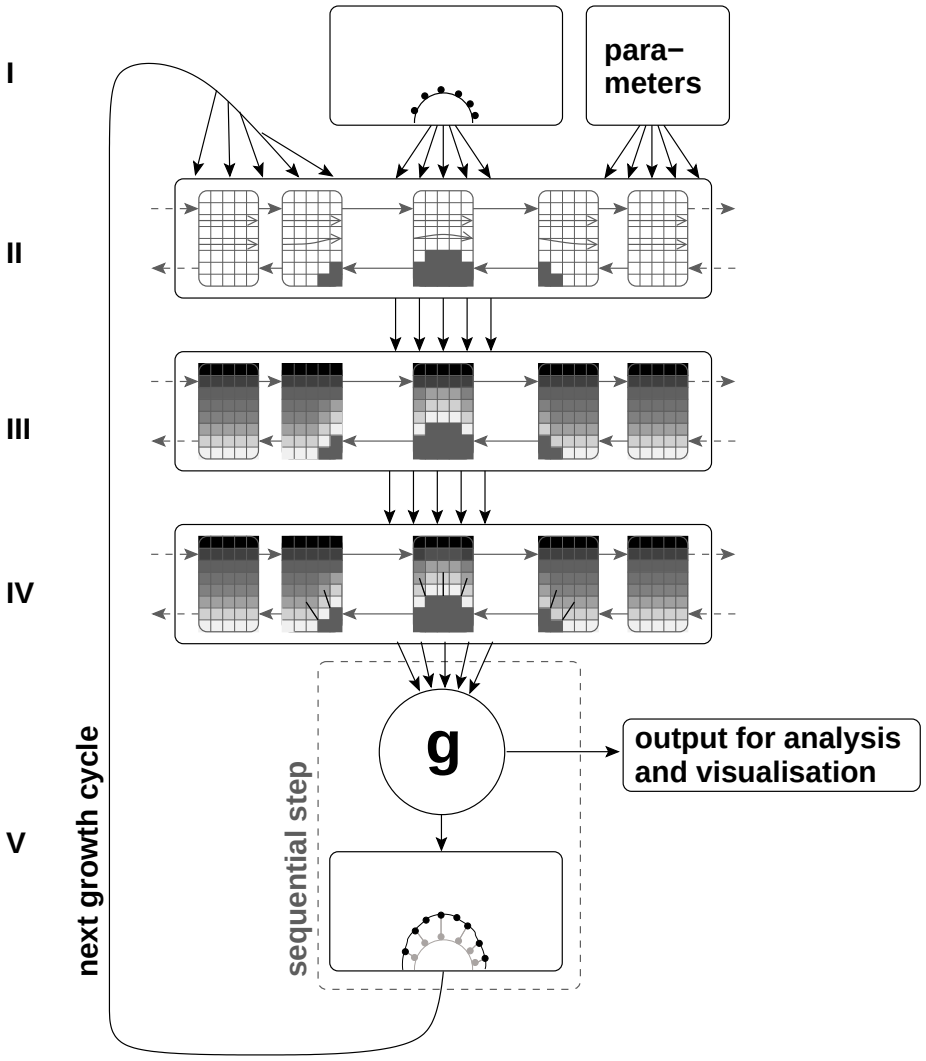

Fig. 6.1: Flow diagram of the accretive coral growth models, consisting of five modules. I. Initial condition. II. Flow calculation. III. Advection-Diffusion IV. Flux measurements. V. Accretion. The modules I and V are replaced for (parallel) modules to obtain the aggregation model.

tional grids. The initial condition is formed by an initial geometry and a set of parameters (I). The next two stages, the dispersion of nutrients through flow and diffusion, are computationally very demanding; therefore this part of the simulation is carried out in parallel. The initial geometry is voxelised and divided over all the processors. If desired, a stable, laminar flow field is calculated (II) using the lattice Boltzmann BGK method (Chen & Doolen, 1998; Succi, 2001; Chapter 2). After this, the advection-diffusion equation is solved using the moment propagation method (Lowe & Frenkel, 1995; Merks *et al.*, 2002; Chapter 2), until a sufficiently stable field has been obtained. Finally, the nutrient fluxes are measured at a number of points scattered over the growing geometry (IV). These flux measurements are sent back to the master processor to carry out a growth step. The *growth function* g determines the thickness of the new growth layer based on these nutrient fluxes and possibly on the measurements of the local curvature of the latest geometry. The new geometry is the input of the next growth cycle. A detailed description of these models is given in Section 4.2. The structure of the aggregation models only partially differs from the accretion models. The geometric description of the morphology is absent, instead the growth form is represented by a cluster of solidified lattice sites. The initial condition is a solid seed in the middle of the simulation box (I). Stages II and III are identical to the accretion models. In stage IV the resource concentration is measured at the nearest neighbours of the aggregate, and aggregation takes place in stage V. A detailed description of the aggregation models is given in Chapter 3.

In Fig. 6.2 we have summarised some of the results of the HIRAG, PORAG and aggregation models. In Fig. 6.2 a. and b. two of the results of HIRAG model are shown. In both of these models the nutrient source was placed at the top of the simulation box, both the ground plane and the coral surface was treated as a nutrient sink. Figs. 6.2c. and d. show two examples of the results of the polyp oriented (PORAG) model. Again the nutrient source were placed at the top of the simulation box, whereas the sinks where placed near the "polyps", as indicated by the black dots. The coral surface itself was impenetrable to the nutrients. In Fig. 6.2c. a nutrient sink was placed at the ground floor, as in Figs. 6.2a. and b. In Fig. 6.2d. the ground floor was made impenetrable to the nutrients, which had a large impact on the overall shape of the "coral", but not on the branching structure. Figs. 6.2 e. and f. show two cross sections of the results of the aggregation models. The two models differ in the growth function that is applied. In Fig. 6.2e. we added a single particle per growth cycle, whereas in f. a number of particles were added in each growth cycle (as in Kaandorp *et al.*, 1996).

6.3 Architecture of the morphogenesis PSE

Fig. 6.3 schematically shows the tiered architecture of the problem solving environment (PSE) and its usage. The PSE consists of four tiers. The computational tiers reside on a parallel machine or the Grid and consist of a developer's tier (tier I) and the user's application (tier II). Tier IV is a web-interface to the simulation and analysis tools, running on a separate web server. The requests to this web interface are mediated by a middleware layer (tier III), the PSE server and client, both written in Perl. The

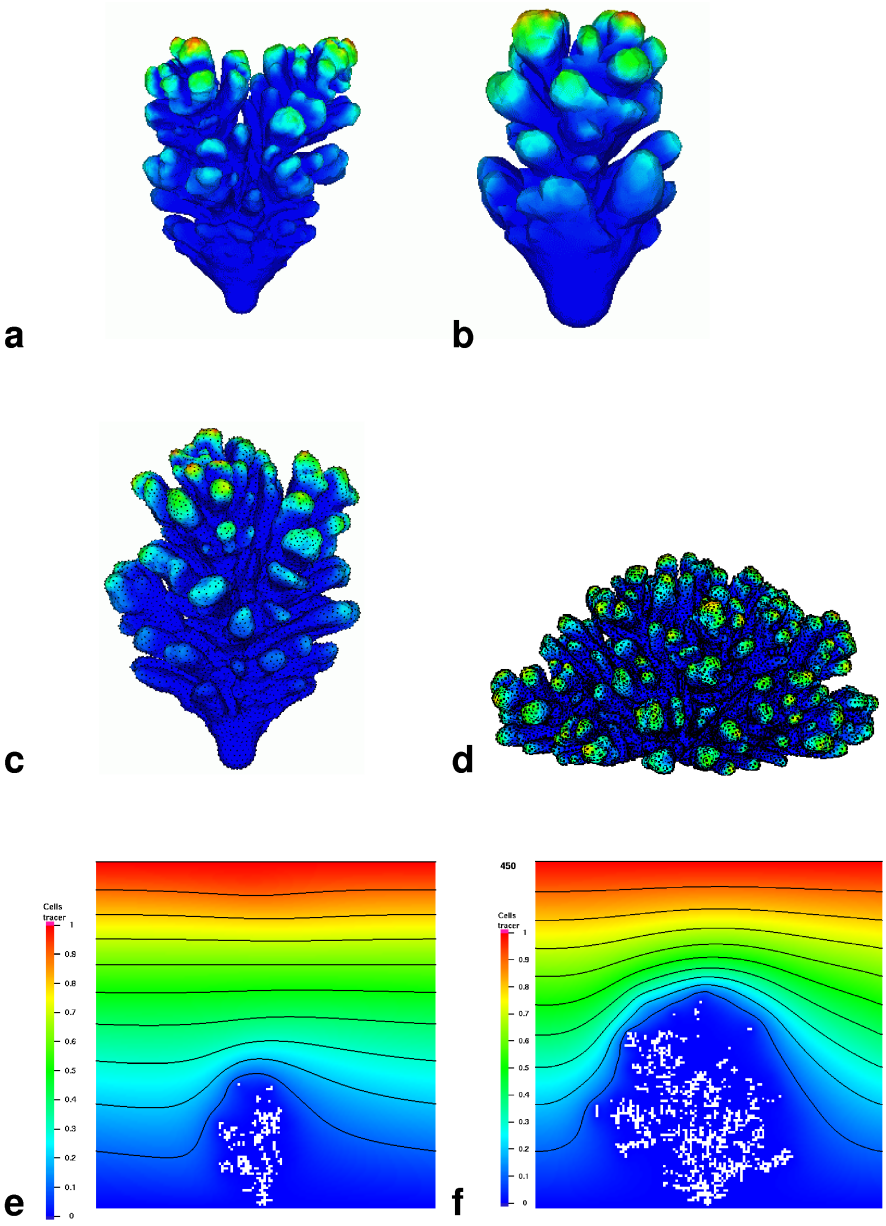

Fig. 6.2: Results of the models covered by the PSE. a-d) Accretion models: a-b) Hydrodynamically influence radiate accretive growth (HIRAG) model c-d) Polyp Oriented Accretive Growth (PORAG) model. Gray scale indicates nutrient flux, white: high flux, black: low flux e-f) Aggregation models. Cross sections of three dimensional simulations. Gray scale indicates resource concentration.

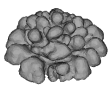

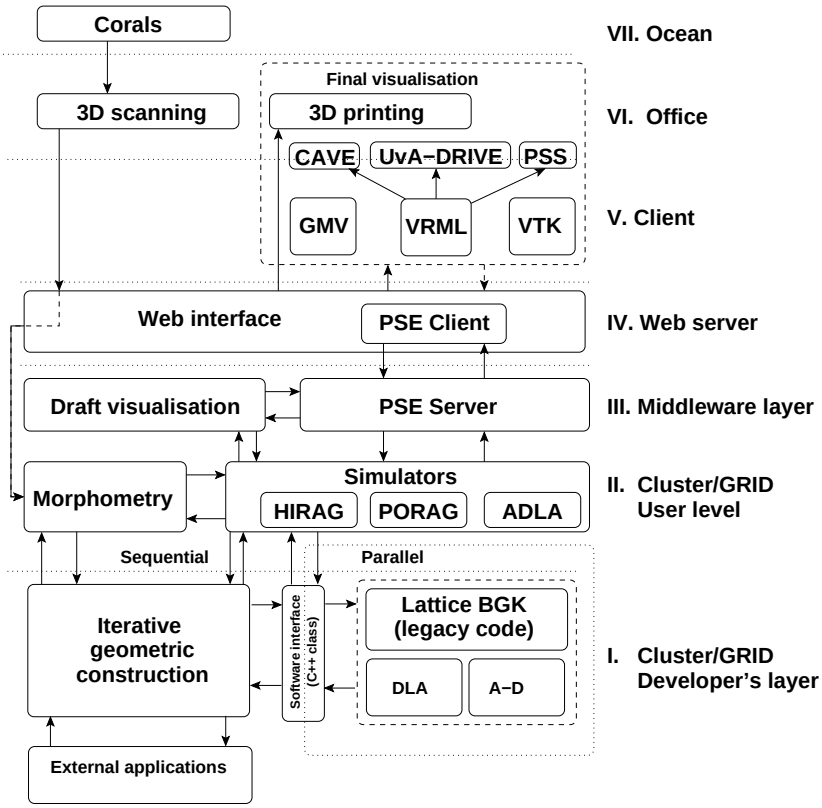

Fig. 6.3: Tiered architecture of the coral growth simulator

PSE client runs on the web server, and handles the web server's requests. It forwards them to the PSE server, which starts the simulators, retrieves data or initiates a draft visualisation of the intermediate results. Below, we describe these tiers in more detail.

The developer's layer (tier I) consists of the sequential library *libGEOM* which carries out the iterative geometric construction of the coral, and a parallel part which carries out the computational fluid dynamics (CFD) and advection-diffusion (A-D) simulations. Rather than using available legacy codes for the iterative geometric construction method (see e.g. Kaandorp, 1994a), we constructed a new library *libGEOM* which makes use of the mesh refinement algorithm introduced in Section 4.2. Unlike the legacy method where undivided triangles occurred next to divided triangles, the simplified mesh refinement algorithm generates standard triangular meshes. This makes it possible to interface our application to external libraries and applications to carry out specific tasks, for example collision detection (with the Proximity Query Package (PQP)[4]) and calculation of convex hulls (using *Qhull* [5]). For the LBGK simulations we

[4] `http://www.cs.unc.edu/~geom/SSV/`
[5] `http://www.geom.umn.edu/software/qhull`

use a legacy code written in C that was developed in our group (Kandhai *et al.*, 1998; Kandhai *et al.*, 1999). This code was interfaced to the rest of the application with a C++ wrapper class which replaces the main program loop of the legacy code with an application programming interface (API). Relative to the use of wrapper scripts around the full application, this interfacing method has the advantage that full and fast access to all the internal data of the legacy code remains possible, whereas the legacy code can still be maintained independently of the rest of the problem solving environment. The modular architecture makes it possible to interface the PSE to alternative (open source) CFD solvers, by writing an alternate wrapper class that implements the same API. The A-D solver and the diffusion limited aggregation (DLA) simulator were also accessed through this API. With slight modifications of the wrapper class, these could be easily swapped for alternative advection-diffusion solvers, such as Van der Sman's method (Van der Sman & Ernst, 2002) (recently extended to three dimensions, Koopman, 2002) or Maier's particle tracking method (Maier *et al.*, 1998).

A web-interface (tier IV) interacts with the user application (tier II), interfaced by the PSE server and client (tier III). Using this web-interface, the user specifies the parameters and initial conditions and starts the simulation by submitting a batch job to the cluster. Three variants of this user application, implementing the HIRAG, PORAG and ADLA models as introduced in the previous section, are made available by the web interface. For more flexibility on the boundary conditions, growth function and the growth method (accretion or aggregation), the user can change the simulation set-up in the user application. This set-up is specified with simple C++ classes that reflect high level model entities. For example, a new layer is built on top of the previous layers by constructing a `Layer` object, based on another `Layer` and a growth function. A simple example code, illustrating this approach, is given in Code 1. The code is then linked to the developer's layer code and the application is started. Although this method adds extra flexibility to the system, it may reduce user accessibility. We therefore plan to make flexible specification of the simulation set-up available through the user interface, which could for example be done using the VLAM-G toolkit (Afsarmanesh *et al.*, 2002; Hendrikse *et al.*, 2002).

Code 1: Example "C++ pseudocode" for specifying the simulation set-up

```
int main() {

  Surface *layer=0; SimBox *simbox=0;

  if (master_processor) {
    // Initial geometry:
    layer=new Sphere(radius, Vector(0,0,0));
    // Construct simulation box:
    simbox = new SimBox(boxsize, bounding_box);
  }
  LBGK *flowfield=new LBGK(boxsize); // Construct flowfield

  do {
```

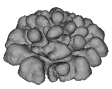

```
    if (master_processor) {
      // Voxelise and fill geometry:
      simbox->Voxelise(*layer);
      simbox->SeedFill(initial_seed);
    }

    flowfield->Geometry(simbox); // Broadcast geometry
    flowfield->SetSolidGroundPlane(); // Boundary conditions
    flowfield->SetVelocityBoundary(velocity, position);

    // Iterate Navier-Stokes and advection-diffusion eq.:
    flowfield->Flow(stability_criterion);
    flowfield->AdvectionDiffusion(stability_criterion);

    Surface *new_layer;
    if (master_processor) {
      // Adsorb tracer to the surface:
      layer->AdsorbTracer(absorbed);
      // Make new layer:
      new_layer=new Layer(*layer, GrowthFunction);
      delete layer;
      layer=new_layer;
    }
  // Write output
  } until ready;
}
```

End of Code 1

Visualisation and morphometry is carried out on the "client side" (tier V), for which several visualisation methods are made available by the PSE. For everyday visualisation at the workstation, we use the General Mesh Viewer (GMV), developed at Los Alamos National Laboratory[6], and several tools developed in our group using the Visualization Toolkit (VTK)[7]. The draft visualisation engine, running on the parallel machine, is based on the batch version of GMV. Simulation output can also be obtained in virtual reality modelling language (VRML) format. This format is used for three-dimensional electronic publishing of the simulation results [8]. The VRML format is also used to display and analyse the simulation results at three-dimensional visualisation systems: the UvA-DRIVE (Belleman *et al.*, 2001), the Personal Space System (PSS) (Mulder & van Liere, 2002; Poston & Serra, 1994) and the CAVE (Cruz-Neira *et al.*, 1993). These systems make use of shutter glasses, giving a three-dimensional illusion, and enable natural visual interaction with the morphology. They adjust the visualisation depending on the user's position, making it possible for the user to watch the morphology from different angles as if it were a statue in a museum. The PSS adds

[6] `http://www-xdiv.lanl.gov/XCM/gmv/`

[7] `http://public.kitware.com/VTK/`

[8] see for example `http://www.science.uva.nl/~roel/iccs2002`, and the CD-ROM accompanying this thesis.

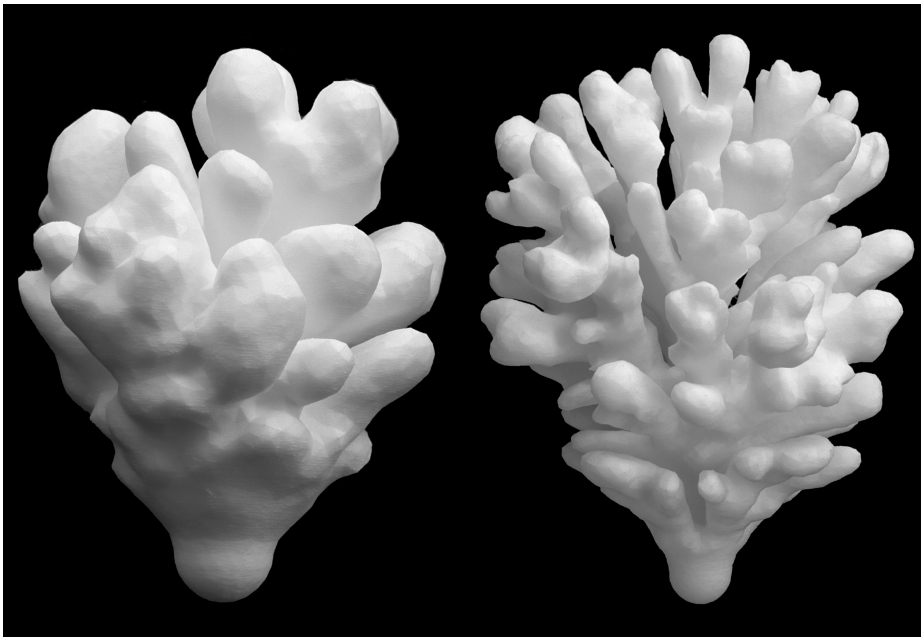

Fig. 6.4: Three-dimensional prints generated with selective laser sintering. Left object: morphology shown in Fig. 5.3a; right object: morphology shown in Fig. 5.4e. Photography: Ronald van Weeren

a further dimension to this. Here the user can manipulate the three-dimensional morphology by handling simple objects. Using a mirror, the virtual image appears at the same position as the user's hands. For demonstration purposes, we have also made use of 3D printing techniques (see Fig. 6.4 and the cover of this thesis). Two morphologies generated by the PORAG model were constructed using the selective laser sintering (SLS) technique (reviewed in Kruth *et al.*, 1998). Such three-dimensional prints make it possible to visually compare the simulated morphologies to real morphologies in the user's office (tier VI).

To enable more extensive comparison between real and simulated morphologies, several corals were scanned using a medical CT-scanner (Kaandorp & Kübler, 2001). These morphologies were converted to a format that can be read by the iterative geometric construction library. In this way the simulated and real objects could be visualised using identical tools (see Fig. 5.12 and Section 5.4), and a fair visual comparison could be made: a "Turing test" (Turing, 1950) for models of morphogenesis. The availability of coral scans also enabled us to apply the analysis tools developed for the simulated corals on the real ones as well. A number of legacy codes for such analysis tools are available in our group, ranging from codes to analyse the coral's three-dimensional branching structure (García Leiva, 2001; Kaandorp & Kübler, 2001) to tools to statistically analyse the compactness of the morphologies (Merks *et al.*, 2003). Ultimately

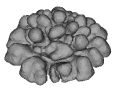

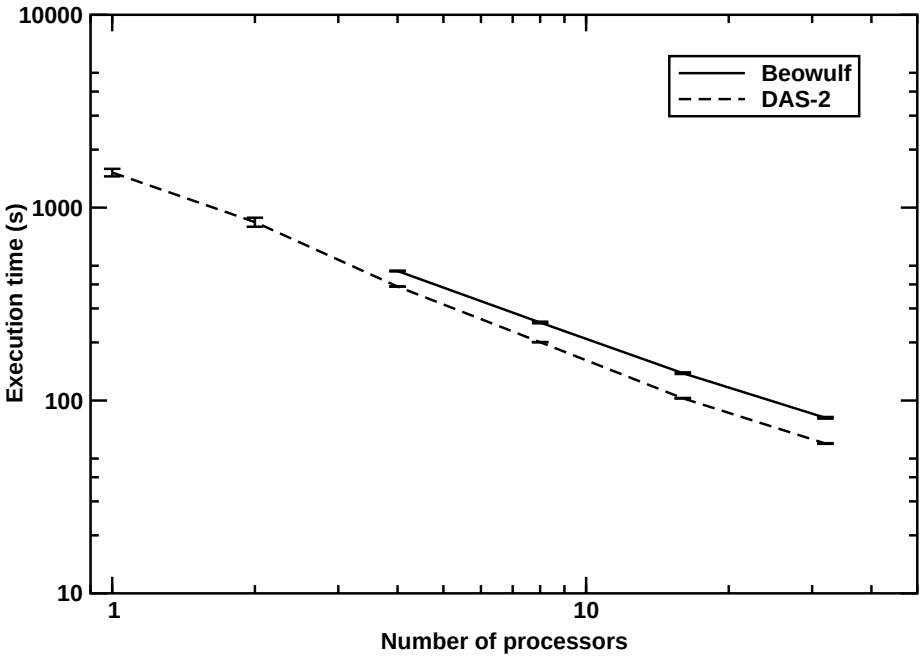

Fig. 6.5: Run time of the first growth cycle on the Beowulf and DAS-2 clusters. Mean and standard deviation are given of 10 simulations each. One and two processor tests could not be run on the Beowulf due to memory constraints.

such tools should be all made available through the PSE.

The dashed arrow pointing from the visualisation back to the user's applications indicates the possibility to use the three-dimensional geometric output as the initial geometry for a new simulation. Also, it indicates the future desire for interactive simulation, where the user would be able to interact with the simulation by manipulating the visualisation. For example, the boundary conditions could be changed, to simulate changing environmental conditions. Another example could be to manipulate the position of the growing coral to simulate transplantation experiments, or to remove branches. Such interactive simulation is already applied in simulations of interactive vascular reconstructions developed in our group (Belleman & Sloot, 2000).

6.4 Performance analysis

We analysed the performance of the simulator on two clusters of work stations. The first system is a Beowulf (Sterling *et al.*, 1995; Ridge *et al.*, 1997) cluster, consisting of 700 MHz AMD Athlon processors with 256Mb (44 nodes) or 512 Mb (12 nodes) of memory. The nodes are interconnected via 100 Mbit switched ethernet and they have a 1 Gbit ethernet connection to the file servers. The second system is the Dis-

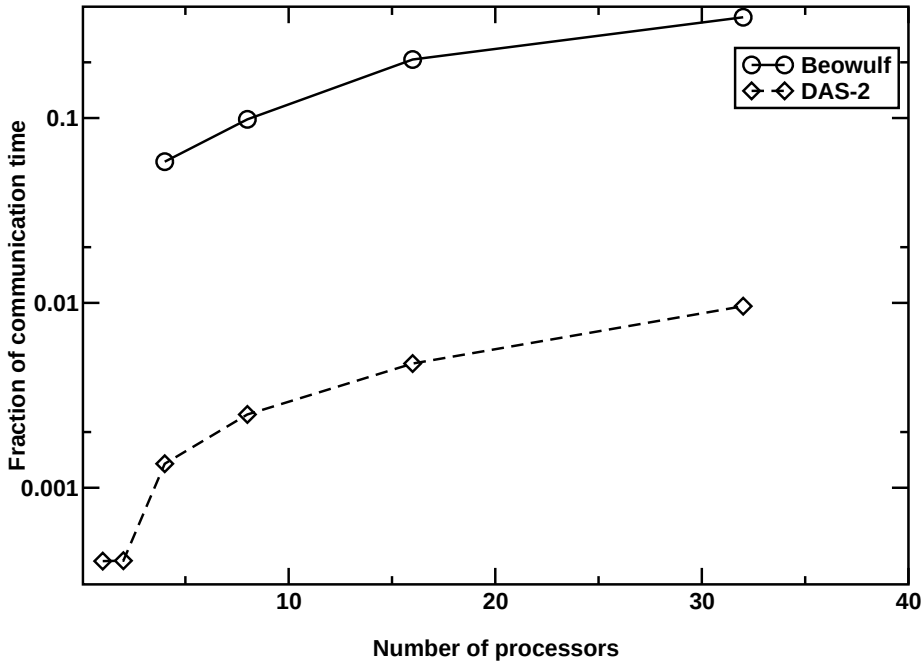

Fig. 6.6: Fraction of communication time spent on the Beowulf and DAS-2 clusters

tributed ASCI Supercomputer 2 (DAS-2) (Bal *et al.*, 2000; Hendrikse *et al.*, 2002), which consists of five clusters geographically distributed over five Dutch universities. Each cluster consists of 32 nodes (except for the 64 node cluster at the Vrije Universiteit), containing two 1 GHz Pentium III processors and 1 GB to 1.5 GB RAM each. The parallel processes communicate through a high speed Myrinet-2000 network (bandwidth over 1 Gbit) between the nodes within a subcluster. The processors within one node communicate through shared memory. File transfer is carried out over Fast Ethernet.

The results of the performance measurements as carried out on the Beowulf and on UvA subcluster of the DAS-2 are shown in Fig. 6.5. We measured the total wall clock time spent in the first growth cycle of a typical run with a 200^3 simulation box, where the code was run on 1 to 32 processors. The mean and standard deviation of ten runs are shown. Due to memory constraints, the execution times of 1 and 2 processor runs could not be measured on the Beowulf cluster. The code is faster at the DAS-2, which can be partly attributed to the faster processors (1 GHz vs. 700 MHz). The code scales a little bit worse than linearly, scaling better on the DAS-2 than on the Beowulf. This can be attributed to the faster network of the DAS-2, as shown in Fig. 6.6. For a 16 processor job the percentage of the total run-time used for interprocess communication on a is 10% to 20% on the Beowulf and less than 1% on the DAS-2.

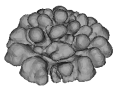

One of the possible performance concerns was the sequential bottleneck generated

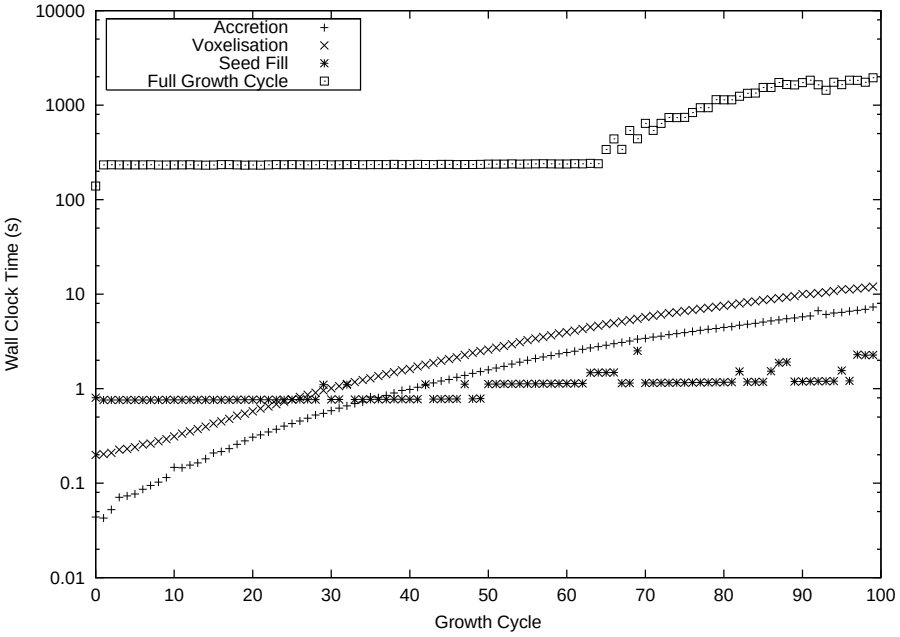

Fig. 6.7: Wall clock time used for the full growth cycle, and the sequential accretion, voxelisation and seed fill steps, for a typical run of 100 growth cycles on 16 processors of the Beowulf cluster.

by the accretion, voxelisation and seed fill steps (see Fig. 6.1). We timed the length of the sequential and parallel steps on the Beowulf and the DAS-2 (Fig. 6.7). This figure shows that only 1% to 5% of the total simulation time was spent in the sequential stage. The triangle voxelisation and seed fill procedures were carried out sequentially, in contrast to a previous implementation of the coral growth system (Kaandorp & Sloot, 1997). Although it would be trivial to parallelise also these two stages of the simulation, the sequential speed of the used voxelisation and seed fill algorithms did not justify the effort of doing so.

The time for a full growth cycle remains almost constant up to growth cycle 65, after which it increases less than exponentially. The full growth cycle timing can be fully attributed to the nutrient dispersion step, because the sequential steps take up a minor fraction of the total simulation time. As indicated by the timing of the accretion and voxelisation steps, the morphology's complexity increases almost exponentially. Hence more iterations of the advection-diffusion equation are needed to obtain a sufficiently stable nutrient field. The stability of the nutrient field is measured once every fifty iterations, which explains the stepwise increase of the needed wall clock time.

6.5 Discussion

In this chapter we have introduced and analysed a prototypical problem solving environment for the simulation of coral morphogenesis. Such a PSE enables marine biologists to experiment with the coral growth simulation, without the need for specific technical training or knowledge about the simulation methods. Using the web front-end, the user can specify simulation parameters, an initial geometry, the growth function, and start the simulation, while the parallel system architecture remains hidden. Currently, our system is not yet able to warn the user in case he would choose combinations of parameters that are known to result in incorrect results. In a future version of the PSE such knowledge will be included. For example, knowledge about the valid combinations of flow velocity and diffusion coefficients (Merks *et al.*, 2002; Chapter 2) can be easily included in the PSE.

Although the interaction through a web-interface makes the simulation system accessible to computationally untrained scientists, it may be limiting to others. Therefore, we have constructed the PSE according to a tiered and modular architecture. The deeper one proceeds in this architecture, the more computational skills are needed, with the gain of more flexibility. For example, if one is not satisfied by simulation set-ups offered by the webserver, a new set-up can be created using high level C++ objects (see Code 1). This requires some basic knowledge on C++ programming, but the deeper geometric library and CFD codes can be safely considered a black box. If desired, such a new simulation set-up could be interfaced to the web-server, but this is not necessarily required.

With some more technical knowledge, the CFD and A-D solvers can be swapped for different solvers, thanks to the modular architecture. Indeed we are planning to do so in the near future, since we are now running into the limits of these solvers. The LBGK method we currently use is not able to simulate turbulent flows and the current A-D method produces incorrect results when advective transport becomes much more important than diffusive transport (Merks *et al.*, 2002).

Simulations of morphogenesis generally are not only high performance applications, but also *high throughput* applications. In order to understand the role of each of the parameters in a model of morphogenesis, one should be able to do parameter sweeps to construct so called “morphospaces” (Raup, 1962; Raup & Michelson, 1965; McGhee, Jr., 1999). These theoretical orderings of morphologies are used to find non-existing shapes produced by the modelled morphogenetic mechanism, and are helpful in analysing the modelled mechanism and in interpreting the functional advantage of existing morphologies. Realistic simulations of morphogenesis are computationally very expensive (a typical simulation of the PORAG model takes 18 to 36 hours on 16 processors of the Beowulf). This makes such extensive parameter sweeps not yet feasible. Conventional high throughput architectures such as Condor (Basney & Livny, 1999) are not suitable for managing high performance applications. Conversely, architectures for dynamically managing high performance applications, such as Dynamite (Iskra *et al.*, 2000) (a Grid enabled version is currently being constructed) would allow efficient execution of the simulators in a dynamic and heterogeneous resource such as the Grid. However, Dynamite was not constructed for high throughput com-

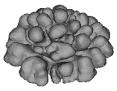

puting. Grid enabled parameter sweep architectures, such as Nimrod/G (Abramson & Giddy, 1997) do enable this. In future work we plan to interface our morphogenesis PSE to a combination of Dynamite and Nimrod/G in order to allow for the efficient construction of morphospaces on computational grids.

6.6 Acknowledgements

We would like to thank Robert van Liere (CWI, Amsterdam) for visualising our simulation results on the Personal Space Station, Robert Belleman (UvA) for the visualisations on the UvA-DRIVE and CAVE systems and Leo E.H. Lampmann (St. Elisabeth Ziekenhuis, Tilburg) for making three-dimensional scans of real corals, that were kindly made available by Mark Vermeij (Cooperative Institute for Marine and Atmospheric Studies, Miami) and Rolf Bak (Netherlands Institute for Sea Research and UvA). We thank Zeger Hendrikse (UvA) and Kamil Iskra (UvA) for fruitful discussions.

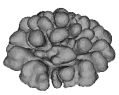

CHAPTER

SEVEN

Summarising Discussion and Future Work

7.1 Summarising discussion

In this thesis we have aimed to reconstruct branching coral morphogenesis and morphologic plasticity from the interactions between the coral tissue, the coral skeleton, and the dispersion of growth resources in the surrounding water. We started by studying physical models of branching morphogenesis, to which we have added more and more biological detail. In this way we could distinguish which aspects of coral morphogenesis can be explained purely by physical processes, and for which aspects the biological factors should be responsible.

Corals are sessile organisms whose most important source of energy is photosynthesis, which is made possible through the endosymbiotic zooxanthellae. In this thesis we have not considered light a limiting resource. In addition to light, however, coral growth is limited by the availability of organic food particles and inorganic resources such as carbonate and calcium ions (see Section 1.3), for whose supply they depend on the surrounding water. To understand the growth of corals, it is thus essential to understand the passive transport of resources to the growing coral. This is a problem of advection and diffusion, which we have modelled using the lattice Boltzmann method in conjunction with the moment propagation method, as introduced in Chapter 2. The moment propagation method was validated against the analytic Taylor-Aris prediction of solute dispersion through a laminar tube flow; we found good agreement between our simulations and the prediction. Unfortunately, the lattice BGK method which we used in this thesis becomes invalid when the velocity becomes too high (Chen & Doolen, 1998; Succi, 2001). Generally, the lattice velocity should be < 0.1 which, depending on the size of the obstacle and the viscosity of the fluid, allows the use of Reynolds numbers of about $Re \approx 1$ to about $Re \approx 10$. In order to be able to study the effect of faster flows on resource transport, an approach often taken is to diminish the diffusion coefficient. This makes advective transport relatively more important than diffusive transport, as expressed by the Péclet number. In Chapter 2 we argued that this cannot be done without limits; when the Péclet number becomes larger than about $\sqrt{2}$ (that

is, when the diffusion coefficient becomes too small), the moment propagation method will produce unphysical results. We gave analytic expressions for the minimum diffusion coefficient for a given flow velocity. After introducing a small modification to the moment propagation method (first published by Warren, 1997), we show that higher Péclet-numbers can be reached. This holds in particular when the velocity becomes small, the typical applicability region of the lattice BGK method.

In Chapter 3 and Chapter 4 we considered two physical metaphors of coral growth, diffusion-limited aggregation and Laplacian growth. The effects of laminar flows on abiotic growth processes may parallel observations of morphologic plasticity in stony corals (see Section 1.3), and its study may provide mechanistic explanations of flow-induced plasticity in corals. Although the resource transport towards coral colonies is characterised by Reynolds-numbers around $Re \approx 100$ to $Re \approx 1000$, and Péclet numbers from $Pe \approx 10$ to $Pe \approx 10^6$, in a previous study low Reynolds-number ($Re < 1$) and low Péclet-number ($Pe \approx 3$) transport was found to affect the compactness of abiotic growth processes (Kaandorp *et al.*, 1996; Kaandorp & Sloot, 2001; Kaandorp, 2001). Since this observation was contradicted by other studies, we have reinvestigated it in Chapter 3. We could not confirm the previous finding that DLA-clusters become more compact as "the flow becomes more important (Pé increases)" (Kaandorp *et al.*, 1996). In our simulations the clusters tended to grow into the direction of the governing flow, but the compactness was not affected. The compactification, as observed by (Kaandorp *et al.*, 1996) occurred in particular when growth becomes fast relative to the transport of resources. This was the case when the diffusion-coefficient was set to low values (in order to set a high Péclet-number) and when multiple particles were added to the cluster at the same time, without intermediate relaxation of the resource field. Note that this reduces the probability of a Mullins-Sekerka instability. If a "bump" appears in the single particle model, it has immediate effect on the resource gradients (see Fig. 1.4). In the multiple particle model however, this effect is postponed until after the addition of other particles which may "smoothen" away the bump.

In Chapter 4 we continued our consideration of physical metaphors of coral growth, and studied Laplacian growth processes. We discussed the relevance of Laplacian growth for understanding coral growth. The Laplacian growth model is based on the accretive growth models by Kaandorp *et al.*, which we introduced in Section 1.4. In the introduction we compared models of biological growth with models of physical growth processes and concluded that in most models of biological growth branching is put in as a model assumption. We reviewed models of branching coral growth and showed that in these models – although triggered by the morphology itself — branching is enforced by a number of rules, such as the so-called *curvature rule*. We studied the hydrodynamically influenced radiate accretive growth (HIRAG) model, introduced by Kaandorp & Sloot (2001). We showed that it is not necessary to include high-level assumptions in our models: branching growth can be obtained by assuming resource flux dependent surface normal growth alone, *if and only if the resource fields are relaxed well enough*. The importance of a well relaxed resource field can be again understood in terms of the Mullins-Sekerka instability. When, by chance, a small bump appears in the "coral" surface, the resource gradient will be locally higher, as shown in Fig. 1.4. Thus the resource flux will be higher at the bump than around it, which sets off the growth of a

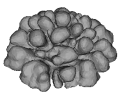

branch. However, if one does not relax the resource fields until stability, the resource gradient at the small bump remains unamplified and the Mullins-Sekerka instability does not appear. This finding explains why the objects in previous simulations of resource dependent growth Kaandorp & Sloot (2001), where the resource fields where relaxed for a limited time only, did not branch without the use of a branch-enforcing curvature rule. A second observation by Kaandorp & Sloot (2001) was similar to the one done in the aggregation model; if the Péclet number was increased (by decreasing the diffusion coefficient) the simulated coral became more compact, which was interpreted as the effect of hydrodynamics. In Chapter 4 we showed that "corals" developed *with* the curvature rule compactify both in the *presence* and in the *absence* of flow when the diffusion coefficient is reduced. Thus, in this model the compactness is not related to flow, but exclusively to the diffusion coefficient.

Our simulations suggest that the Laplacian growth mechanism may in principle be sufficient to explain branching growth in stony corals. Using time scale arguments however, we discussed whether such a mechanism would be feasible. We argued that this would only be the case for actively moving food particles, or when we would assume that turbulent mixing can be approximated as a diffusion process. Most importantly, however, in both cases formation of resource gradients around the coral would be easily disturbed in the dynamical environment which a coral reef is. A fish seeking protection between the coral's branches, a wave rolling over, such common events would preclude the onset of a Mullins-Sekerka instability; hence we conclude that Laplacian growth is not a probable metaphor of coral growth.

In Chapter 5 we introduced more biological detail into the model, by explicitly considering the individual organisms that build the coral skeleton: the coral polyps. In this *polyp oriented* radiate accretive growth (PORAG) model, resources are absorbed exclusively near the model polyps, contrary to the HIRAG model in which the whole "coral" surface absorbed growth resources. In this polyp oriented model we found that the simulated corals formed branches more easily and robustly; it was not necessary to bring the resource fields as close to equilibrium as for the HIRAG model. We explained this finding with the *polyp fanning* hypothesis. At convex portions of the "coral" surface, for example at the branch tips, the "polyps" fan out like the tail of a peacock. The reduced competition between neighbouring "polyps" enhances the resource flux and consequently – assuming a linear relation between resource flux and skeletal accretion rate – the skeletal deposition rate. By contrast, at *concave* positions, the "polyps" fan in and experience strong competition for resources from neighbouring "polyps"; thus the skeletal deposition rate is locally depressed at concave portions of the "coral" surface. polyp fanning thus introduces a curvature effect into the growth model, and may possibly provide a hypothesis explaining branching in corals. One could object that we have reintroduced a "curvature rule" into our model which we were so eager to remove in Chapter 4. However, note that we have not *explicitly* introduced the polyp fanning effect into our model; instead it followed from the lower level dynamics of the "polyps". It is – as it is sometimes called – an "emergent property" of our model.

The polyp fanning effect becomes less strong when the "polyps" are placed further apart; we calculated a morphologic range – or *morphospace* (Raup, 1962; McGhee, Jr., 1999) – for increasing "inter-polyp" distances which showed that the branches be-

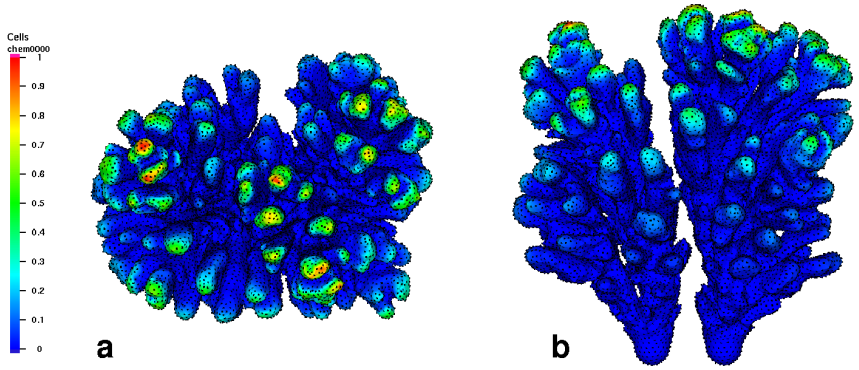

Fig. 7.1: Object grown for 100 cycles with the PORAG model, from two initial spheres placed close to each other in the same simulation box. a) top view b) front view

come thicker and less numerous while the colony as a whole becomes more compact (Fig. 5.4). These observations indicate that the tendency to branch becomes more weak as resource competition between the "polyps" is reduced. It may very well be objected that this observation is explained by a discretisation artifact, because the same effect would occur when the advection-diffusion lattice is refined. It should be noted, however, that the model polyps absorb resource from a small volume. A simple mathematical analysis suggested that the relevant parameter in the polyp fanning effect is the ratio between the total "area of influence" of the "polyp" and the area from which it absorbs resources.

It is sometimes argued that corals are physiologically integrated organisms, rather than colonies of individuals: the "holism" claim (see Rinkevich, 2001; Rinkevich, 2002). In the light of such a view our models would not be sufficient to explain coral morphogenesis, since for the mechanisms we have hypothesised the independence of the polyps seems to be an essential precondition. Two of the observations which are thought to support the holism claim are the following. Firstly, photosynthetates are sometimes observed to be translocated between polyps, most probably through the coenosarc, the tissue which connects the polyps (Rinkevich & Loya, 1983; Oren *et al.*, 1997). In order to test whether this assumption prevents the "corals" in our model from branching, we included some resource translocation in the polyp oriented model (see Fig. 5.11). Moderate resource translocation tends to make the branches more thick and smooth, but branching is not inhibited. Only in the case of very strong resource translocation, which quickly and equally redistributes all the resource over the "coral polyps", hemispherical morphologies were formed in our model. Thus, resource translocation does not necessarily make the proposed branching mechanism unlikely. The second support often given for the "holism" claim is provided by the observation that colonies of *Stylophora pistillata* form hemispherical colonies according to strict architectural rules, which regenerate when part of the colony is damaged (Loya, 1976; Rinkevich, 2001). The absence of spontaneous branch fusion and the occurrence of retreat growth

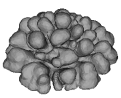

suggests the presence of an "isomone", an extracellular signalling molecule (Rinkevich & Loya, 1985). It is also often observed that two colonies growing next to each other together form a hemispherical colony (Lee Shaish, personal communication), an observation that would further support the existence of an external signalling molecule. However, note that the "colonies" developing in our simulations are mostly symmetric and hemispherical, caused by balanced nutrient supply. The branches never fuse, although no specific "avoidance rule" was included in our model; this is caused by resource depletion zones forming between the branches. Moreover, when we place two initial spheres very close to each-other, a hemispherical morphology develops which is barely distinguishable from a single "coral" when seen from the top (see Fig. 7.1a), reproducing the observation communicated by Lee Shaish (*personal communication*). A similar simulation experiment was carried out earlier, using a diffusion-limited aggregation model, by Witten, Jr. & Meakin (1983). Thus, some observations often used as evidence for the "holism" claim, may not necessarily require full physiological integration of the coral. Note, however, that we have not observed regeneration of damaged spherical colonies in our models; such a disturbance experiment should be carried out in future work.

The relation between the properties of the "polyps", such as their spacing, whether they translocate resources, the particular growth functions used, and the resulting colony morphology, suggests that polyp oriented modelling can be applied to study the relation between micromorphology (the morphology of the polyp and the calix) and macromorphology (the morphology of the colony). The micromorphology is of course genetically regulated, but it is also affected by environmental factors (Foster, 1979; Foster, 1980; Zilberberg & Edmunds, 1999). By constructing large morphospaces parameterised by micromorphology, more insight in the mapping from micromorphology to macromorphogy can be obtained; such an analysis would be similar to analyses of genotype-phenotype mappings (for example in RNA evolution, see e.g. Huynen, 1996).

In Chapter 6 we discussed the computational aspects of carrying out such large-scale simulations of morphogenesis, concentrating on the development of a problem solving environment (PSE) for coral morphogenesis. This prototypical PSE enables computationally untrained marine biologists to experiment with the simulations developed in this thesis. It hides implementation details for the researcher and warns him when invalid parameter combinations would be chosen. Furthermore the PSE enables transparent integration of new codes, such as the iterative geometric construction code *libGEOM*, and legacy codes, such as the LBGK fluid flow solver. A further developed PSE would be very useful for carrying out large morphospace studies, since it could hide the details of scheduling large numbers of parallel jobs on parallel and distributed hardware.

7.2 Future work

7.2.1 The effect of unstable and turbulent flows

In this thesis, we have studied the effect on coral morphogenesis of resource dispersion in laminar, low Reynolds-number ($Re < 1$) and low Péclet-number ($Pe < \sqrt{2}$) flows

(see Chapters 3 and 2). Such Péclet-numbers and Reynolds-numbers are far below the values expected in coral reefs, where one would expect values of $Re \approx 100$ to $Re \approx 1000$, and $Pe \approx 10$ to $Pe \approx 10^6$ depending on the growth resource considered (see Chapter 3). Previous studies reported that a small increase of the Péclet-number up to $P\acute{e} = 3$ affects the compactness of morphologies formed with diffusion-limited aggregation (Kaandorp *et al.*, 1996) and with growth by accretion (Kaandorp & Sloot, 2001; Kaandorp, 2001). Understanding such effects may contribute to understanding the causes of similar effects in more realistic parameter regimes, which motivated our further studies of these phenomena. In our studies low Reynolds-number, low Péclet-number flows neither affected the compactness of DLA-clusters (Chapter 3), nor the compactness of morphologies formed in accretive growth models (Chapter 4).

However, experimental evidence suggests that water flow *does* affect coral growth (Sebens *et al.*, 1997; Kaandorp, 1999), although it is not sure whether the observed effects are due to flow or to other environmental conditions co-occuring with the studied flow conditions. Experimental observations (A. Genin, personal communication) suggest that already at very slow flow velocities the flow around corals is turbulent. Indeed, the flow in the wake of an isolated cylinder becomes instable for about $Re > 49$ (i.e. vortex shedding occurs), from about $Re > 149$ the flow field becomes three-dimensional, but remains periodic, while with further increase of the Reynolds-number the flow becomes turbulent (Berger & Wille, 1972; Williamson, 1996). In fluid flows through arrays of (rectangular) cylinders, which we could consider a crude model of coral morphology, instable flows are found at considerably lower Reynolds numbers (Balachandar & Parker, 2002). In experimental and numerical studies of heat transfer in arrays of rectangular cylinders, it was observed that instable flows enhance heat transfer by bringing far-lying volumes of fluid towards the cylinders, which leads to a thinnened boundary layer (Zhang *et al.*, 1997; De Jong *et al.*, 1998). Given the strong mathematical similarities between heat and solute transport, this may indicate that instable flows enhance the transport of growth resources towards the growing colony. In order to settle the issue of whether the observed effect of flow on coral compactness can be understood using mechanistic (as opposed to adaptive) explanations, we should thus model the transport of resources by means of instable laminar, and possibly turbulent flows.

There are several ways of increasing the Reynolds-number in the LBGK-method which we presently use for the fluid dynamics simulations. The lattice velocity could be increased, but the LBGK-method only recovers incompressible flows in the low Mach-number limit ($Ma << 1$); as a rule of thumb, this is considered valid when the lattice velocity is about $u < 0.1$, although it is safe to stay at about $u < 0.08$ (Chen & Doolen, 1998; Succi, 2001). Higher velocity flows could be reached by using finer lattice spacings, in which case the lattice velocities correspond to higher actual velocities. Note, however, that such an approach would result in enormous increases of the – already large – computation times: a two-fold decrease of the lattice spacing would result in an eight-fold (2^3) increase. Another option is to simulate fluids of smaller kinematic viscosity. In the LBGK method, the kinematic viscosity ν depends on the relaxation time τ as $\nu = (2\tau - 1)/6$ (Chen & Doolen, 1998); low kinematic viscosities can be reached by using a value of τ close to $\frac{1}{2}$, where $\tau > \frac{1}{2}$ to get positive

viscosity. A stability analysis of the LBGK-method at such low values of τ is given by Lallemand & Luo (2000). Preliminary simulations of the PORAG model with low viscosity flows have thus far not indicated any new effects (data not shown). More details on the use of lattice-Boltzmann equations for simulating non-turbulent, high Reynolds-number flows are given in He *et al.* (1997).

For simulating turbulent flows more sophisticated lattice Boltzmann techniques are needed. The LBGK-method is not suitable for simulating turbulent flows, since much of the turbulent dynamics takes place at a scale below that of the grid spacing. The most common work-around for this problem is to introduce subgrid-scale modelling (Hou *et al.*, 1996; Succi, 2001; Zhou, 2002). In this approach one lumps together the effect of subgrid-scale eddies on supergrid-scale processes; mostly this involves introducing a locally variant viscosity (i.e. one varies the relaxation times). Using these techniques, lattice Boltzmann methods are recently routinely used to simulate turbulent flows (see e.g. Crouse *et al.*, 2002; Hill & Koch, 2002; Shock *et al.*, 2002; Lu *et al.*, 2002; Ten Cate *et al.*, 2001). The lattice Boltzmann has become a mature alternative to classical methods for Computational Fluid Dynamics (Ferziger & Perić, 1997) for studying high Reynolds-number flows and turbulence (Hou *et al.*, 1995; see also Chen & Doolen, 1998; Succi, 2001 and references therein).

A more pressing problem is the need for algorithms to simulate high Péclet-number, high Reynolds-number turbulent advection-diffusion. The moment propagation method, which we used in this thesis, produces unphysical results for lattice Péclet-numbers over approximately $\sqrt{2}$ (see Chapter 2). A number of numerical schemes are available for the simulation of higher Péclet-number dispersion in laminar flows (Succi *et al.*, 1999, and more recently Van der Sman & Ernst, 2002, extended to three dimensions by Koopman, 2002). However, these methods are currently not suitable for use in combination with subgrid-scale lattice Boltzmann methods. Two-dimensional turbulent convection has recently been modelled using two coupled lattice-BGK equations by Shi *et al.* (2002). Alternatively, a particle tracking method such as Maier's (Maier & Bernard, 1997) could be used, but such methods are computationally very expensive when smooth resource dispersion fields are desirable.

Apart from these methodological problems, there are also a number of more fundamental problems which will arise when simulating the effect of turbulent flows on coral growth. In the present models, we waited until the resource fields were in (near) equilibrium, before starting a new growth cycle. In turbulent dispersion, such equilibrium will never be reached. Thus, one would need to even more carefully consider the time-scales of resource transport and of coral growth; such a discussion was given for dispersion in laminar flows in Section 4.4.3. In such non-equilibrated fields the Péclet-number should be interpreted carefully, since the diffusion coefficient and the flow velocity have different effects (see Chapter 2). Hence it would be necessary to separately measure their effects on the outcome of the coral growth simulations. It should be noted, however, that at present the inclusion of instable and turbulent flows in our simulations may be highly premature. Numerical studies of heat transfer through three-dimensional instable flows are currently on the edge of what can be done in computational fluid dynamics (see e.g. Zhang *et al.*, 1997; Cui & Tafti, 2002). Thorough understanding of such heat and mass transfer problems and well-developed techniques

for their numerical simulation, are prerequisites for including instable flows in our coral growth simulations.

It may however not be necessary to *simulate* turbulent and instable flows, for understanding its effects on coral growth. Turbulent mixing can often be expressed as a quick diffusion process, where the diffusion coefficient is given by the "eddy diffusivity" (Byron Bird *et al.*, 1960; Altunbas *et al.*, 2002), whose empirical value depends on several flow properties, such as the Reynolds-number, the fluid's velocity and on the sedimentation velocity of the diffusing particles (Altunbas *et al.*, 2002). Given a quick enough nutrient uptake rate, we could simply model turbulent mixing using the presently available tools. The interaction of turbulent flow with the growing object would possible reduce turbulent mixing near the object. Such effects could also be modelled in a subgrid-scale model, in which, depending on the flow's local properties the diffusion coefficient would be varied.

7.2.2 Tracking of polyp trajectories

In Section 5.4.3 we shortly mentioned a possible relation in the PORAG model between the life-time of the "polyps" and the "coral" morphology. It seemed that more model polyps died in finely branched "corals" (through the fusion rule, see Section 4.2), because these contain more concavities in which they become compressed. This observation parallels an experimental observation by Darke & Barnes (1993), who found a relation between the amount of "bumpiness" of massive colonies of the genus *Porites* and the longevity of the polyps. More measurements should be carried out to confirm our preliminary simulation results. Also, visual tools should be developed to track the trajectories of individual "polyps" through the three-dimensional morphology. Collaborations to develop such a tool for the personal space station (Mulder & van Liere, 2002; see also Chapter 6) have been initiated.

7.2.3 Morphologic effects of shear induced food uptake repression

Sebens *et al.* (1997) have shown that colonies of *Madracis mirabilis* with wide branch spacing which are typically found in deep, low flow habitats, capture most particles at low water flow speeds. At higher flow velocities the polyps in were observed to flatten against the colony, interfering with particle capture. Conversely, tightly spaced morphologies (typically found in more shallow, high flow speed habitats) capture most particles at high flow habitats, as the flow is slowed down between the densely packed branches. In Chapter 4 we have only studied the effects of flow on resource transport. The study by Sebens *et al.* (1997) suggests a second effect: shearing flow may interfere with the uptake of food particles by the polyps. With the simulation tools currently available it is straight-forward to study whether and how this could affect morphogenesis. We propose to set up a PORAG simulation as follows. In lattice Boltzmann BGK methods, the shear stress can be directly derived from the particle distribution (Hou *et al.*, 1995; Artoli *et al.*, 2002). After the flow has equilibrated, the shear stress tensor $\sigma_{\alpha\beta}$ will be measured near each of the "polyps". From these shear stress tensors one can derive the principal stresses and, based on the assumed Young's modulus of the

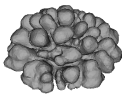

"polyps" and the fluid's viscosity, the resulting deflection of each of the "polyps" due to the shearing flow can be analytically derived. Then, a certain relation between the "polyp's" deflection and the suppression of food uptake should be assumed. Hence the growth function becomes

$$g(\vec{\mu}_i) = \vec{n} R_i \gamma(\sigma_{\alpha\beta,i}, \vec{n}), \tag{7.1}$$

where R_i is the resource uptake rate of the undeflected "polyp", $\vec{n}$ is local surface normal vector, and $\gamma(\sigma_{\alpha\beta,i}, \vec{n})$ is a function translating the principal stresses on the "polyp" (derived from the shear stress tensor and the normal vector) to the resource uptake suppression, expressed by a value between 0 and 1.

7.2.4 Morphometry

There is a strong need for three-dimensional morphometric tools to test the hypotheses generated using our models against real corals. On the one hand one could think of automated methods, which can analyse simulated morphologies and scanned natural morphologies. Such methods mostly focus on the generation of morphological skeletons and the detection of branching points (see for review of two- and three-dimensional tools Kaandorp & Kübler, 2001; see also García Leiva, 2001 and Kaandorp, 1999). However, scanning large amounts of corals is very expensive and time consuming, and moreover, destructive. A second approach would be to develop tools which are simple and equally applicable both in the field and on virtual objects generated with a computer simulation. An example of such a measure is the "compactness" (see Eq. 3.4), the ratio between the volume of the coral and the volume of the "convex hull" of the coral. It would be determined easily and relatively non-destructively in the field, by measuring the volume of the coral and the volume of the same coral tightly wrapped in plastic.[1]

[1] Note that the coral would need to be temporarily removed from the reef, which may affect the coral's vitality.

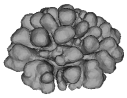

Publications

Merks, R. M. H., Hoekstra, A., & Sloot, P. (2001). Validation of the Lowe-Frenkel tracer dispersion method in the lattice Boltzmann method. In R. Lagendijk, J. Heijnsdijk, A. Pimentel, & M. Wilkinson (Eds.), *Proceedings of the 7th annual conference of the Advanced School for Computing and Imaging*, pp. 137–141.

Merks, R., Hoekstra, A., Kaandorp, J., & Sloot, P. (2002*b*). Spontaneous branching in a polyp oriented model of stony coral growth. In P. Sloot, C. K. Tan, J. J. Dongarra, & A. G. Hoekstra (Eds.), *International Conference on Computational Science (ICCS), Lecture Notes in Computer Science (LNCS)*, Volume 2329, Amsterdam, the Netherlands, pp. 88–96. Springer-Verlag, Berlin.

Merks, R. M. H., Hoekstra, A. G., & Sloot, P. M. A. (2002). The moment propagation method for advection-diffusion in the lattice Boltzmann method: validation and Péclet number limits. *J. Comput. Phys.* **183**, 563–576.

Merks, R. M. H., Hoekstra, A. G., Kaandorp, J. A., & Sloot, P. M. A. (2002*d*). Models of coral growth: Spontaneous branching, compactification and the Laplacian growth assumption. *Journal of Theoretical Biology*, in press.

Merks, R., Hoekstra, A., Kaandorp, J., & Sloot, P. (2002*a*). Branching and compactification in a model of coral growth: a critical reinvestigation of the effect of hydrodynamics. Proceedings of the European Conference on Mathematical Modelling & Computing in Biology and Medicine, Milano, Italy, *in press*.

Merks, R. M. H., Hoekstra, A. G., Kaandorp, J. A., & Sloot, P. M. A. (2002*c*). Branching and morphologic plasticity in stony corals: the polyp oriented approach. Submitted to *Journal of Theoretical Biology*

Merks, R. M. H., Hoekstra, A. G., Kaandorp, J. A., & Sloot, P. M. A. (2003*a*). Towards a problem solving environment for morphogenesis. Submitted.

Merks, R. M. H., Hoekstra, A. G., Kaandorp, J. A., & Sloot, P. M. A. (2003*b*). Diffusion-Limited Aggregation in Laminar Flows. *International Journal of Modern Physics C, in press*.

Merks, R. M. H, Hoekstra, A. G., Kaandorp, J. A., & Sloot, P. M. A. (2003*c*). A problem solving environment for modelling coral morphogenesis. In P. M. A. Sloot, D. Abramson, J. J. Dongarra, A. Zomaya, Y. Gorbachev (Eds.), *International Conference on Computational Science (ICCS), Lecture Notes in Computer Science (LNCS)*, St. Petersburg, Russia, *in press*. Springer-Verlag, Berlin.

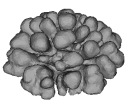

References

Abraham, E. R. (2001). A laplacian model of branching growth. In J. A. Kaandorp & J. E. Kübler (Eds.), *The Algorithmic Beauty of Seaweeds, Sponges and Corals*, pp. 109–113. Springer Verlag.

Abramson, D. & Giddy, J. (1997, September). Scheduling large parametric modelling experiments on a distributed meta-computer. In *PCW '97*, Australian National University, Canberra, pp. P2–H–1 – P2–H–8.

Afsarmanesh, H., Belleman, R. G., Belloum, A. S. Z., Benabdelkader, A., van den Brand, J. F. J., Eijkel, G. B., Frenkel, A., Garita, C., Groep, D. L., Heeren, R. M. A., Hendrikse, Z. W., Hertzberger, L. O., Kaandorp, J. A., Kaletas, E. C., Korkhov, V., de Laat, C. T. A. M., Sloot, P. M. A., Vasunin, D., Visser, A., & Yakali, H. H. (2002). VLAM-G: A Grid-based virtual laboratory. *Scientific Programming: Special Issue on Grid Computing* **10**, 173–181.

Al-Rawahi, N. & Tryggvason, G. (2002). Numerical simulation of dendritic solidification with convection: two-dimensional geometry. *J. Comput. Phys.* **180**, 471–496.

Altunbas, A., Kelbaliyev, G., & Ceylan, K. (2002). Eddy diffusivity of particles in turbulent flow in rough channels. *J. Aerosol. Sci.* **33**, 1075–1086.

Anderson, A. R. A. & Chaplain, M. A. J. (1998). Continuous and discrete mathematical models of tumor-induced angiogenesis. *Bull. Math. Biol.* **60**, 857–899.

Anthony, K. R. N. (1999). Coral suspension feeding on fine particulate matter. *J. Exp. Mar. Biol. Ecol.* **232**, 85–106.

Aris, R. (1956). On the dispersion of a solute in a fluid through a tube. *Proceedings of the Royal Society London A* **235**, 67–77.

Arnéodo, A., Couder, Y., Grasseau, G., Hakim, V., & Rabaud, M. (1989). Uncovering the analytical Saffman-Taylor finger in unstable viscous fingering and diffusion-limited aggregation. *Phys. Rev. Lett.* **63**, 984–987.

Arrayás, M., Ebert, U., & Hundsdorfer, W. (2002). Spontaneous branching of anode-directed streamers between planar electrodes. *Phys. Rev. Lett.* **88**, 174502.

Artoli, A., Hoekstra, A. G., & Sloot, P. M. A. (2002). 3D pulsatile flow with the lattice boltzmann BGK method. *Int. J. Mod. Phys. C* **13**, 1119–1134.

Bal, H. E., Bhoedjang, R., Hofman, R. F. H., Jacobs, C. J. H., Kielmann, T., Maassen, J., Van Nieuwpoort, R., Romein, J., Renambot, L., Rühl, T., Veldema, R., Verstoep, K., Baggio, A., Ballintijn, G., Kuz, I., Pierre, G., Van Steen, M., Tanenbaum, A. S., Doornbos, G., Germans, D., Spoelder, H. J. W., Baerends, E.-J., Van Gisbergen, S., Afsermanesh, H., Van Albada, G. D., Belloum, A., Dubbeldam, D., Hendrikse, Z. W., Hertzberger, L. O., Hoekstra, A. G., Iskra, K., Kandhai, D., Koelma, D., Van der Linden, F., Overeinder, B. J., Sloot, P. M. A., Spinnato, P., Epema, D. H. J., van Gemund, A. J. C., Jonker, P., Radulescu, A., Van Reeuwijk, C., Sips, H. J., Knijnenburg, P. M. W., Lew, M. S., Sluiter, F., Wolters, L., Blom, H., De Laat, C., & Van der Steen, A. (2000). The distributed ASCI supercomputer project. *Operating Systems Review 34*(4), 76–96.

Balachandar, S. & Parker, S. J. (2002). Onset of vortex shedding in an inline and staggered array of rectangular cylinders. *Phys. Fluids* **14**, 3714–3732.

Ball, P. (1998). *The Self-Made Tapestry: Pattern Formation in Nature*. Oxford University Press.

Ball, R. C. & Somfai, E. (2002). Theory of diffusion controlled growth. *Phys. Rev. Lett.* **89**, 135503.

Barber, C. B., Dobkin, D. P., & Huhdanpaa, H. (1996). The quickhull algorithm for convex hulls. *ACM T. Math. Software* **22**, 469–483.

Barnes, D. & Chalker, B. (1990). Calcification and photosynthesis in reef-building corals and algae. In Z. Dubinsky (Ed.), *Coral Reefs. Ecosystems of the world.*, Volume 25, pp. 109–131. Amsterdam: Elsevier Science Publishers B.V.

Barnes, D. J. (1973). Growth in colonial scleractinians. *B. Mar. Sci.* **23**, 280–298.

Barnes, D. J. & Lough, J. M. (1992). Systematic variations in the depth of skeleton occupied by coral tissue in massive colonies of *Porites* from the Great Barrier Reef. *J. Exp. Mar. Biol. Ecol.* **159**, 113–128.

Barra, F., Davidovitch, B., Levermann, A., & Procaccia, I. (2001). Laplacian growth and diffusion limited aggregation: different universality classes. *Phys. Rev. Lett.* **8713**, 134501.

Basney, J. & Livny, M. (1999). Deploying a high throughput computing cluster. In R. Buyya (Ed.), *High Performance Cluster Computing*, Volume 1, Chapter 5. Prentice Hall PTR.

Becker, L. C. & Müller, E. (2001). The culture, transplantation and storage of *Montastraea faveolata*, *Acropora cervicornis* and *Acropora palmata*: what we have learned so far. *Bull. Mar. Sci.* **69**, 881–896.

Bedient, P. B., Rifai, H. S., & Newell, C. J. (1993). *Ground water contamination, transport and remediation*. Englewood Cliffs, New Jersey: Prentice Hall PTR.

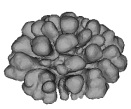

Belleman, R. G. & Sloot, P. M. A. (2000). The design of dynamic exploration environments for computational steering simulations. In M. Bubak, J. Mościński, & M. Noga (Eds.), *Proceedings of the SGI Users' Conference*, Kraków, Poland, pp. 57–74. Academic Computer Centre CYFRONET AGH.

Belleman, R. G., Stolk, B., & De Vries, R. (2001). Immersive Virtual Reality on commodity hardware. In R. L. Lagendijk, J. W. J. Heijnsdijk, A. D. Pimentel, & M. H. F. Wilkinson (Eds.), *Proceedings of the 7th annual conference of the Advanced School for Computing and Imaging*, Heijen, the Netherlands, pp. 297–304. Advanced School for Computing and Imaging (ASCI).

Bensimon, D., Kadanoff, L. P., Liang, S., Shraiman, B. I., & Tang, C. (1986). Viscous flows in two dimensions. *Rev. Mod. Phys.* **58**, 977–999.

Berger, E. & Wille, R. (1972). Periodic flow phenomena. *Annu. Rev. Fluid Mech.* **4**, 313–340.

Börner, U., Deutsch, A., Reichenbach, H., & Bär, M. (2002). Rippling patterns in aggregates of myxobacteria arise from cell-cell collisions. *Phys. Rev. Lett.* **89**, 0.

Brémond, R. & Jeulin, D. (1995). Random media and lattice gas simulations. In M. Armstrong & P. A. Dowd (Eds.), *Geostatistical Simulations*, pp. 89–105. Kluwer Academic Publishers.

Brener, E., Müller-Krumbhaar, H., Temkin, D., & Abel, T. (1998). Morphology diagram of possible structures in diffusional growth. *Physica A* **249**, 73–81.

Brière, C. & Goodwin, B. (1988). Geometry and dynamics of tip morphogenesis in *Acetabularia*. *J. Theor. Biol.* **131**, 461–475.

Bruno, J. F. & Edmunds, P. J. (1997). Clonal variation for phenotypic plasticity in the coral *Madracis mirabilis*. *Ecology* **78**, 2177–2190.

Bruno, J. F. & Edmunds, P. J. (1998). Metabolic consequences of phenotypic plasticity in the coral *Madracis mirabilis* (Duchassaing and Michelotti): the effect of morphology and water flow on aggregate respiration. *J. Exp. Mar. Biol. Ecol.* **229**, 187–195.

Buddemeier, R. & Kinzie III, R. (1976). Coral growth. *Oceanogr. Mar. Biol. Ann. Rev.* **14**, 183–225.

Buss, L. W. (1987). *The evolution of individuality*. Princeton, New Jersey: Princeton University Press.

Bussemaker, H. J., Deutsch, A., & Geigant, E. (1997). Mean-field analysis of a dynamical phase transition in a cellular automaton model for collective motion. *Phys. Rev. Lett.* **78**, 5018–5021.

Byron Bird, R., Stewart, W. E., & Lightfoot, E. R. (1960). *Transport Phenomena*. New York: John Wiley & Sons.

Calí, A., Succi, S., Cancelliere, A., Benzi, R., & Gramignani, M. (1992). Diffusion and hydrodynamic dispersion with the lattice Boltzmann method. *Phys. Rev. A* **45**, 5771–5774.

Callahan, H. S., Pigliucci, M., & Schlichting, C. D. (1997). Developmental phenotypic plasticity: where ecology and evolution meet molecular biology. *Bioessays.* **19**, 519–525.

Carlson, B. A. (1999). Organism responses to rapid change: what aquaria tell us about nature. *Am. Zool.* **39**, 44–55.

Castets, Dulos, E., Boissonade, J., & Kepper, P. D. (1990). Experimental evidence of a sustained standing turing-type nonequilibrium chemical pattern. *Physical Review Letters 64*(24), 2953–2956.

Castro, M., Cuerno, R., Sanchez, A., & Dominguez-Adame, F. (2000). Multiparticle biased diffusion-limited aggregation with surface diffusion: a comprehensive model of electrodeposition. *Phys. Rev. E* **62**, 161–173.

Chambliss, D. D. & Wilson, R. J. (1991). Relaxed diffusion limited aggregation of Ag on Au(111) observed by scanning tunneling microscopy. *J. Vac. Sci. Technol. B* **9**, 928–932.

Chen, S. & Doolen, G. D. (1998). Lattice Boltzmann method for fluid flows. *Annu. Rev. Fluid Mech.* **30**, 329–364.

Clague, D. S., Kandhai, B. D., Zhang, R., & Sloot, P. M. A. (2000). Hydraulic permeability of (un)bounded fibrous media using the lattice Boltzmann method. *Phys. Rev. E* **61**, 616–625.

Crouse, B., Krafczyk, M., Kuhner, S., Rank, E., & van Treeck, C. (2002). Indoor air flow analysis based on lattice Boltzmann methods. *Energy Build.* **34**, 941–949.

Cruz-Neira, C., Sandin, D., & DeFanti, T. (1993, August). Surround-screen projection-based virtual reality: The design and implementation of the CAVE. In *SIGGRAPH '93 Computer Graphics Conference*, pp. 135–142. ACM SIGGRAPH.

Cui, J. & Tafti, D. K. (2002). Computations of flow and heat transfer in a three-dimensional multilouvered fin geometry. *Int. J. Heat Mass Transf.* **45**, 5007–5023.

Darke, W. M. & Barnes, D. J. (1993). Growth trajectories of corallites and ages of polyps in massive colonies of reef-building corals of the genus *Porites*. *Mar. Biol.* **117**, 321–326.

Dauget, J. M. (1991). Application of tree architectural models to reef-coral growth forms. *Mar. Biol.* **111**, 157–165.

Dawson, S. P., Chen, S., & Doolen, G. D. (1993). Lattice Boltzmann computations for reaction-diffusion equations. *J. Chem. Phys.* **98**, 1514–1523.

De Jong, N. C., Zhang, L. W., Jacobi, A. M., Balachandar, S., & Tafti, D. K. (1998). A complementary experimental and numerical study of the flow and heat transfer in offset strip-fin heat exchangers. *J. Heat Transf.-Trans. ASME* **120**, 690–698.

Dorit, R. L., Walker, W. F. J., & Barnes, R. D. (1991). *Zoology*. Saunders College Publishing.

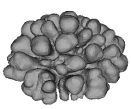

Dormann, S. & Deutsch, A. (2002). Modeling of self-organized avascular tumor growth with a hybrid cellular automaton. In Silico *Biology* **2**, 1–14.

Drazer, G. & Koplik, J. (2001). Tracer dispersion in two-dimensional rough fractures. *Phys. Rev. E* **63**, 056104.

D'Souza, R. M. & Margolus, N. H. (1999). Thermodynamically reversible generalization of diffusion limited aggregation. *Phys. Rev. E* **60**, 264–274.

Eble, G. J. (1999). Developmental and non-developmental morphospaces in evolutionary biology. SFI Working Paper 99-04-027, Santa Fe. to appear in Chapman, R. E., Rasskin-Gutman, D. and Wills, M. (eds.): *Morphospace Concepts and Applications*.

Ellers, O. (1993). A mechanical model of growth in regular sea urchins: predictions of shape and a developmental morphospace. *Proceedings: Biological Sciences* **254**, 123–129.

Ferziger, J. H. & Perić, M. (1997). *Computational Methods for Fluid Dynamics*. Berlin: Springer.

Flekkøy, E. G. (1993). Lattice Bhatnagar-Gross-Krook models for miscible fluids. *Phys. Rev. E* **47**, 4247–4257.

Foster, A. B. (1979). Phenotypic plasiticity in the reef corals *Montastrea annularis* (Ellis & Solander) and *Sidastrea siderea* (Ellis & Solander). *J. Exp. Mar. Biol. Ecol.* **39**, 25–54.

Foster, A. B. (1980). Environmental variation in skeletal morphology within the caribbean reef corals *Montastrea annularis* and *Sidastrea siderea*. *B. Mar. Sci. 30*(3), 678–709.

Foster, I., Kesselman, C., & Tuecke, S. (2001). The anatomy of the Grid: Enabling scalable virtual organization. *The International Journal of High Performance Computing Applications 15*(3), 200–222.

Frenkel, D. (1989). Long-time decay of velocity autocorrelation function of two-dimensional lattice gas cellular automata. In P. Manneville, N. Boccara, G. Vichniac, & R. Bidaux (Eds.), *Cellular automata and modeling of complex physical systems*, Volume 46 of *Proceedings in Physics*, pp. 144–154. Springer.

Frenkel, D. & Ernst, M. H. (1989). Simulation of diffusion in a two-dimensional lattice-gas cellular automaton - a test of mode-coupling theory. *Phys. Rev. Lett.* **63**, 2165–2168.

Gallopoulos, E., Houstis, E., & Rice, J. R. (1994). Computer as thinker/doer: Problem-solving environments for computational science. *IEEE Comput. Sci. Eng. 1*(2), 11–23.

García Leiva, R. A. (2001). Morphological analysis of branching structures. Master's thesis, University of Amsterdam, Section Computational Science.

Gardella, D. J. & Edmunds, P. J. (2001). The effect of flow and morphology on boundary layers in the scleractinians *Dichocoenia stokesii* (Milne-Edwards and

Haime) and *Stephanocoenia michilini* (Milne-Edwards and Haime). *J. Exp. Mar. Biol. Ecol.* **256**, 279–289.

Gateno, D., Israel, A., Barki, Y., & Rinkevich, B. (1998). Gastrovascular circulation in an octocoral: evidence of significant transport of coral and symbiont cells. *Biol. Bull.* **194**, 178–186.

Gattuso, J. P., Allemand, D., & Frankignoulle, M. (1999). Photosynthesis and calcification at cellular organismal and community levels in coral reefs: a review on interactions and control by carbonate chemistry. *Am. Zool.* **39**, 160–183.

Gierer, A. & Meinhardt, H. (1972). A theory of biological pattern formation. *Kybernetic* **12**, 30–39.

Glazier, J. A. & Graner, F. (1993). Simulation of the differential adhesion driven rearrangement of biological cells. *Phys. Rev. E* **47**, 2128–2154.

Gödde, R. & Kurz, H. (2001). Structural and biophysical simulation of angiogenesis and vascular remodeling. *Dev. Dyn.* **220**, 387–401.

Goodwin, B. (1994). *How the leopard changed its spots*. Weidenfeld & Nicholson.

Goreau, T. (1963). Calcium carbonate deposition by coralline algae and corals in relation to their roles as reef-builders. *Ann. N.Y. Acad. Sci.* **109**, 127–167.

Grasso, L. C., Hayward, D. C., Trueman, J. W. H., Hardie, K. M., Janssens, P. A., & Ball, E. E. (2001). The evolution of nuclear receptors: evidence from the coral *Acropora*. *Mol. Phylogenet. Evol.* **21**, 93–102.

Graus, R. R. & Macintyre, I. G. (1976). Light control of growth form in colonial reef corals: computer simulation. *Science* **193**, 895–897.

Graus, R. R. & Macintyre, I. G. (1982). Variation in growth forms of the reef coral *Montastrea annularis* (Ellis and Solander): A quantitative evaluation of growth response to light distribution using computer simulations. *Smithson. Contrib. Mar. Sci.* **12**, 441–464.

Halsey, T. C. (2000). Diffusion-limited aggregation: a model for pattern formation. *Phys. Today* **53**, 36–41.

Harriott, V. J. (1999). Coral growth in subtropical eastern Australia. *Coral Reefs* **18**, 281–291.

He, X. Y., Luo, L. S., & Dembo, M. (1997). Some progress in the lattice Boltzmann method: Reynolds number enhancement in simulations. *Physica. A.* **239**, 276–285.

Hendrikse, Z. W., Belloum, A. S. Z., De Laat, C. T. A. M., Jonkergouw, P. M. R., Eijkel, G. B., Hertzberger, B. L. O., Korkhov, V., & Vasunin, D. (2002). Evaluating the VLAM-G toolkit on the DAS-2. To be published in *Future Generation Computer Systems*, Special Issue on iGrid-2002.

Hill, R. J. & Koch, D. L. (2002). The transition from steady to weakly turbulent flow in a close- packed ordered array of spheres. *J. Fluid Mech.* **465**, 59–97.

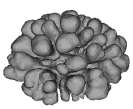

Hogeweg, P. (2000). Evolving mechanisms of morphogenesis: on the interplay between differential adhesion and cell differentiation. *J. Theor. Biol.* **203**, 317–333.

Hogeweg, P. & Hesper, B. (1974). Model study on biomorphological description. *Pattern Recogn.* **6**, 165–179.

Holloway, D. M. & Lantin, M. (2002). Maintaining Apical Dominance in the Fern Gametophyte. *Ann Bot 89*(4), 409–417.

Holm, E. A., Glazier, J. A., Srolovitz, D. J., & Grest, G. S. (1991). Effects of lattice anisotropy and temperature on domain growth in the 2-dimensional Potts-model. *Phys. Rev. A* **43**, 2662–2668.

Horzman, R. & Genin, A. (2002). unpublished data.

Hou, S., Sterling, J., Chen, S., & Doolen, G. (1996). A lattice subgrid model for high Reynolds number flows. *Fields Institute Communications* **6**, 151–166.

Hou, S. L., Zou, Q., Chen, S. Y., Doolen, G., & Cogley, A. C. (1995). Simulation of cavity flow by the lattice Boltzmann method. *J. Comput. Phys.* **118**, 329–347.

Huang, J., Yagel, R., Filippov, V., & Kurzion, Y. (1998). An accurate method for voxelizing polygon meshes. In *1998 ACE/IEEE Symposium on Volume Visualization*, pp. 119–126. ACE/IEEE.

Hut, P. & Makino, J. (1999). Computational physics - astrophysics on the GRAPE family of special-purpose computers. *Science* **283**, 501–505.

Huynen, M. A. (1996). Exploring phenotype space through neutral evolution. *J. Mol. Evol.* **43**, 165–169.

Ihle, T. & Müller-Krumbhaar, H. (1994). Fractal and compact growth morphologies in phase transitions with diffusion transport. *Phys. Rev. E* **49**, 2972–2991.

Iskra, K. A., Belleman, R. G., Van Albada, G. D., Santoso, J., Sloot, P. M. A., Bal, H. E., Spoelder, H. J. W., & Bubak, M. (2002). The polder computing environment: a system for interactive distributed simulation. *Concurr. Comput.-Pract. Exp.* **14**, 1313–1335.

Iskra, K. A., Hendrikse, Z. W., van Albada, G. D., Overeinder, B. J., & Sloot, P. M. A. (2000, July). The implementation of Dynamite — an environment for migrating PVM tasks. *Operating Systems Review 34*(3), 40–55.

Jiang, Y., Swart, P. J., Saxena, A., Asipauskas, M., & Glazier, J. A. (1999). Hysteresis and avalanches in two-dimensional foam rheology simulations. *Phys. Rev. E* **59**, 5819–5832.

Jülicher, F. (1996). The morphology of vesicles of higher topological genus: conformal degeneracy and conformal modes. *J. Phys. II France* **6**, 1797–1824.

Kaandorp, J. (1994*a*). *Fractal modelling: growth and form in biology*. Berlin, New York: Springer-Verlag.

Kaandorp, J. & Kübler, J. (Eds.) (2001). *The algorithmic beauty of seaweeds, sponges and corals*. The virtual laboratory. Berlin Heidelberg New York: Springer.

Kaandorp, J. A. (1991). Modelling growth forms of the sponge *Haliclona oculata* (Porifera, Demospongiae) using fractal techniques. *Mar. Biol.* **110**, 203–215.

Kaandorp, J. A. (1994*b*). A formal description of radiate accretive growth. *J. Theor. Biol.* **166**, 149–161.

Kaandorp, J. A. (1995). Analysis and synthesis of radiate accretive growth in three dimensions. *J. Theor. Biol.* **175**, 39–55.

Kaandorp, J. A. (1999). Morphological analysis of growth forms of branching marine sessile organisms along environmental gradients. *Mar. Biol.* **134**, 295–306.

Kaandorp, J. A. (2001). In J. A. Kaandorp & J. Kübler (Eds.), *The algorithmic beauty of seaweeds, sponges and corals*, The virtual laboratory, Berlin, Heidelberg, New York, pp. 114–144. Springer Verlag.

Kaandorp, J. A., Lowe, C. P., Frenkel, D., & Sloot, P. M. A. (1996). Effect of nutrient diffusion and flow on coral morphology. *Phys. Rev. Lett.* **77**, 2328–2331.

Kaandorp, J. A. & Sloot, P. M. A. (1997). Parallel simulation of accretive growth and form in three dimensions. *Biosystems* **44**, 181–192.

Kaandorp, J. A. & Sloot, P. M. A. (2001). Morphological models of radiate accretive growth and the influence of hydrodynamics. *J. Theor. Biol.* **209**, 257–274.

Kandhai, D., Koponen, A., Hoekstra, A., Kataja, M., Timonen, J., & Sloot, P. M. A. (1999). Implementation aspects of 3D lattice-BGK: boundaries accuracy and a new fast relaxation method. *J. Comput. Phys.* **150**, 482–501.

Kandhai, D., Koponen, A., Hoekstra, A. G., Kataja, M., Timonen, J., & Sloot, P. M. A. (1998). Lattice-Boltzmann hydrodynamics on parallel systems. *Comput. Phys. Commun.* **111**, 14–26.

Kandhai, D., Vidal, D. J. E., Hoekstra, A. G., Hoefsloot, H., Iedema, P., & Sloot, P. M. A. (1998). A comparison between lattice-Boltzmann and finite-element simulations of fluid flow in static mixer reactors. *Int. J. Mod. Phys. C* **9**, 1123–1128.

Kessler, J. (1986). Individual and collective fluid dynamics of swimming cells. *J. Fluid Mech.* **173**, 191–205.

Kleypas, J. A., Buddemeier, R. W., Archer, D., Gattuso, J. P., Langdon, C., & Opdyke, B. N. (1999). Geochemical consequences of increased atmospheric carbon dioxide on coral reefs. *Science* **284**, 118–120.

Knutson, D. W., Buddemeier, R. W., & Smith, S. V. (1972). Coral chronometers: seasonal growth bands in reef corals. *Science* **177**, 270–272.

Kolb, M., Botet, R., & Jullien, R. (1983). Scaling of kinetically growing clusters. *Phys. Rev. Lett.* **51**, 1123–1126.

Kondo, S. & Asai, R. (1995). A reaction-diffusion wave on the skin of the marine angelfish *Pomacanthus*. *Nature* **376**, 765–768.

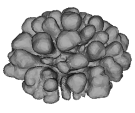

Koopman, E. A. (2002). A comparison of a particle tracking and a lattice boltzmann based method for advection-diffusion problems. Master's thesis, University of Amsterdam, Computational Physics.

Koponen, A., Kandhai, D., Hellen, E., Alava, M., Hoekstra, A., Kataja, M., Niskanen, K., Sloot, P., & Timonen, J. (1998). Permeability of three-dimensional random fiber webs. *Phys. Rev. Lett.* **80**, 716–719.

Kovács, T. & Bárdos, G. (1997). Cluster growth by diffusion-limited aggregation in shear flow. *Physica A* **247**, 59–66.

Kruth, J., Leu, M., & Nakagawa, T. (1998). Progress in additive manufacturing and rapid prototyping. *Annals of the CIRP* **47**, 525–540. Keynote paper.

Kuffner, I. B. (2002). Effects of ultraviolet radiation and water motion on the reef coral, *Porites compressa* Dana: a transplantation experiment. *J. Exp. Mar. Biol. Ecol.* **270**, 147–169.

Kumar, R., Nivarthi, S. S., Davis, H. T., Kroll, D. M., & Maier, R. S. (1999). Application of the lattice-Boltzmann method to study flow and dispersion in channels with and without expansion and contraction geometry. *Int. J. Numer. Methods Fluids* **31**, 801–819.

Lajeunesse, E. & Couder, Y. (2000). On the tip-splitting instability of viscous fingers. *J. Fluid Mech.* **419**, 125–149.

Lallemand, P. & Luo, L. S. (2000). Theory of the lattice boltzmann method: dispersion dissipation, isotropy, Galilean invariance, and stability. *Phys. Rev. E* **61**, 6546–6562.

Langdon, C., Takahashi, T., Sweeney, C., Chipman, D., Goddard, J., Marubini, F., Aceves, H., Barnett, H., & Atkinson, M. J. (2000). Effect of calcium carbonate saturation state on the calcification rate of an experimental coral reef. *Glob. Biogeochem. Cycle* **14**, 639–654.

Lantin, M. (1999). *An environment for the simulation of biological cells*. Ph. D. thesis, Simon Fraser University.

Le Tissier, M. D. A., Clayton, B., Brown, B. E., & Davis, P. S. (1994). Skeletal correlates of coral density banding and an evaluation of radiography as used in sclerochronology. *Mar. Ecol.-Prog. Ser.* **110**, 29–44.

Lee, K.-J., McCormick, W. D., Pearson, J. E., & Swinney, H. L. (1994). Experimental observation of self-replicating spots in a reaction-diffusion system. *Nature* **369**, 215–218.

Lesser, M. P., Weis, V. M., Patterson, M. R., & Jokiel, P. L. (1994). Effects of morphology and water motion on carbon delivery and productivity in the reef coral, *Pocillopora damicornis* (Linnaeus): Diffusion barriers, inorganic carbon limitation, and biochemical plasticity. *J. Exp. Mar. Biol. Ecol.* **178**, 153–179.

Lindenmayer, A. (1968). Mathematical models for cellular interaction in development, parts i and ii. *Journal of Theoretical Biology* **18**, 280–315.

López-Tomàs, L., Claret, J., & Sagues, F. (1993). Quasi-2-dimensional electrodeposition under forced fluid-flow. *Phys. Rev. Lett.* **71**, 4373–4376.

Lough, J. M. & Barnes, D. J. (1997). Several centuries of variation in skeletal extension density and calcification in massive *Porites* colonies from the great barrier reef: A proxy for seawater temperature and a background of variability against which to identify unnatural change. *J. Exp. Mar. Biol. Ecol.* **211**, 29–67.

Lough, J. M. & Barnes, D. J. (2000). Environmental controls on growth of the massive coral *Porites*. *J. Exp. Mar. Biol. Ecol.* **245**, 225–243.

Lowe, C. P. & Frenkel, D. (1995). The super long-time decay of velocity fluctuations in a two-dimensional fluid. *Physica A* **220**, 251–260.

Lowe, C. P. & Frenkel, D. (1996). Do hydrodynamic dispersion coefficients exist? *Phys. Rev. Lett.* **77**, 4552–4555.

Loya, Y. (1976). Skeletal regeneration in a red sea scleractinean coral population. *Nature* **261**, 490–491.

Lu, Z. Y., Liao, Y., Qian, D. Y., McLaughlin, J. B., Derksen, J. J., & Kontomaris, K. (2002). Large eddy simulations of a stirred tank using the lattice boltzmann method on a nonuniform grid. *J. Comput. Phys.* **181**, 675–704.

Magdaleno, F. X. & Casademunt, J. (1998). Surface tension and dynamics of fingering patterns. *Phys. Rev. E* **57**, R3707–R3710.

Maier, R. S. & Bernard, R. S. (1997). Accuracy of the lattice-boltzmann method. *Int. J. Mod. Phys. C* **8**, 747–752.

Maier, R. S., Kroll, D. M., Davis, H. T., & Bernard, R. S. (1998). Pore-scale flow and dispersion. *Int. J. Mod. Phys. C* **9**, 1523–1533.

Makino, J. (1996). Postcollapse evolution of globular clusters. *Astrophys. J.* **471**, 796–803.

Manica, A. & Carter, R. (2000). Morphological and fluorescence analysis of the *Montastrea annularis* species complex in florida. *Mar. Biol.* **137**, 899–906.

Marée, A. F. M. & Hogeweg, P. (2001). How amoeboids self-organize into a fruiting body: Multicellular coordination in *Dictyostelium discoideum*. *PNAS 98*(7), 3879–3883.

Marée, A. F. M. & Hogeweg, P. (2002). Modelling *Dictyostelium discoideum* morphogenesis: the culmination. *Bull. Math. Biol.* **64**, 327–353.

Marinescu, D. C. & Boloni, L. (2000). A component-based architecture for problem solving environments. *Math. Comput. Simul.* **54**, 279–293.

Marshall, A. T. (1996). Calcification in hermatypic and ahermatypic corals. *Science* **271**, 637–639.

Marubini, F., Barnett, H., Langdon, C., & Atkinson, M. J. (2001). Dependence of calcification on light and carbonate ion concentration for the hermatypic coral *Porites compressa*. *Mar. Ecol.-Prog. Ser.* **220**, 153–162.

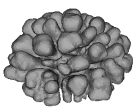

McGhee, Jr., G. R. (1999). *Theoretical Morphology: The concept and its applications*. Colombia University Press.

McDougall, S. R., Anderson, A. R. A., Chaplain, M. A. J., & Sherratt, J. A. (2002). Mathematical modelling of flow through vascular networks: implications for tumour-induced angiogenesis and chemotherapy strategies. *Bull. Math. Biol.* **64**, 673–702.

Meakin, P. (1983*a*). Diffusion-controlled cluster formation in 2-6 dimensional space. *Phys. Rev. A 27*(3), 1495–1507.

Meakin, P. (1983*b*). Formation of fractal clusters and networks by irreversible diffusion-limited aggregation. *Phys. Rev. Lett.* **41**, 1119–1122.

Meakin, P. (1986). A new model for biological pattern formation. *J. Theor. Biol.* **118**, 101–113.

Meakin, P. (1999). A historical introduction to computer models for fractal aggregates. *J. Sol-Gel Sci. Technol.* **15**, 97–117.

Meakin, P., Ramanlal, P., Sander, L. M., & Ball, R. C. (1986). Ballistic deposition on surfaces. *Physical Review A 34*(6), 5091–5103.

Meinhardt, H. (1995). *The Algorithmic Beauty of Sea Shells*. The Virtual Laboratory. New York, Berlin, Heidelberg, London, Paris, Tokyo, Hong Kong: Springer-Verlag.

Meinhardt, H. & Gierer, A. (2000). Pattern formation by local self-activation and lateral inhibition. *Bioessays* **22**, 753–760.

Merks, R., Hoekstra, A., Kaandorp, J., & Sloot, P. (2002*a*, April). Spontaneous branching in a polyp oriented model of stony coral growth. In P. Sloot, C. K. Tan, J. J. Dongarra, & A. G. Hoekstra (Eds.), *International Conference on Computational Science (ICCS), Lecture Notes in Computer Science (LNCS)*, Volume 2329, Amsterdam, the Netherlands, pp. 88–96. Springer-Verlag, Berlin.

Merks, R. M. H., Hoekstra, A., & Sloot, P. (2001). Validation of the Lowe-Frenkel tracer dispersion method in the lattice Boltzmann method. In R. Lagendijk, J. Heijnsdijk, A. Pimentel, & M. Wilkinson (Eds.), *Proceedings of the 7th annual conference of the Advanced School for Computing and Imaging*, pp. 137–141.

Merks, R. M. H., Hoekstra, A. G., Kaandorp, J. A., & Sloot, P. M. A. (2002*b*). Branching and morphologic plasticity in stony corals: the polyp oriented approach. Submitted.

Merks, R. M. H., Hoekstra, A. G., Kaandorp, J. A., & Sloot, P. M. A. (2003). Models of coral growth: Spontaneous branching, compactification and the Laplacian growth assumption. *Journal of Theoretical Biology*, in press.

Merks, R. M. H., Hoekstra, A. G., & Sloot, P. M. A. (2002). The moment propagation method for advection-diffusion in the lattice Boltzmann method: validation and Péclet number limits. *J. Comput. Phys.* **183**, 563–576.

Meroz, E., Brickner, I., Loya, Y., Peretzman-Shemer, A., & Ilan, M. (2002). The effect of gravity on coral morphology. *Proc. R. Soc. Lond. B* **269**, 717–720.

Meyer, M., Desbrun, M., Schröder, P., & Barr, A. H. (2002). Discrete differential-geometry operators for triangulated 2-manifolds. International Workshop on Visualization and Mathematics, Berlin-Dahlem (Germany).

Meyer-Hermann, M., Deutsch, A., & Or-Guil, M. (2001). Recycling probability and dynamical properties of germinal center reactions. *J. Theor. Biol.* **210**, 265–285.

Miller, M. (1995). Growth of a temperate coral: effects of temperature, light, depth and heterotropy. *Mar. Ecol.-Prog. Ser.* **122**, 217–225.

Mineev-Weinstein, M. B. & Dawson, S. P. (1994). Class of nonsingular exact-solutions for Laplacian pattern formation. *Phys. Rev. E* **50**, R24–R27.

Muko, S., Kawasaki, K., Sakai, K., Takasu, F., & Shigesada, N. (2000). Morphological plasticity in the coral *Porites sillimaniani* and its adaptive significance. *Bull. Mar. Sci.* **66**, 225–239.

Mulder, J. & van Liere, R. (2002). The personal space station: Bringing interaction within reach. In *Proceedings of VRIC2002; 4th Virtual Reality International Conference*, Laval, France, pp. 73–81.

Mullins, W. W. & Sekerka, R. F. (1963). Morphological stability of a particle growing by diffusion or heat flow. *Journal of Applied Physics* **34**, 323–329.

Mullins, W. W. & Sekerka, R. F. (1964). Stability of a planar interface during solidification of a dilute binary alloy. *Journal of Applied Physics* **35**, 444–451.

Muthukumar, M. (1983). Mean-field theory for diffusion-limited cluster formation. *Phys. Rev. Lett. 50*(11), 839–842.

Nagatani, T. (1991). Modified laplacian growth under shear-flow. *J. Phys. Soc. Jpn.* **60**, 2700–2705.

Nagatani, T. & Sagues, F. (1991). Morphological-changes in convection-diffusion-limited deposition. *Phys. Rev. A* **43**, 2970–2976.

Newman, S. A. (2002). Developmental mechanisms: putting genes in their place. *J. Biosci.* **27**, 97–104.

Newman, S. A. & Muller, G. B. (2000). Epigenetic mechanisms of character origination. *J. Exp. Zool.* **288**, 304–317.

Nicolis, G. & Prigogine, I. (1977). *Self-Organization in Nonequillibrium Systems*. New York: Wiley-Interscience.

Nicolis, G. & Prigogine, I. (1989). *Exploring Complexity: An introduction*. New York: W. H. Freeman and company.

Nittmann, J. & Stanley, H. E. (1986). Tip splitting without interfacial tension and dendritic growth patterns arising from molecular anisotropy. *Nature* **321**, 663–668.

Oren, U., Rinkevich, B., & Loya, Y. (1997). Oriented intra-colonial transport of C^{14}-labeled materials during coral regeneration. *Mar. Ecol.-Prog. Ser.* **161**, 117–122.

Palsson, E. (2001). A three-dimensional model of cell movement in multicellular systems. *Futur. Gener. Comp. Syst.* **17**, 835–852.

Parrish, J. K. & Edelstein-Keshet, L. (1999). Complexity, Pattern, and Evolutionary Trade-Offs in Animal Aggregation. *Science 284*(5411), 99–101.

Pasko, V. P., Stanley, M. A., Mathews, J. D., Inan, U. S., & Wood, T. G. (2002). Electrical discharge from a thundercloud top to the lower ionosphere. *Nature* **416**, 152–154.

Paterson, L. (1984). Diffusion-limited aggregation and two-fluid displacements in porous media. *Phys. Rev. Lett.* **52**, 1621–1624.

Picioreanu, C., Van Loosdrecht, M. C. M., & Heijnen, J. J. (2000). Effect of diffusive and convective substrate transport on biofilm structure formation: a two-dimensional modeling study. *Biotechnol. Bioeng.* **69**, 504–515.

Pigliucci, M. (1996). How organisms respond to environmental changes: from phenotypes to molecules (and vice versa). *Trends Ecol. Evol.* **11**, 168–173.

Plapp, M. & Karma, A. (2000*a*). Multiscale finite-difference-diffusion Monte-Carlo method for simulating dendritic solidification. *J. Comput. Phys.* **165**, 592–619.

Plapp, M. & Karma, A. (2000*b*). Multiscale random-walk algorithm for simulating interfacial pattern formation. *Phys. Rev. Lett.* **84**, 1740–1743.

Portegies Zwart, S. F., McMillan, S. L. W., Hut, P., & Makino, J. (2001). Star cluster ecology - IV. Dissection of an open star cluster: photometry. *Mon. Not. Roy. Astron. Soc.* **321**, 199–226.

Poston, T. & Serra, L. (1994, August 23-26). The virtual workbench: Dextrous VR. In S. K. F. G. Singh & D. Thalmann (Eds.), *Proceedings of the VRST'94—Virtual Reality Software and Technology*, Singapore, pp. 111–122. World Scientific.

Prusinkiewicz, P. & Lindenmayer, A. (1990). *The Algorithmic Beauty of Plants*. The Virtual Laboratory. New York, Berlin, Heidelberg, London, Paris, Tokyo, Hong Kong: Springer-Verlag.

Qian, Y. H., D'Humières, D., & Lallemand, P. (1992). Lattice BGK models for Navier-Stokes equation. *Europhys. Lett.* **17**, 479–484.

Raup, D. M. (1962). Computer as aid in describing form in gastropod shells. *Science* **138**, 150–152.

Raup, D. M. & Michelson, A. (1965). Theoretical morphology of the coiled shell. *Science* **147**, 1294–1295.

Rice, J. R. & Boisvert, R. F. (1996). From scientific software libraries to problem solving environments. *IEEE Comput. Sci. Eng.* **3**, 44–53.

Ridge, D., Becker, D., & Merkey, P. (1997). Beowulf: Harnessing the power or parallelism in a pile-of-pcs. In *Proceedings of the 1997 IEEE Aerospace Conference*, Volume 2, pp. 79–91. IEEE.

Rinkevich, B. (2001). Genetic regulation in the branching stony coral *Stylophora pistillata*. In J. A. Kaandorp & J. E. Kübler (Eds.), *The algorithmic beauty of seaweeds, sponges, and corals*, pp. 62–66. Springer Verlag.

Rinkevich, B. (2002). The branching coral *Stylophora pistillata*: contribution of genetics in shaping colony landscape. *Isr. J. Zool.* **48**, 71–82.

Rinkevich, B. & Loya, Y. (1983). Oriented translocation of energy in grafted reef corals. *Coral Reefs* **1**, 243–247.

Rinkevich, B. & Loya, Y. (1985). Coral isomone: a proposed chemical signal controlling intraclonal growth patterns in a branching coral. *B. Mar. Sci.* **36**, 319–324.

Rosenboom, T. (2002). *Aanvallend spel: Vier lezingen over schrijven*. Amsterdam: Em. Querido's Uitgeverij.

Sander, L. M. (1986). Fractal growth processes. *Nature* **322**, 789–793.

Savill, N. J. & Hogeweg, P. (1997). Modelling morphogenesis: from single cells to crawling slugs. *J. Theor. Biol.* **184**, 229–235.

Schwarzer, S., Lee, J., Havlin, S., Stanley, H. E., & Meakin, P. (1991). Distibution of growth-probabilities for off-lattice diffusion-limited aggregation. *Phys. Rev. A* **43**, 1134–1137.

Sebens, K. P., Witting, J., & Helmuth, B. (1997). Effects of water flow and branch spacing on particle capture by the reef coral *Madracis mirabilis* (Duchassaing and Michelotti). *J. Exp. Mar. Biol. Ecol.* **211**, 1–28.

Segel, L. A. (2001). Computing an organism. *PNAS 98*(7), 3639–3640.

Shi, B. C., Guo, Z. L., & Wang, N. C. (2002). Lattice Bhatnagar-Gross-Krook simulations of turbulent natural convection in a cavity. *Chin. Phys. Lett.* **19**, 515–517.

Shock, R. A., Mallick, S., Chen, H., Yakhot, V., & Zhang, R. (2002). Recent results on two-dimensional airfoils using a lattice boltzmann-based algorithm. *J. Aircr.* **39**, 434–439.

Shraiman, B. & Bensimon, D. (1984). Singularities in nonlocal interface dynamics. *Phys. Rev. A* **30**, 2840–2842.

Sterling, T. L., Savarese, D., Becker, D. J., Dorband, J. E., Ranawake, U. A., & Packer, C. V. (1995). Beowulf: A parallel workstation for scientific computation. In P. Banerjee (Ed.), *Proceedings of the 1995 International Conference on Parallel Processing*, Volume I: Architecture, pp. 11–14. CRC Press.

Succi, S. (2001). *The Lattice Boltzmann Equation: for Fluid Dynamics and Beyond*. Numerical Mathematics and Scientific Computation. Oxford New York: Oxford University Press.

Succi, S., Chen, H. D., Teixeira, C., Bella, G., De Maio, A., & Molvig, K. (1999). An integer lattice realization of a Lax scheme for transport processes in multiple component fluid flows. *J. Comput. Phys.* **152**, 493–516.

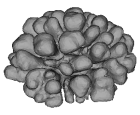

Ten Cate, A., Derksen, J. J., Kramer, H. J. M., Van Rosmalen, G., & Van den Akker, H. E. A. (2001). The microscopic modelling of hydrodynamics in industrial crystallisers. *Chem. Eng. Sci.* **56**, 2495–2509.

Thompson, D. (1917). *On Growth and Form* (Abridged edition, 1961, 1995, Cambridge University Press ed.). Cambridge University Press.

Tong, S. & Yuan, F. (2001). Numerical simulations of angiogenesis in the cornea. *Microvasc. Res.* **61**, 14–27.

Toussaint, J., Debierre, J. M., & Turban, L. (1992). Deposition of particles in a 2-dimensional lattice gas-flow. *Phys. Rev. Lett.* **68**, 2027–2030.

Trigueros, P. P., Claret, J., Mas, F., & Sagues, F. (1991). Pattern morphologies in zinc electrodeposition. *J. Electroanal. Chem.* **312**, 219–235.

Turing, A. M. (1950, October). Computing machinery and intelligence. *Mind: A quarterly review of psychology and philosophy 59*(236), 433–460.

Turing, A. M. (1952). The chemical basis of morphogenesis. *Phil. Trans. Roy. Soc. B* **237**, 37–72.

Turner, S. & Sherratt, J. A. (2002). Intercellular adhesion and cancer invasion: a discrete simulation using the extended Potts model. *J. Theor. Biol.* **216**, 85–100.

Van der Hoef, M. A. & Frenkel, D. (1990). Long-time tails of the velocity autocorrelation function in 2- dimensional and 3-dimensional lattice-gas cellular automata - a test of mode-coupling theory. *Phys. Rev. A* **41**, 4277–4284.

Van der Sman, R. & Ernst, M. H. (2002). Gallilean invariant convection-diffusion lattice boltzmann scheme for rectangular lattices. Submitted.

Van der Sman, R. G. M. (1999). Solving the vent hole design problem for seed potato packagings, with the lattice Boltzmann scheme. *Int. J. Comput. Fluid Dyn.* **11**, 237–248.

Van der Sman, R. G. M. & Ernst, M. H. (2000). Convection-diffusion lattice Boltzmann scheme for irregular lattices. *J. Comput. Phys.* **160**, 766–782.

Van Veghel, M. & Bak, R. (1993). Intraspecific variation of a dominant Caribbean reef building coral, *Montastrea annularis*: genetic, behavioral and morphometric aspects. *Mar. Ecol. Prog. Ser.* **92**, 255–265.

Vasiev, B. & Weijer, C. J. (1999). Modeling chemotactic cell sorting during *Dictyostelium discoideum* mound formation. *Biophys. J.* **76**, 595–605.

Vermeij, M. J., Barnes, D. J., & Muko, S. (2001). Scleractinian stony corals (hexacorals). In J. A. Kaandorp & J. E. Kübler (Eds.), *The algorithmic beauty of seaweeds, sponges, and corals*, pp. 51–56. Springer Verlag.

Vermeij, M. J. A. & Bak, R. P. M. (2002). How are coral populations structured by light? Marine light regimes and the distribution of *Madracis*. *Mar. Ecol.-Prog. Ser.* **233**, 105–116.

Vogel, S. (1988). *Life's devices: the physical world of animals and plants*, Chapter 8: Diffusion versus convection, pp. 158–176. Princeton, New Jersey: Princeton University Press.

Vold, M. (1959). A numerical approach to the problem of sediment volume. *J. Coll. Sci.* **14**, 168–174.

Warren, P. B. (1997). Electroviscous transport problems via lattice-Boltzmann. *Int. J. Mod. Phys. C* **8**, 889–898.

Warren, P. B., Ball, R. C., & Boelle, A. (1995). Convection-limited aggregation. *Europhys. Lett.* **29**, 339–344.

Weast, R. C., Astle, M. J., & Beyer, W. H. (Eds.) (2000). *CRC Handbook of Chemistry and Physics* (3rd electronic ed.). Boca Raton, Florida: CRC Press.

Weil, E. & Knowlton, N. (1994). A multi-character analysis of the caribbean coral montastraea- annularis (ellis and solander, 1786) and its 2 sibling species, m-faveolata (ellis and solander, 1786) and m-franksi (gregory, 1895). *Bull. Mar. Sci.* **55**, 151–175.

Wellington, G. (1982). An experimental analysis of the effect of light and zooplankton on coral zonation. *Oecologia* **52**, 311–320.

Williamson, C. H. K. (1996). Vortex dynamics in the cylinder wake. *Annu. Rev. Fluid Mech.* **28**, 477–539.

Witten Jr., T. & Sander, L. (1981). Diffusion-limited aggregation, a kinetic critical phenomenon. *Phys. Rev. Lett.* **47**, 1400–1403.

Witten, Jr., T. A. & Meakin, P. (1983). Diffusion-limited aggregation at multiple growth sites. *Physical Review B* **28**, 5632–5642.

Zajac, M., Jones, G. L., & Glazier, J. A. (2000). Model of convergent extension in animal morphogenesis. *Phys. Rev. Lett.* **85**, 2022–2025.

Zemlin, C. (2000). Numerical schemes to solve diffusion on a triangular mesh. unpublished.

Zhang, L. W., Balachandar, S., & Tafti, D. K. (1997). Effects of intrinsic three dimensionality on heat transfer and friction loss in a periodic array of parallel plates. *Numer. Heat Tranf. A-Appl.* **31**, 327–353.

Zhang, L. W., Balachandar, S., Tafti, D. K., & Najjar, F. M. (1997). Heat transfer enhancement mechanisms in inline and staggered parallel-plate fin heat exchangers. *Int. J. Heat Mass Transf.* **40**, 2307–2325.

Zhou, J. G. (2002). A lattice boltzmann model for the shallow water equations with turbulence modeling. *Int. J. Mod. Phys. C* **13**, 1135–1150.

Zilberberg, C. & Edmunds, P. J. (1999). Patterns of skeletal structure variability in clones of the reef coral *Montastraea franksi*. *Bull. Mar. Sci.* **64**, 373–381.

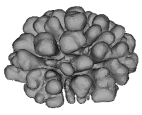

Nederlandse samenvatting

Het begrijpen van morfogenese, de ontwikkeling van de *vorm* van organismen, is een van de meest boeiende en fundamentele problemen in de biologie. Uit een bevruchte eicel kan een volledig ontwikkeld dier ontstaan, met pootjes, oogjes, een neusje, en vaak haartjes. Bij andere organismen, zoals bij planten of koralen, kan een onderdeel van de ouder, een "stekje", uitgroeien tot een volledig volwassen organisme. Die ene bevruchte eicel of dat ene stekje bevatten schijnbaar genoeg informatie om de volledige ontwikkeling van het volwassen dier of de uitgegroeide plant te beschrijven. Deze informatie, die vaak het *ontwikkelingsprogramma* wordt genoemd, naar analogie van een computerprogramma, is in elke cel van het organisme als DNA opgeslagen.

Dit is echter een sterke versimpeling van de werkelijkheid. Stel je eens voor dat een archeoloog over duizenden jaren het stof van een stapel ponskaarten[1] zou blazen. Misschien zou hij een serie enen en nullen kunnen aflezen, maar zonder kennis van de computer die de op de ponskaarten opgeslagen programma's oorspronkelijk kon uitvoeren, zal deze informatie van beperkte waarde zijn. Hetzelfde geldt voor genetische informatie. Zonder grondige kennis van de structuur en werking van de *apparatuur* die de instructies van het "ontwikkelingsprogramma" opvolgt, de cellen, weefsels, en externe skeletdelen, blijft het onbegrijpelijk hoe het DNA de vorm en functie van planten en dieren reguleert.

De cellen, weefsels en skeletdelen van planten en dieren nemen vaak door hun structuur en wederzijdse interactie *uit zichzelf*, passief een vorm aan. Denk bijvoorbeeld aan een heel simpele celachtige structuur, een door een membraan omhulde druppel vloeistof. Deze structuur zal zonder verdere bijsturing de vorm aannemen van een bolletje, zoals een vetdruppeltje op de soep ook rond is. De genetische informatie zal in veel gevallen, door de eiwitten die het codeert, een effect hebben op deze "eigen" vorm. In de meeste cellen worden, gestuurd door de genetische informatie, skeleteiwitten aangemaakt. Deze eiwitten vormen een skelet dat de cel als de stokken in een tent in vorm houdt. We moeten ons dus niet verwonderen over bolvormige cellen — dat is immers de vorm die we op grond van hun meeste simpele structuur verwachten — we zouden ons juist moeten verbazen over de meer complexe vormen: langgerekte

[1] Kartonnen kaarten met gaatjes die tot in de jaren zeventig van de twintigste eeuw werden gebruikt om computergegevens mee op te slaan.

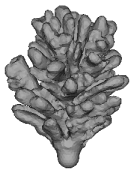

cellen in spieren, de schijfvormige rode bloedcellen, en de vertakte zenuwcellen. In dit proefschrift heb ik een soortgelijke gedachtengang toegepast op koraalgroei. Wat voor vormen verwachten we op grond van het groeiproces in koralen, en voor welke vormen verwachte we dat er extra, meer complexe factoren meespelen, zoals bijsturing door de erfelijke informatie?

De meeste steenkoralen zijn kolonies van kleine diertjes, de poliepen. Dit zijn kleine zee-anemonen, die met elkaar verbonden zijn via weefselbruggen. Ze bouwen een skelet van aragoniet, een soort kalk. Als de poliepen dood zijn, blijft het vaak prachtig vertakte, witte koraal over dat soms (helaas) in toeristenwinkels wordt verkocht. De poliepen leven op dit skelet in skeletstructuurtjes, de calyx, die in het Engels ook wel de "skeletal cup", vrij vertaald het "skeletnapje" wordt genoemd (zie Figuur 1.5). De koraalpoliepen zetten op de bodem van het skeletnapje en bij de verbindende weefselbruggen nieuwe kalk af op het oude kalkskelet, waardoor het skelet als geheel groeit. Bij de meeste koraalsoorten groeit het skelet niet sneller dan enkele centimeters per jaar (zie Tabel 4.3). Op bolle stukken van een koraal zullen de poliepen door de groei van het skelet uit elkaar worden gedreven. Denk maar aan een gestipte ballon, de stippen komen steeds verder uit elkaar te staan bij het opblazen. Als de poliepen een zekere afstand tot elkaar krijgen, zal er een nieuwe poliep tussen worden geplaatst. Bij welke afstand dat gebeurt, hangt af van de soort. Op holle gedeelten worden de poliepen door de groei van het skelet juist dichter op elkaar gedrongen. Niet alle poliepen overleven dit, waardoor de poliepen gelijk over het koraaloppervlak verdeeld blijven. Koralen halen een belangrijk deel van hun energie uit licht. De poliepen bieden onderdak aan eencellige algen, die in ruil voor een veilige, goed verlichte haven met name suikers aan het koraal afstaan. De rest van hun voedsel, zoals bijvoorbeeld kleine kreeftjes en los organisch materiaal, en een grote hoeveelheid kalkzouten en andere anorganische stoffen die nodig zijn voor het skelet, nemen de poliepen op uit het water.

Uit het relatief eenvoudige groeiproces van koralen komen veel vormen voort. Er zijn vertakte koralen, zoals de exemplaren van *Madracis mirabilis* op de omslag, maar er bestaan ook bolvormige, gelobde en korstvormige koralen. De uiteindelijke vorm van de koraalkolonie wordt voor een belangrijk deel bepaald door de soort waartoe het behoort, zodat koraalbiologen de soort vaak aan de vorm kunnen herkennen. Dit lukt ze echter niet altijd. Dat komt doordat de kolonievormen mede afhangen van de omgeving waarin het koraal groeit. Zo blijken koralen die in stromend water groeien vaak robuuster, compacter te zijn dan hun wijdvertakte soortgenoten die in stilstaand water groeien. Ook blijken sommige koralen meer takken te hebben op sterk verlichte groeiplaatsen dan op donkerder plaatsen. Dit fenomeen wordt *morfologische plasticiteit* genoemd.

Biologen zijn het niet eens over de oorzaak van morfologische plasticiteit. Sommigen denken dat het koraal *actief* op een milieufactor reageert. Door zijn groeidynamiek aan te passen, zou het koraal een vorm kunnen aannemen die het gunstigst is voor de omgeving waarin het groeit. Zo kunnen fijnvertakte koralen meer voedsel opvangen in stilstaand water, en onderscheppen dicht vertakte, compacte groeivormen meer voedsel in stromend water. Zij stellen dat het groeiproces zeer sterk genetisch bepaald is, en dat plasticiteit een genetisch gereguleerde reactie is. Anderen vermoeden dat de oorzaak ook *passief* kan zijn. In deze zienswijze wordt de vorm van het koraal

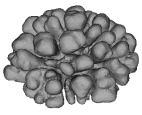

minder sterk in een "genetisch keurslijf" geperst, zodat de omgeving het groeimechanisme kan beïnvloeden. Zo zou de hoeveelheid voedsel die het koraal opneemt mede beïnvloed kunnen worden door de waterstroming, waardoor de groei — en daardoor de kolonievorm — door de omgeving wordt bepaald.

Het is lastig een onderscheid te maken tussen deze twee mogelijke verklaringen. Immers, beide theorieën doen dezelfde voorspelling, namelijk dat koraalvormen afhangen van hun omgeving. Wetenschappers gaan daarom vaak uit van een stelling door Willem van Ockham (ca. 1285-1349), bekend als *Ockham's razor*, het scheermes van Ockham. Deze Fransiscaner monnik, die lesgaf in Oxford, stelde "*pluralitas non est ponenda sine neccesitate*", poneer geen veelvoud zonder noodzaak. Als twee verklaringen dezelfde uitwerking hebben, dan is de verklaring waar het minste aantal factoren in meespeelt het waarschijnlijkst. Als het licht in mijn huis uitvalt, maar alle lampen in de buurt doen het nog wel, dan zou de elektriciteitscentrale kapot kunnen zijn, terwijl al mijn buren een noodaggregaat hebben. Of mijn eigen stoppen zijn doorgeslagen.

Dit is de belangrijkste reden om een computermodel te gebruiken. In een computermodel kunnen we elementen die volgens ons van belang zijn op elkaar laten inwerken, om uit te testen of deze elementen *voldoende* zijn om de observaties, of een gedeelte daarvan, te reproduceren. In dit proefschrift heb ik een serie, steeds iets complexere computermodellen gebruikt om te testen of de minimale aanname dat koraalpoliepen meer skelet afzetten als ze meer voedsel uit het water kunnen opnemen, voldoende is voor het ontstaan van vertakkende groei. Bovendien heb ik onderzocht of waterstroming van invloed is op de groeivormen die zo ontstaan.

Doordat de poliepen voedsel opnemen uit het water, zal het water rondom het koraal op den duur uitgeput raken, en moeten er nieuwe voedingsstoffen vanuit het omringende water worden aangevoerd. Als eerste stap in de opbouw van mijn model had ik dus een correct berekeningsmodel van het voedseltransport nodig. Watermoleculen en de daarin opgeloste voedingsstoffen dansen door de warmte als kleine knikkertjes heen en weer, waardoor ze langzamerhand worden vermengd. Deze langzame, passieve vermenging wordt diffusie genoemd. De stoffen die in het water zijn opgelost worden ook meegevoerd door de stroming van het water. In **Hoofdstuk twee** bespreek ik een methode om te berekenen hoe het transport van opgeloste stoffen door diffusie en stroming in een vloeistof zal verlopen. Deze methode is al langer in gebruik, maar tot nu toe was nog niet uitvoerig getest of de methode ook inderdaad correcte resultaten oplevert. In 1956 bepaalden de natuurkundigen Taylor en Aris (Aris, 1956) wiskundig hoe een stroming door een ronde buis een opgeloste stof zal verspreiden. Wij hebben onze berekeningen met deze wiskundige voorspelling van Taylor en Aris vergeleken en gelukkig bleek dat ze, binnen bepaalde limieten, met hun voorspellingen overeenkwamen. We hebben ook laten zien dat de methode alléén correcte resultaten oplevert zolang het transport door stroming niet te sterk is ten opzichte van het transport door diffusie.

In 1996 publiceerden mijn co-promotor dr. Jaap Kaandorp, mijn promotor prof. dr. Peter Sloot en een aantal anderen een artikel in *Physical Review Letters* waarin ze een eenvoudig model van vertakkende koraalgroei bestudeerden (Kaandorp *et al.*, 1996). Dit *Diffusie-geLimiteerde Aggegratiemodel* (DLA), dat in 1981 is geïntroduceerd, begint met een klein, vastgeklonken deeltje, zie het als een koraallarve. Er wordt een

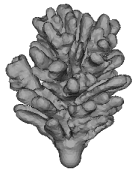

tweede "voedsel"-deeltje losgelaten dat zich op een regelmatig rooster volgens een "dronkenmanswandeling" voortbeweegt. Het zet telkens een stapje in een willekeurige richting naar een naburig knooppunt in het rooster. Als het wandelende deeltje het vaste deeltje raakt, blijft het er aan plakken. Het wordt zo als het ware in koraalskelet omgezet. Door dit proces te herhalen ontstaat een vertakte vorm, zoals die in Fig. 3.2. Kaandorp en Sloot onderzochten de invloed van stroming op dit proces. De "dronkenmanswandelingen" konden ze benaderen met een diffusieproces, en met de methode beschreven in Hoofdstuk 2 modelleerden ze het gecombineerde effect van stroming en diffusie. Ze hielden de stroomsnelheid op een vaste waarde, en varieerden in plaats daarvan de "snelheid" van de diffusie. Bij een langzaam diffusieproces, wanneer de stroming relatief belangrijker werd, vonden ze compactere groeivormen, net zoals bij echte koralen. Dit was een ondersteuning voor de *passieve* verklaring van morfologische plasticiteit.

In **Hoofdstuk drie** heb ik dit model opnieuw bestudeerd, maar ik vond niets terug van deze effecten. Hoogstens groeide het cluster een klein beetje in de richting van de stroming. Ik heb laten zien dat de conclusies van Kaandorp en Sloot op een misverstand berustten. Om de groei wat sneller te laten verlopen — de computers waren toen veel langzamer dan nu — voegden ze een groot aantal deeltjes tegelijkertijd aan het koraal toe. Bovendien kreeg het diffusieproces te weinig tijd, zodat bij langzame diffusie het "voedsel" bij de groeivorm onvoldoende was uitgeput. Hierdoor groeide het "koraal" overal even hard, en vertakte het niet. Het effect had dus niets met stroming te maken, maar viel te verklaren door een fout in het model.

In 2001 publiceerden Kaandorp en Sloot een tweede artikel over dit onderwerp, nu in *Journal of Theoretical Biology*. Ze gebruikten hier een gedetailleerder model van koraalgroei. Dit was het *accretiemodel*, waarin het "koraal" laagje over laagje aangroeit. De dikte van een laagje hangt af van de hoeveelheid voedsel die er op die plek uit de modelvloeistof wordt opgenomen. Dit model was een betere benadering van het koraalgroeiproces dan het vorige. Maar het bleek dat de koralen niet vertakten als de groei alléén afhing van de voedselopname. Daarom voegden ze een nieuwe modelregel toe. Het "koraal" groeide het hardst op bolle gedeelten, en de groei werd onderdrukt op platte en holle gedeelten. Het idee achter deze regel was dat er op bolle gedeelten een "beter contact" bestond met de omgeving. Met de extra regel werd de vertakking in feite afgedwongen, zodat dit model niet kon worden gebruikt om te begrijpen *hoe* koralen vertakken. Wel was het geschikt om te bestuderen hoe de volledige groeivorm reageert op stroming. Kaandorp en Sloot gebruikten hetzelfde model van voedseltransport als in hun vorige artikel. Weer stelden ze de stroomsnelheid in op een vaste waarde, en varieerden in plaats daarvan hoe snel het diffusieproces verliep. Net als in hun vorige publicatie werden de groeivormen compacter als de stroming schijnbaar belangrijker werd.

In **Hoofdstuk vier** heb ik dit model opnieuw opgebouwd en bestudeerd. Ik zag dat de modelkoralen wel degelijk vertakten als de groei alleen afhangt van de voedselopname (zie Fig. 4.6). Een extra modelregel bleek overbodig. Wel moest er een balans zijn tussen de aanvoer en de opname van voedsel, voor we een nieuw laagje toevoegden. Er wordt door uitstekende stukjes, hoe klein ook, altijd iets meer "voedsel" opgenomen dan elders. Hierdoor groeien ze iets harder en versterkt het proces zichzelf, zodat

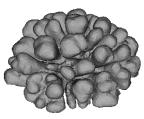

er takken worden gevormd. Eigenlijk was dit geen verbazingwekkende ontdekking, aangezien dit model erg lijkt op *Laplaciaanse groeimodellen* uit de natuurkunde. Deze worden gebruikt voor het bestuderen van uiteenlopende fenomenen waarin vertakkingen een rol spelen, zoals bliksemschichten, de verplaatsing van aardolie door het inpompen van water en de vorming van kristallen. Het was al langer bekend dat in deze modellen spontane vertakkingen optreden. Wel zijn drie-dimensionale modellen van dergelijke processen relatief nieuw.

Ik bestudeerde vervolgens de invloed van stroming op deze groeivormen, maar opnieuw zag ik bij de stroomsnelheden die Kaandorp en Sloot gebruikt hadden, de "koralen" alleen een beetje in de richting van de stroming groeien (zie Fig. 4.8). Maar waarom vonden zij dan dat de groeivormen compacter werden onder invloed van stroming? De verklaring lag opnieuw in het feit dat Kaandorp en Sloot te weinig tijd toelieten voor het voedseltransport. Het voedsel raakt door de opname rondom de "takken" van het modelkoraal uitgeput. Hier vindt dus geen groei plaats, zodat de takken een zekere afstand tot elkaar houden. Ze stelden het diffusieproces langzamer af om stroming te simuleren. In dat geval worden de uitputtingszones kleiner en houden de takken minder afstand tot elkaar. Dat is geen stromingseffect. In mijn studies trad dit effect inderdaad zowel mét als zonder stroming op.

In ons model vertakken de "koralen" spontaan als de aanvoer en opname van voedsel in balans zijn. Maar is dat een realistische aanname? Na een vergelijking van de tijd die nodig is voor het voedseltransport en de tijd die nodig is voor de groei van echte koralen, concludeerden we dat deze processen zo langzaam zijn, dat de balans al vele malen is verstoord voor hij zich heeft ingesteld. Een golf of een langszwemmende vis zou de voedselverdelingen in het water zodanig verstoren dat het vertakkingsmechanisme waarschijnlijk niet op kan treden.

In **Hoofdstuk vijf** poneer ik een aanvulling op dit model. In de vorige modellen werd het koraaloppervlak als één geheel beschouwd, en werd het voedsel over het hele oppervlak opgenomen. In het *poliep-georiënteerde* model beschouw ik de poliepen afzonderlijk van elkaar. Elke poliep absorbeert zijn voedsel vanuit een klein gedeelte van de vloeistof op een kleine afstand van het koraaloppervlak, die overeenkomt met de hoogte van een werkelijke koraalpoliep. Het koraaloppervlak neemt zelf geen voedsel op. In dit model bleek ook spontane vertakking op te treden, maar het trad al op als de aanvoer en opname van voedsel minder sterk in balans zijn. Dit mechanisme is dus minder gevoelig voor de vele verstoringen in een koraalrif. De oorzaak is een extra vertakkingsmechanisme. Op bolle stukken van het oppervlak waaieren de "poliepen" een beetje uit. Hierdoor hebben ze minder concurrentie van elkaar kunnen ze iets meer voedsel opnemen dan de andere "poliepen" op platte en holle gedeelten. De animatie op de rechterpagina is een resultaat van dit model. Je zou verwachten dat het waaiereffect minder sterk wordt als de poliepen minder dicht op elkaar staan. De "poliepen" hebben dan immers hoe dan ook al minder last van elkaar, zodat het uitwaaieren relatief minder voordeel oplevert. Inderdaad vertakken de "koralen" minder sterk, en krijgen ze dikkere takken, als de poliepen minder dicht op elkaar staan (zie Fig. 5.4). De animatie op de linkerpagina laat een dergelijke groeivorm zien, waarbij bovendien de aanvoer van voedsel iets anders verloopt.

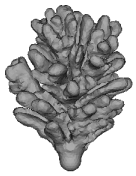

De meeste onderzoekers die gebruik maken van rekenmodellen, moeten hun pro-

grammatuur zelf ontwikkelen, en ik was hierin geen uitzondering. Hoewel ik hierdoor precies weet hoe de modellen in elkaar zitten, kleeft er ook een groot nadeel aan. Het gebruik van modellen is nu alleen bereikbaar voor onderzoekers die zich kunnen inlezen in het onderzoeksonderwerp — koralen in mijn geval — en tegelijkertijd kennis en vaardigheden hebben in de technische aspecten van het simulatieprogramma. Het risico bestaat dat de onderzoeker hierbij op één van beide kanten de nadruk legt. De laatste jaren is er binnen de *computational science,* de berekeningswetenschap, een ontwikkeling gaande waarbij men probeert dit probleem te vermijden. Zou het niet mooi zijn als de taken konden worden gescheiden? De koraalbioloog concentreert zich op het correct modelleren van het groeiproces, terwijl natuurkundigen de vloeistofstroming correct modelleren en informatici bestuderen hoe het model zo efficiënt mogelijk op grote paralelle machines kan worden gesimuleerd. Het werk van de koraalbioloog concentreert zich zo op het *oplossen van probleem,* de systemen heten dan ook *problem solving environments,* probleemoplossingsomgevingen. In **Hoofdstuk zes** beschrijf en bediscussieer ik een dergelijke probleemoplossingsomgeving die we gebouwd hebben om de koraalsimulatie bereikbaar te maken voor biologen die niet opgeleid zijn in de berekeningswetenschap.

In dit proefschrift hoop ik aannemelijk te hebben gemaakt dat er eenvoudige mechanismen bestaan die aspecten van de vertakkende groei van koralen kunnen reproduceren. Dergelijke mechanismen zouden een rol kunnen spelen in de vertakkende groei van echte koralen. Genetische regulatiemechanismen zijn niet noodzakelijk voor vertakkende groei. In deze modellen zetten we alle regels van de simulatie van te voren klaar, en kwamen we niet in de verleiding later nieuwe regels, zoals een curvatureregel, toe te voegen. Dit proefschrift begon met een motto van Thomas Rosenboom uit *Aanvallend spel* (Rosenboom, 2002), een serie lezingen over schrijven:

> *— maar nieuwe elementen worden na het begin niet meer toegevoegd, de schrijver had ze allemaal al klaargezet in de opening en hoefde ze alleen nog maar te gebruiken, net zoals een goede kok eerst alle benodigde ingrediënten klaarzet voor hij begint te koken, en net zoals een schaakspeler speelt met de stukken die al vanaf het begin op het bord staan, zonder bij te zetten.*

Ik zou het citaat als volgt willen aanvullen: *— en net zoals een wetenschapper zijn simulaties construeert uit de onderdelen van het natuurlijke systeem, zonder extra regels toe te laten.*

De tweede vraag, of morfologische plasticiteit als gevolg van waterbeweging kan worden veroorzaakt door een passief effect op het groeiproces, heb ik niet kunnen beantwoorden. Wel heb ik laten zien dat twee eerdere modelresultaten die een dergelijke "passieve" verklaring leken te ondersteunen, berustten op een verkeerde interpretatie van de simulaties. De stroming in koraalriffen is meestal echter veel hoger dan de stroming die bereikt kon worden in die simulaties. Bij dergelijke stromingen zullen er turbulenties optreden rond de takken van koraal. Deze zullen het transport van voedsel sterk beïnvloeden. Toekomstige modelstudies van koraalgroei zouden zich daarom moeten richten op het effect van turbulent voedseltransport.

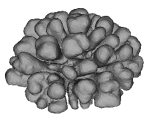

Dankwoord

Veel mensen zijn belangrijk geweest voor dit proefschrift. Mijn promotor, Peter Sloot, wil ik hartelijk bedanken voor zijn enthousiaste begeleiding. Je soms kritische vragen hebben veel verbeterd aan mijn onderzoek. Mijn co-promotores Alfons Hoekstra en Jaap Kaandorp hadden de “dagelijkse begeleiding” in handen. Jaap, mijn kritische benadering van je vroegere werk moet niet altijd even gemakkelijk voor je zijn geweest. De fundamenten van mijn onderzoek zijn echter door jou gelegd. Ondanks de enkele rotte balk die ik misschien heb vervangen in dit boekje, staat je koraalgroeionderzoek nog als een huis. Van onze uitvoerige wetenschappelijke discussies, waarin we het lang niet altijd eens werden, heb ik enorm veel geleerd. Alfons, jouw rol in de voortzetting van dit onderzoek is van onschatbare waarde geweest. Toen ik ongeveer een jaar in SCS-groep werkte, vroeg ik of je een gedeelte van mijn begeleiding op je wilde nemen. En hoewel je het al behoorlijk druk had, reageerde je meteen enthousiast en heb je vanaf het begin veel tijd in dit onderzoek gestoken. Officieel ben je ingeschakeld voor de natuurkundige aspecten van mijn promotieonderzoek, maar het moet gezegd dat je ook aan de biologische kant veel hebt bijgedragen. Aan onze vele, vruchtbare discussies over lattice Boltzmann, advectie-diffusie, Péclet-getallen, koraalpoliepjes, skeletdichtheden, groeisnelheden en *problem solving environments* zal ik met plezier terugdenken. Dick, je adviezen en onverwachtse gezichtspunten, die ik soms terloops van je kreeg terwijl je op weg was naar Piero, zijn vaak erg nuttig voor me geweest. Walter, ik durf je hier wel op te biechten dat ik je planten een keertje vergeten ben, maar tot mijn opluchting hebben ze het overleefd!

Zonder de antwoorden van mijn collega-AiO’s, OiO’s, postdocs en studenten op mijn vele vragen over Unix, C, C++, wiskunde, rooster-Boltzmann, natuurkunde, netwerken, visualisatie, informatica-jargon, waarvoor ik op de meest ongelegen momenten hun kamers meende te kunnen binnenstormen, hadden mijn simulaties nooit gewerkt. En zonder hun LaTeX-tips hadden mijn papers en dit proefschrift er maar rommelig uitgezien. Maar hun belangrijkste bijdragen aan de afgelopen vier jaar waren hun gezelligheid, steun, humor, plezier, etentjes en drinkentjes.

Piero, without you as my office-mate my research would have been a dull job. Thanks for all the nice discussions about the university, politics, art, the world, food, the universe, our many struggles with our computers, and life in general. And thank

you so much for your Italian turbo-coffee which dragged me through the last months. Rosella, it was a pleasure to take some of your time, whenever you dropped by to see Piero. Your and Piero's Italian dishes were the best I have ever tasted. I wish you both all the best for your new life in Trento, and I do hope to see you again! Alessia, with your arrival *those* astronomers became the majority in room F.222... but your presence has been a real pleasure. Thanks for coping with my continuous grumbles and sighs uttered to my always stubborn computer!

Zeger en Kamil, ik noem jullie in één adem. Jullie kamer is een soort van toevluchtsoord met reddende engeltjes voor me geweest. Kamil, hoe hopeloos mijn programmeerproblemen soms ook leken, jij wist de oplossing. Ik heb meer dan eens met stomme verbazing toegekeken hoe je mijn codes, maar ook draaiende programma's op de ontleedtafel legde en vroeg of laat je vinger op de fout legde. Zeger, je hebt me enorm geholpen met de lineaire algebra en vectorberekeningen die ik nodig had voor de ontwikkeling van mijn koraalcodes. Later heb je me een stoomcursus tensorcalculus gegeven, die onmisbaar was voor een aantal berekeningen in Hoofdstuk 2. En altijd kon ik bij jou en Kamil terecht voor de dagelijkse klets en de laatste roddels, en een portie *mental coaching* zoals je het zelf graag noemt.

Artoli, your knowledge of physics in general, and of lattice-Boltzmann in particular has been extremely helpful to me. But above all, I thank you for the endless hospitality to your room, your support, the cups of tea, the fun we had. Zhiming, Roman, Denis, Elena, Alfredo and Heidi, thanks for our lunches, hikes and fiestas. Robert, tijdens onze 'laatste loodjes' hebben we veel aan elkaar gehad. Simon, jouw komst naar de SCS-groep heeft veel leven in de brouwerij gebracht. Wonderlijk, hoe we als bioloog en sterrenkundige zowel in Tokio als in Amsterdam door stom toeval op dezelfde gang terecht kwamen! Bedankt voor je vele relativeringen, die na hóógstens één of twee biertjes... het miserabele leven als AiO een heel stuk draaglijker maakten. En Merei, bedankt voor je gezelligheid.

Wouter, het was leuk om je afstudeeronderzoek te begeleiden. Rafael, Evert, Lee, Chris and Antony, Simon, it was a pleasure and very stimulating to discuss your research projects. David, bedankt voor onze vele praatjes! Ook mijn vroegere collega's Leen, Drona, Benno, Arjen, Martin en David ben ik natuurlijk niet vergeten! Erik, Marianne, Jacqueline, Jan, en het systeembeheer van Sara en de DAS-2, bedankt voor jullie onmisbare ondersteuning!

Fan, thank you so much for our interesting discussions about cellular automata and biological modelling. No words can suffice to express everyone's shock about the fact you will never read these sentences. The strength and humour you found to bear your illness have deeply impressed me.

Han, hartelijk dank voor het fantastische omslagontwerp, Ronald voor de geweldige foto's van de koraalmodellen.

In een dankwoord schijnen de belangrijkste mensen altijd op de laatste plaats te moeten komen. Mam en Pap, Jan en Marlies, (schoon-)broers en (schoon-)zussen, vrienden: ontzettend bedankt voor jullie liefde, vriendschap, steun, en vertrouwen dat het allemaal goed zou komen! Taco en Marjolein, bedankt dat jullie als paranimfen mijn handje vasthouden! Lieve, lieve Bart, bedankt voor je liefde, je luisterend oor, je geduld, etentjes op het juiste moment. Zonder jou was het nooit gelukt!

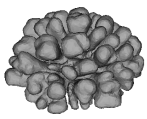

Curriculum vitae

Roeland Merks werd geboren te Groningen op 29 november 1972 en groeide op in Nijmegen. Hij voltooide het Atheneum B aldaar op het Dominicus College in 1991. In hetzelfde jaar begon hij een studie Diergeneeskunde aan de Universiteit Utrecht. Hij behaalde zijn propedeuse in 1992. Vanaf 1993 studeerde hij Biologie, ook aan de Universiteit Utrecht. Hij studeerde af in 1997 met als specialisaties Ontwikkelingsbiologie en Theoretische Biologie, op onderzoeken naar patroonvorming in de klauwkikker en de evolutie van morfogenese. In 1998 verbleef hij met een beurs van het Nuffic Talentenprogramma aan de Tokyo University in Japan. Van 1999 tot 2003 was hij als promovendus verbonden aan de Sectie Computational Science aan de Universiteit van Amsterdam, waar hij werkte aan de modellering van vertakkende koraalgroei. De resultaten van dit onderzoek staan beschreven in dit proefschrift.

Roeland Merks was born in Groningen, The Netherlands on November 29, 1972. He grew up in Nijmegen, where he finished high school in 1991. In the same year he started studying Veterinary Medicine at Utrecht University. He obtained his propedeutic diploma in 1992. From 1993 he studied Biology, also at Utrecht University, where he specialised in Developmental Biology and Theoretical Biology. He obtained a Master's degree in 1997 on research of pattern formation in *Xenopus laevis* and the evolution of morphogenesis. He gained a "Nuffic Talentenprogramma" fellowship for a stay at Tokyo University, Japan, in 1998. From 1999 to 2003 he worked as a PhD-student in the Section Computational Science at the University of Amsterdam, where he worked on modelling branching coral growth. The results of this research are described in this thesis.

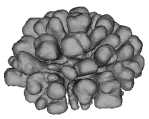

List of Symbols

A_i	area of influence of polyp v_i
α	tube radius
b	number of lattice velocities
C	compactness
c_s	speed of sound
c_i	lattice velocities
D_m	diffusion coefficient
$D(t)$	time dependent dispersion coefficient
$D_{\min}$	minimum valid diffusion coefficient
d	Euclidean dimensionality
Δt	time interval
Δ	amount of rest particles
Δ^*	fraction of rest particles
Δx	space interval
$\Delta_{\max}$	maximum valid Δ
$\delta_{\alpha\beta}$	Kronecker delta
δ	mean free path
$\delta(x_i)$	δ-function, 1 when x_i is solid, 0 when x_i is fluid
F_r	fractal dimension (from radius of gyration)
f_i	lattice Boltzmann particle distribution
f_i^{eq}	equillibrium distribution
$f_{\min}$	minimum value of distribution f_i
$g()$	growth function
$\gamma()$	function translating strains on polyp to food uptake inhibition
$h2_i$	local measurement function
K	dispersion coefficient
k	turn over of resource flux to growth velocity
$\bar{\kappa}$	mean curvature
κ	geometry dependent paramter in Taylor-Aris expression
κ_1, κ_2	principal curvatures
L	characteristic length

l_{reach}	polyp size
$\vec{l}_i$	longitudinal growth element placed at v_i
$\vec{\Lambda}_{ij}$	link from v_i to v_j
$\vec{m}_1$	first order moment
$\vec{m}_2$	second order moment
$\vec{\mu_i}$	vector of growth parameters measured locally to v_i
$\vec{n}_i$	normal vector at v_i
ν	kinematic viscosity
Ω_i	collision operator
$Pé$	Péclet-number
$Pé_{\text{lat}}$	lattice Péclet-number
P_{aggr}	aggregation probability
p	pressure
ϕ_i	resource flux at vertex v_i
$Q_{i\alpha\beta}$	$c_{i\alpha\beta} - c_s^2\delta_{\alpha\beta}$
R	resource (= tracer)
R_g	radius of gyration
$R_{\max}$	maximum resource concentration found among all v_i
r	radius
Re	Reynolds number
ρ	fluid density
s	maximum thickness of growth layer
σ_x	first order moment in x-direction
$\sigma_x^2 x$	second order moment in x-direction
$\sigma_{\alpha\beta}$	shear stress tensor
t	time
t_p	equillibrium density for $\vec{u} = 0$, where $p = \vec{c}_i.\vec{c}_i$
t_D	diffusion time
τ	relaxation time
Θ_1, Θ_2	threshold functions
θ_{NS}	stability threshold Navier-Stokes
θ_{AD}	stability threshold advection-diffusion
θ_{INS}	insertion threshold
θ_{FUSE}	fusion threshold
θ	maximum accretion per growth cycle
tr	minimum accretion
$\vec{u}$	fluid velocity
$\vec{u}_{\max}$	maximum velocity occurring in simulation
V	variance
V_n	Volume of n
v_i	vertex, or polyp in PORAG model
w_i	"weight" of connection (compare t_p)
$\vec{x}$	lattice position
x_i, y_i, z_i	spatial coordinate

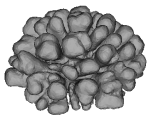

Subject Index

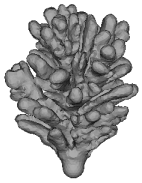

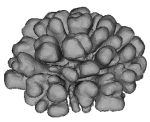

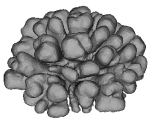

Author Index